Development of automated microfluidic devices for quantifying nutrient uptake and release from murine adipose tissue with fluorescence imaging

by

Md Moniruzzaman

A dissertation submitted to the Graduate Faculty of
Auburn University
in partial fulfillment of the
requirements for the Degree of
Doctor of Philosophy in Chemistry

Auburn, Alabama
December 9, 2023

Keywords:
Microfluidic, Photolithography, Tissue Engineering, Linear flow, Droplet, Multiplex Assay

Approved by

Christopher J. Easley, Chair, C. Dent Williams Professor, Dept. of Chemistry & Biochemistry

Wei Zhan, Professor, Dept. of Chemistry & Biochemistry

Leonardo De La Fuente, Professor, Dept. of Entomology & Plant Pathology

Ahmed Hamid, Assistant Professor, Dept. of Chemistry & Biochemistry

Abstract

This study aims to advance the knowledge of diabetes-associated biological assays such as white adipose tissue secreted glycerol and fatty acid uptake and secretion assays by leveraging the incorporation of microfluidic platforms. The investigation involves several dimensions, spanning from diabetes and obesity to the innovation of modern microfluidic devices.

The first chapter initiates a comprehensive exploration of the relationships among diabetes, obesity, and adipose tissue. These relationships lay the groundwork for the ensuing chapters and underscores the pivotal significance of microfluidic tools as unique instruments in addressing complexities of adipose tissue function.

In the second chapter, automated microfluidic devices, microfluidic digital analog converters (μDAC), are designed to expedite cell and tissue stimulation at high temporal resolution (5 seconds). This pioneering approach not only streamlines experimentation but also showcases the potential for modulating stimuli, thereby offering deeper insights into dynamic cellular responses and the intricacies of disease (diabetes) mechanisms.

Chapter three unveils the application of valve-controlled droplet-based microfluidics, enabling precise sampling from *ex vivo* adipose tissue. Through multiplexed sensing of glycerol and fatty acid secretion, this technique presents a novel avenue for dissecting adipose tissue dynamics, unveiling implications for metabolic disorders such as diabetes.

Shifting focus to nucleic acid driven sensing through electrochemistry, the fourth chapter introduces an innovative automated microfluidic device for biosensor preparation on electrode

surfaces. This approach streamlines the process of electrode fabrication, potentially elevating the efficiency of nucleic acid-based sensors and paving the way for more precise diagnostic outcomes.

Cumulatively, this research underscores the pivotal role of microfluidics in propelling forward bioanalysis, particularly when applied to diabetes research. By combining chapters that span from comprehending diseases to automating assays and multiplexed sensing, this dissertation contributes to the evolving landscape of diabetes research and diagnostic methodologies. It is our hope that the advancements showcased herein will stimulate novel insights, streamlined techniques, and transformative breakthroughs in the future to aid in managing diabetes and its related metabolic intricacies.

Acknowledgments

I am deeply grateful for the invaluable opportunity to pursue my postgraduate (Doctoral) studies in bioanalytical chemistry within the esteemed Department of Chemistry and Biochemistry at Auburn University. The nurturing and welcoming environment that permeates Auburn's campus has been instrumental in facilitating my comprehensive understanding of this specialized field. I am hopeful that the knowledge I have acquired during my tenure at Auburn will be of benefit to numerous individuals, especially those pursuing similar academic paths.

I extend my heartfelt appreciation to my mentor, Prof. Chris Easley, for his unwavering support and invaluable guidance throughout my doctoral journey. His mentorship has not only enriched my scientific perspective but also broadened my comprehension of research in profound ways. Gratitude is also extended to Prof. Wei Zhan, Dr. Leonardo De La Fuente, and Dr. Ahmed Hamid for their commitment as esteemed committee members. Special recognition is reserved for Dr. Adriana Avila- Flores, who served as the university reader for this dissertation.

I extend my commendations to the entire Easley lab team, whose contributions have significantly shaped my Auburn experience. I extend my gratitude to former lab members, including Dr. Xiangpeng Li, Dr. Juan Hu, Dr. Subramaniam Somasundaram, Dr. Kat Ford, Dr. Mark Holtan, Dr. Niamat Khuda, and Dr. Nan Shi. Their mentorship, guidance, and amity have played an instrumental role in my growth and development as a graduate student. I am equally thankful to my current lab colleagues, including Dr. Asanka, Dr. Amanda, Mohib, Yvette, Andresa, Joanne, Mainul, Sabita, and Josh, who have become an integral part of my academic journey. Their unwavering support has made my lab experience both delightful and productive. A

special note of gratitude goes to Dr. Nan Shi, Mohib and Andresa for their assistance in my research related to microfluidic device development and fluorescence assay development.

As an international student from South Asia, the transition to American culture seemed daunting. However, I am profoundly indebted to my dear friend Chase Richburg for his steadfast companionship. To my American friends, your support since my arrival in the USA has been deeply appreciated. I was fortunate to find a vibrant Bangladeshi community at Auburn University, and I am especially grateful to Mohib, Russel, Dr. Kamal Hossain, Dr. Shamim Begum, Dr. Ashraf Uddin, Moin Islam, and Dr. Emran Al. Your presence has truly made Auburn feel like a second home. Our impromptu outings, movie nights, potlucks, and adventures have been a source of solace during challenging times.

Undoubtedly, my PhD journey would not have been possible without the constant support of my parents. Mama (Sajeda Begum) and papa (Abdul Mazid), your constant encouragement has been my foundation throughout these years. A special acknowledgment goes to my elder brother (Abdur Rahman), whose commitment to education has continuously inspired me. Despite the miles that separate us, our daily conversations have served as a wellspring of motivation. During moments of self-doubt, your unwavering belief has propelled me forward. Words cannot adequately convey the depth of my gratitude for your enduring support.

List of Contents

List of Tables

List of Figures

Chapter 1

Introduction

This portion of this chapter is adopted from the published book chapter "Tissue engineering and analysis in droplet microfluidics" (N. Shi, M. Moniruzzaman and C. J. Easley In: Droplet Microfluidics, R. Soc. Chem. Cambridge, UK 2020)

1.1 Obesity

Obesity is a serious public health problem that has been increasing in prevalence worldwide over the past few decades. It is defined as having a body mass index (BMI) of 30 or higher, and it is associated with a number of negative health outcomes, including type 2 diabetes, cardiovascular disease, and certain cancers[1]. In this passage, we will review some of the empirical research on obesity and its impacts on health. One study published in The Lancet in 2017 found that the global prevalence of obesity has more than doubled since 1980, with an estimated 603.7 million adults and 107.7 million children being classified as obese in 2015[2]. The study also found that obesity rates have increased more rapidly in low- and middle-income countries compared to high-income countries.

Another study published in JAMA in 2019 analyzed data from over 6 million people and found that higher levels of body fat were associated with an increased risk of all-cause mortality, as well as an increased risk of death from cardiovascular disease, respiratory disease, and cancer[3]. The study also found that the optimal BMI for survival was in the range of 20-25, which is considered a healthy weight. In addition to its impacts on physical health, obesity is also associated with negative mental health outcomes. A systematic review published in Obesity Reviews in 2018 found that obesity was associated with an increased risk of depression and anxiety, as well as lower

quality of life and self-esteem[4]. Efforts to address the obesity epidemic have focused on a variety of approaches, including public health campaigns to promote healthy eating and physical activity, policies to improve the availability and affordability of healthy food options, and interventions to support individuals in achieving and maintaining a healthy weight. However, the effectiveness of these interventions has been mixed, highlighting the complexity of the issue.

Obesity is a major public health problem that has significant impacts on physical and mental health. Efforts to address this epidemic will require a multifaceted approach that considers both individual and societal factors. The disease is a complex disorder that results from a combination of genetic, behavioral, and environmental factors[5]. Obesity has been associated with several health problems, including cardiovascular diseases, diabetes, cancer, and decreased life expectancy[6]. One of the primary causes of obesity is an imbalance between energy intake and energy expenditure, where individuals consume more calories than they burn[7]. Research has shown that the availability of unhealthy food and beverages in schools, workplaces, and communities is also a significant environmental contributor to obesity[8]. A study conducted by the Centers for Disease Control and Prevention found that in the United States, the prevalence of obesity increased from 30.5% in 1999-2000 to 42.4% in 2017-2018[9]. The World Health Organization recommends a combination of healthy eating, physical activity, and behavior changes to prevent and manage obesity[10]. Public health interventions, such as taxes on sugary drinks and restrictions on unhealthy food marketing, have been shown to be effective in reducing obesity rates[8]. A comprehensive approach, including individual and environmental interventions, is necessary to address the obesity epidemic[8].

1.1.1 Obesity and Adipose Tissue: Understanding the Connection

One of the key factors in the development of obesity is the accumulation of adipose tissue, or body fat, which can lead to a number of negative health outcomes. In this passage, we will explore

the relationship between obesity and adipose tissue and review some of the empirical research on this topic. Adipose tissue is a complex and metabolically active tissue that plays a critical role in energy homeostasis (**Figure 1.1**), as well as the regulation of appetite and satiety[11]. However, excess adipose tissue can lead to the development of obesity, which is associated with a number of negative health outcomes, including type 2 diabetes, cardiovascular disease, and certain cancers[10].

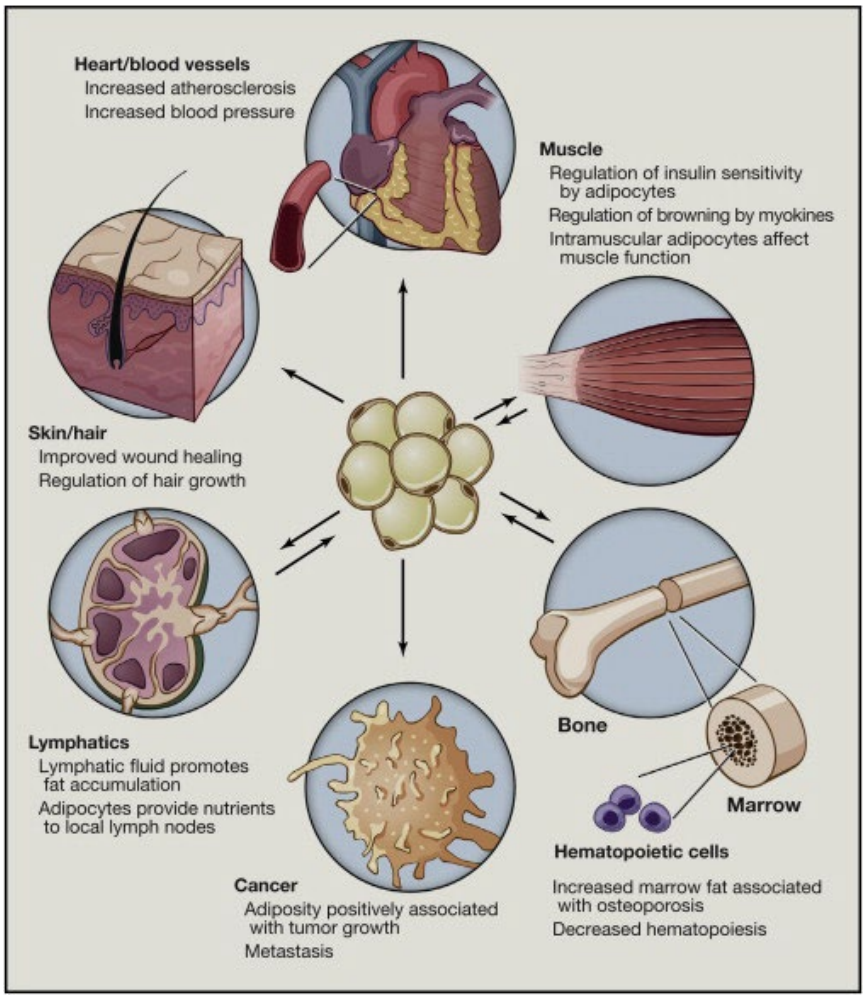

Figure 1. 1 Relation of adipose tissue with other tissues: Adipocytes store and release calories to the body generally, but numerous examples have emerged that demonstrate additional roles of fat in a wide array of biological processes. Adapted from Ref.[11] with permission from the Elsevier article, Copyright © 2014 Elsevier Inc. All rights reserved.

One study published in *Nature* in 2017 found that the accumulation of adipose tissue is regulated by a complex network of genetic, epigenetic, and environmental factors[12]. The study identified several key genetic pathways that are involved in the regulation of adipose tissue mass, including pathways related to lipid metabolism, insulin signaling, and inflammation. Another study published in *Cell* in 2019 found that adipose tissue also plays an important role in the regulation of systemic metabolism and immune function[13]. The study identified several key signaling pathways that are involved in the crosstalk between adipose tissue and other organs, including the liver, pancreas, and gut.

Efforts to address obesity and its associated health outcomes have focused on a variety of approaches, including lifestyle interventions, pharmacotherapy, and bariatric surgery. One area of active research is the development of novel therapies that target adipose tissue directly, either by reducing its mass or by modifying its metabolic function. Adipose tissue is a complex and metabolically active tissue that plays a critical role in energy homeostasis and the regulation of systemic metabolism and immune function. However, excess adipose tissue can lead to the development of obesity and a number of negative health outcomes. Further research is needed to better understand the relationship between adipose tissue and obesity, and to develop effective strategies for preventing and treating obesity-related diseases.

1.1.2 The Role of Adipose Tissue in Obesity Development

One of the key functions of adipose tissue is to store excess energy in the form of triglycerides. When energy intake exceeds energy expenditure, the excess energy is stored in adipose tissue.

However, when energy intake consistently exceeds energy expenditure, the size and number of adipocytes, or fat cells, increase, leading to the development of obesity[14].

Several studies have investigated the relationship between adipose tissue and obesity development. A study published in the New England Journal of Medicine in 2019 found that individuals with obesity have a greater number of adipocytes than individuals with normal weight, which leads to an increase in total body fat mass[15]. This finding suggests that the accumulation of adipose tissue is a critical factor in the development of obesity. Another study published in the Journal of Clinical Endocrinology and Metabolism in 2016 investigated the impact of adipose tissue inflammation on obesity development[16]. The study found that chronic inflammation in adipose tissue, which can result from a range of factors including poor diet, physical inactivity, and stress, can lead to insulin resistance and the development of obesity.

Efforts to address obesity and its associated health outcomes have focused on a variety of approaches, including lifestyle interventions, pharmacotherapy, and bariatric surgery. However, targeting adipose tissue directly may also hold promise as a therapeutic strategy for preventing and treating obesity. For example, a study published in Nature in 2018 found that the use of a protein called BMP8b can increase energy expenditure and reduce adipose tissue mass in mice, suggesting that targeting adipose tissue metabolism may be a promising avenue for the development of obesity treatments[17]. The accumulation of adipose tissue is a critical factor in the development of obesity. Further research is needed to better understand the complex interplay between adipose tissue and obesity development, and to develop effective strategies for preventing and treating obesity-related diseases.

1.2 Microfluidics

Microfluidics is a rapidly evolving field that focuses on manipulating small volumes of fluids in channels or chambers with dimensions in the range of micrometers. It has applications in various fields such as chemical synthesis, biotechnology, drug discovery, and microfabrication. Microfluidic devices offer several advantages over conventional devices, such as reduced sample volumes, increased throughput, enhanced reaction control, and reduced costs.

One area of microfluidics research that has gained significant attention is the development of microfluidic platforms for biomedical applications, particularly in disease diagnosis and drug discovery. For example, microfluidic systems have been used to isolate and analyze circulating tumor cells (CTCs) from blood samples for cancer diagnosis[18]. In another study, a microfluidic chip was developed to perform high-throughput screening of drug candidates for treating tuberculosis[19]. Microfluidics has also been applied in neuroscience research, particularly in the study of the behavior of neurons and synapses. For instance, a microfluidic device was developed to study the effects of drug treatments on synaptic activity in cultured neurons[20]. The device allowed for the continuous perfusion of different drugs while monitoring synaptic activity in real-time.

Moreover, microfluidic devices have been used for environmental monitoring and analysis. In a study, a microfluidic chip was developed for the detection of waterborne pathogens, such as E. coli, using an electrochemical sensor[21]. The chip was able to detect E. coli in water samples with a high degree of accuracy and sensitivity. Microfluidics is a rapidly advancing field with various applications in diverse areas such as biomedical research, drug discovery, neuroscience, and environmental monitoring. The development of microfluidic devices has enabled researchers to perform experiments with greater precision, accuracy, and efficiency.

1.2.1 Fundamentals and Applications of Microfluidics

Microfluidics is a field that deals with the manipulation of small volumes of fluids in microscale channels or chambers. It has gained significant attention in recent years due to its potential applications in various fields such as chemical synthesis, biotechnology, and biomedical research. Microfluidic devices offer several advantages over conventional devices, such as enhanced reaction control, reduced sample volumes, increased throughput, and reduced costs. The fundamental principles of microfluidics are based on the behavior of fluids at the microscale. At this scale, the properties of fluids differ significantly from those observed in bulk, due to the dominance of surface forces and viscous forces over inertial forces. The physics of microfluidics is characterized by low Reynolds numbers, which result in laminar flow and reduced turbulence. Microfluidic devices are typically fabricated using microfabrication techniques such as photolithography and soft lithography. The channels and chambers in microfluidic devices are typically made from materials such as silicon, glass, or polymers.

Microfluidics has several applications in various fields, including biomedical research, drug discovery, and environmental monitoring. For example, microfluidic devices have been used to study cell behavior, such as migration and differentiation, and to develop organ-on-a-chip systems for drug screening[22]. In another study, a microfluidic platform was used to study the effect of shear stress on the growth and differentiation of stem cells[23]. Moreover, microfluidic devices have been applied in chemical synthesis and analysis, such as the development of microreactors for organic synthesis[24].

Microfluidics is a rapidly growing field with a wide range of applications in various fields such as biomedical research, drug discovery, and environmental monitoring. The fundamental

principles of microfluidics, coupled with the ability to fabricate complex devices, enable researchers to perform experiments with greater precision, accuracy, and efficiency.

1.2.2 Design and Fabrication of Microfluidic Devices for Lab-on-a-Chip Applications

The design and fabrication of microfluidic devices for lab-on-a-chip applications has become an increasingly important area of research in recent years. These devices offer several advantages over traditional laboratory techniques, including reduced sample volumes, increased automation, and improved sensitivity and specificity. Microfluidic devices have been developed for a variety of applications, including point-of-care diagnostics, drug discovery, and environmental monitoring. The design of microfluidic devices for lab-on-a-chip applications involves several key considerations, including the selection of appropriate materials, channel and chamber geometry, and flow control mechanisms. Materials used in microfluidic devices should be biocompatible, transparent, and have low autofluorescence to minimize interference with experimental measurements[25]. Channel and chamber geometry can be optimized to improve mixing, reduce sample volumes, and increase sensitivity[26]. Flow control mechanisms, such as pneumatic or electrokinetic pumping, can be used to precisely manipulate fluids within the device[27].

Fabrication of microfluidic devices typically involves microfabrication techniques such as photolithography, soft lithography, or injection molding. These techniques allow for precise control over device geometry and the creation of complex fluidic architectures[28]. In addition, 3D printing has emerged as a promising approach for the rapid prototyping of microfluidic devices[29]. Empirical research has demonstrated the utility of microfluidic devices for lab-on-a-chip applications. For example, microfluidic devices have been developed for point-of-care diagnostics

of infectious diseases, such as HIV and malaria[30]. In another study, a microfluidic device was developed for the high-throughput screening of drug candidates for the treatment of cancer[31]. Microfluidic devices have also been used for environmental monitoring, such as the detection of heavy metals in water samples[32].The design and fabrication of microfluidic devices for lab-on-a-chip applications has become a critical area of research in recent years. These devices offer several advantages over traditional laboratory techniques and have been developed for a variety of applications. Advances in microfabrication techniques, such as 3D printing, are expected to continue to drive the development of new and innovative microfluidic devices.

1.2.3 Fluid Dynamics in Microchannels: Modeling and Simulation Techniques

Fluid dynamics in microchannels is a complex and important topic in the field of microfluidics. Microchannels are channels with dimensions on the order of micrometers, where fluid flow is dominated by viscous forces rather than inertial forces. Modeling and simulation techniques are essential for understanding and predicting fluid behavior in microchannels, as experimental characterization can be challenging due to the small length scales and high surface area-to-volume ratios.

One important aspect of fluid dynamics in microchannels is the study of flow regimes. Microfluidic flow can be classified into laminar, transitional, or turbulent regimes, depending on the Reynolds number, which is a dimensionless number that relates the inertial forces to the viscous forces in the fluid. In microchannels, laminar flow is the most common regime due to the low Reynolds numbers typically encountered[26].

Modeling and simulation techniques can be used to predict flow behavior in microchannels. Numerical simulations, such as finite element or finite difference methods, can be used to solve

the Navier-Stokes equations, which describe the motion of a fluid. These simulations can provide detailed information on fluid velocity, pressure, and shear stress distributions within microchannels[33]. Empirical research has demonstrated the utility of modeling and simulation techniques for understanding fluid dynamics in microchannels. For example, a study used numerical simulations to investigate the effect of channel geometry on the flow behavior of a microchannel with a T-junction. The simulations showed that varying the angle of the T-junction had a significant effect on the flow behavior, with a 90-degree angle producing the most uniform flow[34].

Fluid dynamics in microchannels is a complex and important topic in the field of microfluidics. Modeling and simulation techniques are essential for understanding and predicting fluid behavior in microchannels, and empirical research has demonstrated the utility of these techniques for investigating the effect of various parameters on fluid flow behavior. Advances in modeling and simulation techniques are expected to continue to drive the development of new and innovative microfluidic devices.

1.2.4 Biomedical Applications of Microfluidics: Diagnostics, Drug Delivery, and Tissue Engineering

Microfluidics has emerged as a revolutionary technology with a wide range of biomedical applications, spanning diagnostics, drug delivery, and tissue engineering. This field focuses on manipulating fluids at the microliter or nanoliter scale within microchannels, allowing for precise control over fluid behavior. Biomedical researchers have harnessed this technology to develop innovative solutions that address various challenges in healthcare. In diagnostics, microfluidic platforms offer rapid and cost-effective solutions for detecting diseases and pathogens. These devices integrate complex biochemical assays into compact and portable systems, enabling point-

of-care testing with minimal sample volumes. For instance, the work of Martinez et al. demonstrated a paper-based microfluidic device that enabled colorimetric detection of biomarkers associated with diseases such as malaria and HIV[35]. This approach significantly streamlined diagnostic processes, particularly in resource-limited settings.

Furthermore, microfluidics plays a pivotal role in enhancing drug delivery methods. Traditional drug administration can be imprecise and result in unwanted side effects. Microfluidic devices offer the ability to tailor drug release profiles by precisely controlling fluid flow rates and drug concentrations. Research by Kim et al. showcased a microfluidic chip capable of producing monodisperse drug-loaded microspheres for sustained and controlled drug delivery[36]. Such systems improve therapeutic outcomes by ensuring the right dose reaches the target site at the right time. Tissue engineering is yet another domain benefiting from microfluidics. Creating functional tissues in the lab involves precise control over cell microenvironments and nutrient delivery. Microfluidic platforms enable the design of intricate culture systems that mimic in vivo conditions. For instance, a study by Huh et al. demonstrated a lung-on-a-chip device that recapitulated the mechanical and biochemical cues of human lung tissue, enabling real-time drug testing and disease modeling[37].

Microfluidics has ushered in a new era of biomedical innovation, offering unprecedented opportunities for diagnostics, drug delivery, and tissue engineering. By providing precise control over fluid behavior at the microscale, this technology empowers researchers and clinicians to develop more efficient, accurate, and personalized healthcare solutions.

1.2.5 Emerging Trends in Microfluidics: From Single-Cell Analysis to Organ-on-a-Chip Technologies

Microfluidics has rapidly advanced in recent years, leading to the emergence of new trends and applications. One such trend is the focus on single-cell analysis, which enables the characterization of individual cells in complex biological systems. Another trend is the development of organ-on-a-chip technologies, which aim to recreate the structure and function of human organs in vitro. These emerging trends in microfluidics have the potential to revolutionize a range of fields, from drug discovery to personalized medicine.

Single-Cell Analysis: Microfluidic devices have been increasingly used for single-cell analysis due to their ability to precisely manipulate small volumes of fluids. For example, microfluidic devices can be used to isolate and lyse individual cells, enabling the analysis of their genomic, transcriptomic, and proteomic profiles[38]. Furthermore, microfluidic devices can be used to study cell-cell interactions and signaling events, providing insights into the complex biology of multicellular systems[39].

Organ-on-a-Chip: Organ-on-a-chip technologies are an emerging application of microfluidics that aim to mimic the structure and function of human organs in vitro. These devices consist of microfluidic channels lined with cells, which can be used to model the physiology of specific organs or tissues[37]. Organ-on-a-chip devices have the potential to revolutionize drug discovery and toxicology testing by enabling the testing of new drugs and therapies in a more physiologically relevant context[40]. Additionally, these devices can be used to study disease mechanisms and develop personalized medicine approaches.

Empirical research has demonstrated the utility of microfluidics in these emerging trends. For example, a study used a microfluidic device to isolate and analyze the transcriptomic profiles of

individual cells from breast cancer patients, providing insights into the heterogeneity of cancer cells and potential therapeutic targets[41]. Another study used an organ-on-a-chip device to model the blood-brain barrier, demonstrating the potential of this technology for drug discovery and delivery applications. Emerging trends in microfluidics, such as single-cell analysis and organ-on-a-chip technologies, have the potential to revolutionize a range of fields, from basic research to drug discovery and personalized medicine. Empirical research has demonstrated the utility of microfluidics in these areas, and ongoing advancements are expected to lead to new and innovative applications.

1.3 Droplet Microfluidics

Droplet microfluidics is a rapidly growing field that utilizes small droplets of fluid to perform a range of chemical and biological assays. This technology has enabled high-throughput experimentation and has found numerous applications in biology, chemistry, and materials science. Droplet microfluidics has several advantages over traditional microfluidics, including better control over reagent delivery, reduced sample volumes, and high throughput.

Empirical research has demonstrated the versatility of droplet microfluidics. For example, a study utilized droplet microfluidics to perform high-throughput screening of bacterial cells for antibiotic resistance[42]. The study found that the use of droplet microfluidics improved the screening efficiency and reduced the number of reagents required compared to traditional screening methods. Another study used droplet microfluidics to perform single-cell sequencing of cancer cells, providing insights into the heterogeneity of cancer cells and potential therapeutic targets[43]. Droplet microfluidics has also found applications in materials science. For instance, droplet microfluidics has been utilized to synthesize polymer particles with controlled size and morphology[44]. This

technique has the potential to improve the design and performance of drug delivery vehicles and other materials.

Additionally, droplet microfluidics has been used in the development of point-of-care diagnostic devices. Droplet microfluidics is a rapidly growing field that has found numerous applications in biology, chemistry, and materials science. Empirical research has demonstrated the versatility and potential of this technology, including high-throughput screening, single-cell analysis, materials synthesis, and diagnostic applications.

1.3.1 Design and Fabrication of Droplet Microfluidic Devices

Droplet microfluidics is a rapidly growing field with numerous applications in biology, chemistry, and materials science. The design and fabrication of droplet microfluidic devices is critical to achieving precise and reliable droplet generation, manipulation, and analysis. This requires the use of microfabrication techniques and specialized materials to create microfluidic channels with the necessary properties, such as hydrophobicity or hydrophilicity, to control droplet behavior.

Empirical research has demonstrated the importance of device design and fabrication in achieving reliable and efficient droplet microfluidics. For example, one study explored the design and optimization of a droplet-based microfluidic system for high-throughput single-cell analysis[45]. The researchers used computer simulations and experimental testing to optimize the device design for efficient droplet generation, manipulation, and analysis. The resulting device achieved high-throughput analysis of thousands of individual cells in a single experiment, demonstrating the importance of device design in achieving efficient droplet microfluidics. Another study focused on the fabrication of droplet microfluidic devices using soft lithography techniques[46]. The researchers explored the effects of various fabrication parameters, such as mold surface energy

and curing time, on the properties of the resulting microfluidic channels. They found that careful control of these parameters was critical to achieving uniform and reliable droplet generation and manipulation.

In addition to device design and fabrication, the choice of materials is also critical in droplet microfluidics. For instance, a study demonstrated the use of biocompatible materials for droplet microfluidic devices to perform high-throughput screening of bacterial cells for antibiotic resistance[42]. The use of biocompatible materials improved the compatibility of the device with biological samples and reduced the potential for contamination, highlighting the importance of material selection in droplet microfluidics.

The design and fabrication of droplet microfluidic devices are critical to achieving precise and reliable droplet generation, manipulation, and analysis. Empirical research has demonstrated the importance of careful optimization of device design and fabrication parameters, as well as the choice of materials, in achieving efficient droplet microfluidics.

1.3.2 Droplet Generation and Manipulation Techniques in Microfluidics

Droplet generation and manipulation are critical processes in droplet microfluidics, enabling precise control over droplet size, composition, and behavior. A variety of techniques have been developed for droplet generation and manipulation in microfluidic devices, each with their own advantages and limitations. Empirical research has been conducted to optimize these techniques and improve their reliability and efficiency.

One common technique for droplet generation is flow-focusing, where two immiscible fluids are forced to flow through a small channel, resulting in the formation of droplets at the channel outlet[47]. Research has been conducted to optimize flow-focusing for droplet generation in various applications, such as high-throughput cell analysis and drug discovery[42, 48]. For example,

one study explored the use of flow-focusing to generate uniform droplets containing mammalian cells for high-throughput drug screening[42]. The researchers optimized the flow rates and channel dimensions to achieve reliable and consistent droplet generation, highlighting the importance of careful optimization of this technique. Another technique for droplet generation is the use of microfluidic T-junctions, where two fluids are brought together at a T-shaped junction to form droplets[49]. Research has demonstrated the use of T-junctions for droplet generation in applications such as single-cell analysis and emulsion polymerization[50]. For instance, one study used a microfluidic T-junction to generate droplets containing single bacterial cells for high-throughput screening of antibiotic resistance[50]. The researchers optimized the T-junction dimensions and flow rates to achieve uniform droplet generation and efficient cell encapsulation.

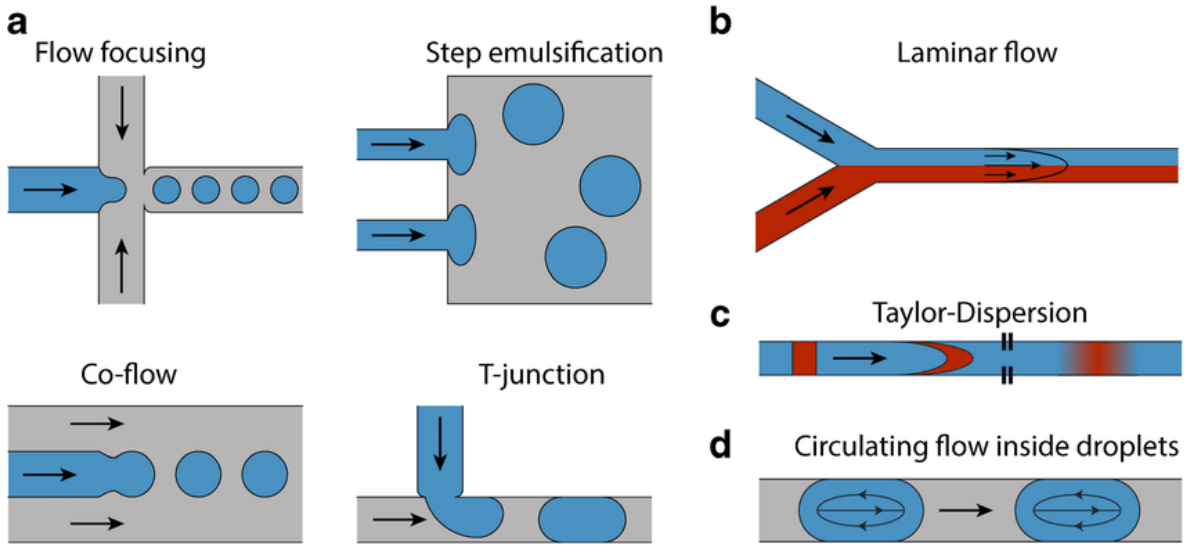

Figure 1. 2 Droplet generation modes. In a, the four most popular droplet generator geometries, namely flow focusing, step emulsification, co-flow, and T-junction are shown. b In pressure-driven continuous flows, a parabolic flow profile across the channel and laminar flow are observed. Adapted from Ref.[51] with permission from the Springer article, Copyright © 2019, Springer-Verlag GmbH Germany, part of Springer Nature.

Droplet manipulation techniques include methods for merging, splitting, and sorting droplets based on their properties. One common technique for droplet merging is the use of passive microfluidic structures, such as Y-junctions or H-junctions, where droplets are brought together through laminar flow[52]. Research has explored the use of passive droplet merging for various applications, such as the synthesis of complex particles and emulsions[24, 53]. For example, one study demonstrated the use of a passive microfluidic mixer for the synthesis of Janus particles, which have different properties on each side[53]. The researchers optimized the mixer design to achieve efficient droplet merging and uniform particle synthesis. Another droplet manipulation technique is the use of droplet sorting based on their properties, such as size, composition, or fluorescence[54]. Research has demonstrated the use of various sorting techniques, such as droplet electrophoresis and droplet dielectrophoresis, for applications such as cell sorting and drug screening[55]. For instance, one study used droplet dielectrophoresis to sort droplets containing different types of cells based on their electrical properties[55]. The researchers optimized the sorting conditions to achieve high efficiency and purity of sorted droplets.

Droplet generation and manipulation techniques are critical to achieving precise and reliable droplet microfluidics. Empirical research has demonstrated the importance of careful optimization of these techniques for various applications, highlighting the potential of droplet microfluidics for a wide range of fields.

1.3.3 Quantification of Analytes in Droplet Microfluidics

Droplet microfluidics has emerged as a powerful platform for high-throughput analysis of analytes in small volumes, such as single cells or molecules. Quantification of analytes in droplet microfluidics typically involves measuring the fluorescence or absorbance of droplets containing

the analyte of interest. Empirical research has been conducted to optimize and improve the accuracy and sensitivity of these measurements.

One common technique for quantification in droplet microfluidics is fluorescence detection, where a fluorescent label is attached to the analyte of interest and detected using a fluorescence microscope or flow cytometer[25]. Research has been conducted to optimize the sensitivity and accuracy of fluorescence detection in droplet microfluidics. For example, one study developed a microfluidic device for single-cell RNA sequencing, where fluorescence detection was used to quantify the amount of RNA in each droplet[56]. The researchers optimized the fluorescence detection conditions, including the excitation and emission wavelengths and exposure time, to achieve high sensitivity and accuracy. Another technique for quantification in droplet microfluidics is absorbance detection, where the optical density of droplets containing the analyte of interest is measured using a spectrophotometer[57]. For example, one study developed a microfluidic device for neurotransmitter detection, where electrochemical detection was used to quantify dopamine and norepinephrine in single cells[58]. The researchers optimized the device design and measurement conditions to achieve high sensitivity and selectivity.

The quantification of analytes in droplet microfluidics is a powerful tool for high-throughput analysis in various fields, such as genomics, proteomics, and metabolomics. Empirical research has demonstrated the importance of careful optimization of detection techniques and measurement conditions for achieving high sensitivity, accuracy, and reliability.

1.4 Tissue Engineering and Analysis in Droplet Microfluidics

1.4.1 Introduction

In this section, we will provide an extensive overview of systems that integrate tissue engineering with droplet microfluidics. This comprehensive review will encompass five key areas: cell and tissue cultivation, small-scale bioanalysis, existing practical applications, the obstacles faced, and prospects for the future. To start, this introductory section will offer a brief explanation of traditional tissue engineering and microscale tissue engineering, as well as the incorporation of tissue engineering into the realm of microfluidics. As we conclude this chapter, we will delve into the potentially groundbreaking uses of tissue engineering within the context of droplet-based microfluidic systems.

1.4.2 Tissue Engineering

Millions of solid organ transplantations are performed globally every year, yet a significant number of patients succumb to the extended waiting period to secure compatible donor organs[59]. Additionally, the persistent threats of chronic rejection and immune system-mediated organ damage present formidable challenges in the field of organ transplantation. These pressing concerns have driven the emergence of tissue engineering as an innovative solution. Current technology offers the possibility of implanting engineered biological substitutes or utilizing ex-vivo perfusion systems as viable alternatives to traditional organ transplantation[60]. Tissue engineering, by definition, revolves around the creation of new, fully functional living tissues. This process combines living cells, device engineering, novel materials, biochemical agents, and physicochemical techniques[61] to fabricate tissues. The core elements of this technology are living cells or tissues, often considered the "heart" around which devices and systems are meticulously engineered. These cells are derived from either fluid or solid tissues and are typically categorized into seven groups based on their sources: autologous cells, allogeneic cells, xenogenic cells, syngeneic/isogenic cells, primary cells, secondary cells, or stem cells.

To replicate the extracellular environment of native tissue and facilitate in vitro cell growth, scaffolds are frequently synthesized and play an indispensable role in tissue engineering. These scaffolds provide cells with three-dimensional (3D) structures necessary for tissue formation and favorable cellular interactions[62]. Specific requirements are essential for these scaffolds to effectively reconstruct tissues in vitro. Firstly, they must feature interconnected pores with adequate sizes to support cell integration and vascularization[63]. Furthermore, biocompatibility is a crucial factor to prevent undesirable tissue responses to implants, while biodegradability ensures that scaffolds are absorbed by surrounding tissues, obviating the need for surgical removal and promoting new tissue formation[64]. In selecting scaffold materials, various factors come into play, including material chemistry, polymer molecular weight, surface properties, structure, shape, degradation characteristics, and water absorption. These materials must also interact with cells in a manner that fosters cellular attachment, growth, and the development of new tissue[65]. Over the past decades, extensive research has explored a plethora of materials, encompassing natural substances like polysaccharides, polypeptides, and proteins, synthetic materials such as polyglycolic acid (PGA), polylactic acid (PLA), and poly-ε-caprolactone (PCL), as well as biomaterials like hydroxyapatite (HA) and tricalcium phosphate (TCP), for their potential in tissue engineering[66]. Moreover, a wide array of methodologies has been developed to create porous scaffolds for use in tissue engineering, including techniques like nanofiber self-assembly, textile technologies, solvent casting, particulate leaching, gas foaming, emulsification, freeze-drying, thermally-induced phase separation, electrospinning[67, 68] or blow spinning[69], CAD/CAM technologies, and laser-assisted bioprinting[70]. To address the challenges of oxygen and nutrient delivery (mass transport) in tissue engineering, various assembly methods have been explored. These methods encompass self-assembly, liquid-based template assembly, additive

manufacturing, and scaffolding. Additionally, the field of tissue engineering incorporates other critical aspects, such as tissue culture, the development of interconnected cellular and tissue networks, as well as on-chip or off-chip analyses.

1.4.3 Microscale Tissue Engineering

While tissue engineering presents significant advantages, it is accompanied by several formidable challenges that require attention, such as the creation of vascular networks and the accurate replication of authentic tissue functions[71]. The uninterrupted supply of oxygen and nutrients to cells, as well as the efficient removal of waste and carbon dioxide through blood vessels, are fundamental to cellular survival within the body[72]. While certain tissues, like skin, cartilage, or the cornea, can rely on diffusion from distant blood vessels to facilitate oxygen and nutrient delivery, the majority of body tissues necessitate the presence of well-developed blood vessel systems situated less than 200 μm away from the tissue[73]. Therefore, establishing an effective blood vessel system, whether through actual vascularization or suitable mimics, is a critical aspect of tissue engineering. One approach for achieving vascularization is by enhancing angiogenesis within tissue scaffolds through the introduction of endothelial cells (ECs) capable of releasing growth factors to stimulate blood vessel formation. However, a drawback to this strategy lies in its lack of precise control, potentially leading to growth instabilities that raise the risk of failure. The timing of vascularization or re-vascularization also presents a challenge, as cells may lose viability before proper vessels can form. Alternatively, there is the option of synthetically producing vascularized scaffolds before implanting cells, a method made feasible through the use of various biological and synthetic materials and fabrication technologies.

Another major challenge revolves around ensuring the proper functioning of cells or tissues post-implantation. As scientists strive for improved standardization and reproducibility of engineered tissues, they have unearthed various unique issues[74-76]. It is well-understood that cell-to-cell contact and tissue architecture significantly influence cell behavior. On a microscopic level, the entire scaffold provides the boundaries for cell self-assembly, a crucial step in facilitating interactions and communication between cells to form functional tissue. Yet, achieving uniform cell seeding throughout the scaffold is difficult, given the rapid attachment and proliferation of cells on the scaffold periphery, which hinders other cells from penetrating to the core[77]. While traditional perfusion systems can address this challenge of low seeding efficiency by altering culture conditions, these techniques have inherent limitations within in vitro systems[78]. Therefore, the development of optimized scaffolds that facilitate both cell and nutrient flow to the center of their architecture is essential.

In recent years, microtechnology has emerged as an effective platform for addressing these challenges in the biomedical and biological fields. Particularly, the application of soft lithography in fabricating microfluidics has seamlessly merged the realms of tissue engineering and microscale technology. Microfluidic cell and tissue culture systems have exhibited tremendous potential in addressing the aforementioned issues[63]. Firstly, the scale of microtechnology aligns well with that of living tissues, providing a substantial surface-to-volume ratio for efficient nutrient and cell delivery without necessitating complete vascular systems. For instance, typical mammalian cell diameters range from 8 to 30 μm, closely matching the common sizes of microfluidic channels, which range from 10 to 200 μm[79]. Secondly, polydimethylsiloxane (PDMS), a commonly used substrate in the fabrication of microfluidic devices, boasts numerous advantages when used as the bulk material for engineered tissues. PDMS is cost-effective, optically transparent, gas-permeable,

non-toxic, biocompatible, and deformable. Therefore, microfluidic devices can provide cells with the required nutrients and oxygen through straightforward or specially designed networks of channels and reservoirs. Thirdly, the application of various physiological stimuli to tissues and the monitoring or sampling of their responses can be achieved with exceptional precision, accuracy, and resolution using microfluidics, surpassing traditional methods. Furthermore, the potential for scaling up to complex and powerful micro-bioreactors has enabled researchers to reach ambitious objectives, such as organs-on-chips, which have already made a significant impact on biomedical and clinical applications. In recent years, numerous studies have explored the convergence of tissue engineering and microfluidics[80-90], and we will delve into these studies in the context of droplet-based microfluidics in this chapter. Several recent examples of microscale tissue engineering are depicted in **Figure 1.4.1**[83, 91-93]

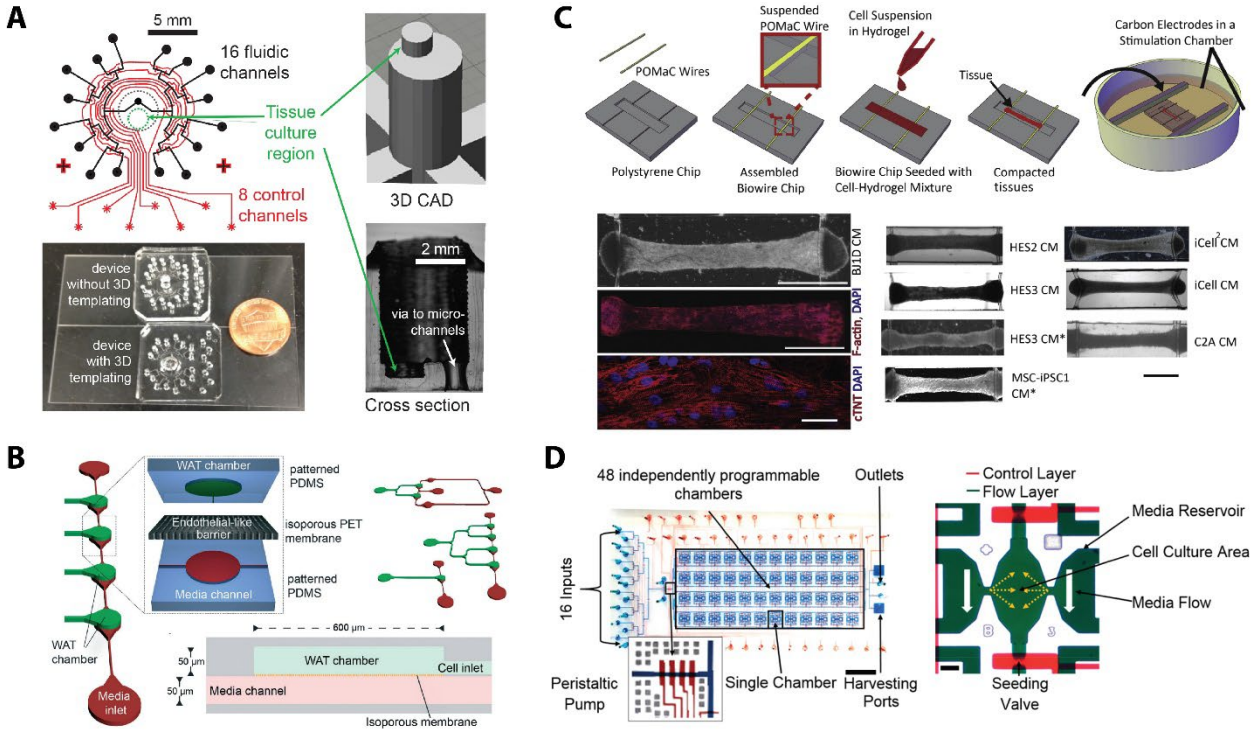

Figure 1.4. 1 Engineered tissue at the microscale. (A) A fully automated, 16-channel microfluidic input/output multiplexer (µMUX) for endocrine tissue culture and secretion sampling. Adapted

from Ref. [83] with permission from the Royal Society of Chemistry, Copyright 2017. (B) Integration of a physiologically relevant microfluidic system for modelling of white adipose tissue (WAT-on-a-chip). Adapted from Ref. [92] with permission from the Royal Society of Chemistry, Copyright 2017. (C) Biowire II platform for generation of chamber-specific cardiac tissues. Adapted from Ref. [93] with permission from Elsevier, Copyright 2019. (D) Microfluidic system for dynamic stimulation and tracking of single cells. Adapted from Ref. [91] with permission from the American Chemical Society, Copyright 2018.

1.4.4 Analysis of Tissues at the Microscale

As tissue engineering scales down to smaller dimensions, the need for analytical and bioanalytical methods suitable for this reduced scale becomes evident. Two primary strategies are employed for analyzing micro-engineered tissues: off-chip analysis and on-chip (integrated) analysis. Conventional off-line analysis methods are still predominantly used to examine samples from microfluidic devices, mainly because many of these methods have not been effectively or economically integrated on-chip. Certain widely accepted techniques only become quantitative or usable after undergoing multiple-step processes such as mixing, incubation, purification, heating, or amplification, among others. Additionally, some analytes necessitate sophisticated instrumentation like mass spectrometers, PCR instruments, plate readers, or methods like genomic sequencing, gel electrophoresis, and immunoassays[83, 88, 90]. While off-chip methods continue to be the standard, numerous challenges remain. Compared to common end-point measurements, dynamic monitoring offers greater accuracy and significance in tissue detection and medical diagnosis. Nevertheless, off-chip sampling analysis tends to compromise temporal resolution, limiting our ability to comprehend the dynamic activities of cells and tissues in vivo. The sample volumes collected from on-chip tissues can be exceedingly small and often do not meet the lowest detection volume requirements of certain instruments. Furthermore, the process of sample

collection and handling can lead to contamination or even the inactivation of the targeted analytes. In contrast, traditional methodologies usually demand more time, human resources, and costs compared to equivalent on-chip methods[94].

Direct on-chip measurement proves to be a more convenient and efficient approach for sample analysis compared to off-chip methods. The inherently small sizes of microfluidic channels, chambers, or reservoirs can provide robust platforms for quantifying targets with minimal volumes, minimizing dilution from cell or tissue samples. Conducting all sampling, reaction, and detection processes on-chip reduces the risk of human errors and contamination while minimizing waste generated by manual operations and transportation. Droplet-based microfluidics, which is the focus of this chapter, can enhance the temporal resolution of tissue sampling and detection[84, 95, 96], aligning with the need for dynamic measurements. Nonetheless, there are certain constraints associated with integrated on-chip analysis. Firstly, the application of heterogeneous assays is limited on microchips because additional steps involving mixing, washing, and purification are more challenging to achieve on-chip. For more convenient mix-and-read homogeneous assays[84], addressing the requirements for mixing multiple reactants and/or extended incubation times remains a significant challenge for on-chip applications. Secondly, the hydrophobic properties of PDMS can lead to the adsorption of chemical or biological assay reagents unless effective coating procedures are implemented and maintained.

To address these challenges in on-chip analyses, several techniques have been introduced in recent years. To facilitate complex or multi-step biochemical reactions within a microfluidic device, on-chip manipulations like mixing, sorting, and washing are sometimes necessary. Techniques such as electric fields, magnetic fields, and surface acoustic waves have been applied to enhance the flexibility of microfluidic devices by various research groups[97-102]. Similarly, Our

group has also employed on-chip valves to automate processes involving cell and tissue sampling, mixing, droplet formation, reaction, and detection[84, 96]. Pioneering work by the Ramsey and Kennedy groups integrates microfluidics with mass spectrometry, allowing assays to function within the microdevice platform before directly transferring products into mass spectrometers for high-performance detection and identification[88, 103, 104]. Another popular approach used by the Roper and Kennedy groups couples microfluidic chips with capillary electrophoresis to achieve integrated separation and detection on-chip[105, 106]. Given that on-chip integrated techniques should be compatible with ultra-small volumes, low analyte concentrations, or both, optical detection presents an appealing and relatively straightforward choice. While the small dimensions of microfluidic channels often render optical absorbance detection impractical for most analytes due to the limited optical path lengths, highly sensitive detection via fluorescence excitation and emission is less constrained by small channels. Consequently, fluorescence, detectable with a standard fluorescence microscope or a custom optical system, is the most commonly used analytical readout for on-chip detection, although it necessitates the use of fluorophore-labeled reagents.

1.4.5 Use of Droplet Microfluidics in Engineering and Analysis of Tissue

In conventional biochemical assays, tubes or well-plates are the predominant tools for assessing secretions from cells or tissues. However, these tube- or well-based sampling methods demand a substantial quantity of tissues or cells and often yield information that significantly deviates from in vivo conditions. The dynamic behaviors of cells tend to be lost due to diffusion and dispersion effects, depriving researchers of vital insights into the target tissues. Since the early days of technology, microfluidics has been recognized as a valuable and highly efficient instrument for

the analysis and manipulation of tissues. Over time, numerous research groups have harnessed continuously flowing fluidics to combine tissue perfusion and culture with downstream analyses. For instance, rapid-injection electrophoretic immunoassays have enabled in vivo tissue culture and stimulation, along with continuous monitoring of cellular activity[107, 108]. While there are some limitations to these systems, such as the complexity of flow control and electrophoresis setup or the temporal resolution loss during tissue sampling dispersion, these studies have unequivocally demonstrated that microfluidic systems possess a unique capability for the temporal investigation of cells[84].

In recent decades, droplet microfluidics has emerged as an enticing platform for exploring cellular biology. Within a typical droplet-based microfluidic device, monodisperse droplets exhibit diameters ranging from nanometers to micrometers, offering several significant advantages to researchers. Firstly, each droplet serves as an isolated and well-protected unit for assays and reactions, which can be individually manipulated for operations like delivery, mixing, sorting, or analysis[109]. Secondly, ultra-small volume reactions (~femtoliters to nanoliters) can take place within these droplets, resulting in substantial savings on experimental reagents and enabling unique analyses on single cells or even single molecules[110, 111]. Thirdly, compared to traditional reaction scales, droplet reactors facilitate faster reaction times due to reduced mass transfer times over very short diffusional distances. Furthermore, generating high-throughput monodisperse droplets (often at kHz frequencies) that are nearly identical empowers scientists to investigate biological systems and generate data sets on a larger scale than previously achievable[49]. Over the past years, droplet microfluidics has empowered numerous biological and clinical applications, including single-cell genome sequencing analysis[112], protein and nucleic acid quantification[113-115], and cellular secretion detection[116].

As discussed in this review, droplet microfluidics exhibits remarkable potential for both analytical and preparative purposes in the field of tissue engineering. For instance, in cellular secretion sampling, the temporal record of secretory events can be preserved with high resolution and reconstructed after encapsulated samples in droplets are measured. In contrast to continuous flow systems where longitudinal broadening limits resolution, temporal chemical and biological information can be retained by digitizing the analog secretion signal with a droplet-based microfluidic system[84, 95, 117]. Droplet microfluidics also garners significant attention for its precision in single-cell analysis, revealing inaccuracies that arise from averaging behaviors across entire cell populations[118]. Encapsulating single cells in individual droplets enables the sorting and cultivation of specific cells from large populations for various downstream purposes[116, 119], such as accumulating and quantifying metabolites or even mapping the genetics of single cells[120, 121]. Furthermore, this relatively straightforward method of generating numerous individual droplets permits the examination of phenotypic and genetic variabilities at the single-cell level on an ultra-high-throughput scale[122]. Furthermore, this relatively straightforward method of generating numerous individual droplets permits the examination of phenotypic and genetic variabilities at the single-cell level on an ultra-high-throughput scale.

1.4.6 Cell and Tissue Culture

One primary purpose of cell and tissue culture involves the isolation of distinct components from the entire organism, creating experimentally controlled environments for study. For example, by extracting tissue from an organism, it becomes possible to sustain its vitality within a precisely regulated synthetic medium, thus maintaining tissue functionality for extended periods conducive to tissue engineering or analysis. The requirement for standardized nutrients, salts, and biological

media like serum has been well-established. These techniques originated from early ex vivo investigations involving whole organs or tissue fragments maintained in vitro for varying durations [123]. While the fundamental methods have been in use for many years, novel concepts persistently emerge, including spheroid systems and microfluidic culture systems. A significant number of these innovations revolve around the three-dimensional organization of cells and the creation or synthesis of tissue-specific extracellular matrices[124]. Such research has made substantial contributions to our comprehension of mammalian biology and physiology.

1.4.7 Cell and Tissue Culture Fundamentals

A variety of techniques for culturing cells and tissues were available prior to the onset of the 20th century, many of which were designed to address specific research needs[125]. The primary objective of culturing conditions is to preserve the structure, function, behavior, and biology of cells in vitro. To achieve this, it is essential to employ sterilized equipment and procedures, prepare suitable culture media, perform cell passaging, adequately freeze and store samples, ensure proper recovery of frozen stocks, and typically quantify viable cells[126]. These diverse culture methodologies have ushered in a new era of advancements in various fields, including virology, morphogenesis, cytology, cytochemistry, toxicology, and molecular biology.

Traditionally, two major categories of cultures have existed: primary cultures and cultures of established cell lines. Primary cell and tissue cultures originate from tissues directly obtained from a living organism, in contrast to immortalized cell lines that divide indefinitely. One of the significant advantages of primary cell extraction and culture is that these cells have traversed the various developmental stages of the organism within the ideal in vivo environment. Researchers have developed comprehensive protocols to maintain an in vitro environment post-extraction,

ensuring cell viability over varying durations. Additionally, the availability of knock-out animal models provides a unique opportunity to, for instance, compare cells extracted from a wild-type mammal with those derived from a genetically altered mammal[127]. This methodology also proves invaluable for neurobiological studies, allowing the direct study of brain tissue. When a brain is removed from an animal, it can be sectioned into thin slices using a vibratome and kept alive in slice culture. Alternatively, a brain slice or a specific brain region can be meticulously dissected to create an explant culture. This explant culture can be enzymatically broken down into individual cells, resulting in a dissociated cell culture[127]. It is important to note that primary cells often exhibit significantly different behaviors and morphologies compared to in vitro cultured cell lines[96, 128, 129], and our group has recently shown this to be true for oscillatory function in adipose tissue [96]. As depicted in Figure 1.4.2, primary pancreatic islet tissue constitutes a highly interconnected multicellular system, displaying complex spatiotemporal electrical activity, including full-tissue waves of calcium influx[129]. These robust, coordinated calcium waves are not observed in dish-based cell culture. However, a notable drawback of primary cell culture is the limited lifespan of the tissue in vitro, which significantly contributed to the development of immortalized cell lines.

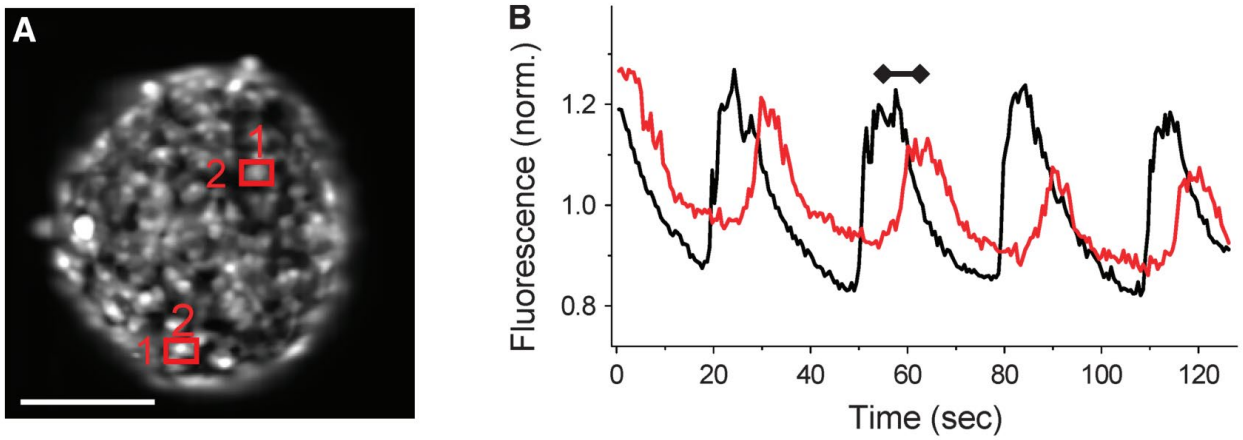

Figure 1.4. 2 Gap junctional coupling in primary pancreatic islet tissue is exemplified by the existence of unique calcium waves. (A) Fluorescence intensity of an islet stained with a calcium

binding dye (Fluo-4) in a microfluidic flow device, with two regions of interest (ROIs) marked. (B) Time course of strong calcium waves is shown from each ROI in part A, with a time delay showing evidence of the propagating wave in the tissue. Scale bar represents 100 μm. Adapted from Ref. [129] with permission from Elsevier, Copyright 2008.

An immortalized cell line represents a permanently established cell culture that enables the systematic examination of gradual changes in the cellular structure, biology, and genetics under well-controlled conditions[130]. This type of cell culture is more or less standardized and does not necessitate extensive coverage within this chapter. Although cell lines may not fully replicate the functionality of in vivo tissues, they are still highly valuable, especially for complex tissues like the pancreas, which comprises various cell types and is challenging to investigate at the single-cell level in vivo[130]. Notably, organ-on-a-chip-based microfluidic systems have recently spurred significant advancements in the utility of cell lines, allowing for more realistic modeling of in vivo organisms even within controlled laboratory settings[131].

1.4.8 Off-Chip Cell and Tissue Culture

In the context of microfluidics, the term "off-chip" cell and tissue culture pertains to the use of conventional culture vessels like flasks, petri dishes, roller bottles, or multi-well plates, rather than microfluidic chips. Off-chip culture methodologies typically necessitate a laminar-flow hood or a biosafety cabinet, in addition to a humidity-controlled incubator equipped with feedback mechanisms for temperature and CO2 regulation. It's noteworthy that even in contemporary biological research, many investigations rely on culturing individual cell types in petri dishes, employing standard culture systems that require manual and periodic media replenishment, usually at intervals ranging from 1 to 7 days[132]. As elaborated further in this chapter, microfluidic systems

have emerged as a conduit bridging the gap between such traditional culture models and those that more closely emulate the true in vivo environment.

1.4.9 On-Chip Cell and Tissue Culture

Looking through the lens of microfluidics, "on-chip" cell and tissue culture represents a rethinking of the conventional cell culture vessel, moving beyond petri dishes towards a physical, chemical, and biological milieu that faithfully emulates in vivo conditions. Researchers have harnessed their insights into chemical, biological, biochemical, engineering, and physical systems to devise microfluidic devices and methodologies for cultivating and investigating cells within more contextually appropriate microenvironments[131, 133]. Through the fusion of microfluidics and cell biology, scientists have not only proposed the construction of entire functional organs from human stem cell lines but have also aimed to intentionally fabricate minimal functional units that replicate tissue and organ-level functions[133]. In one illustrative instance, cells can be precisely positioned using micropatterns of extracellular matrix (ECM) in linear arrangements within a microfluidic chamber, enabling the meticulous measurement of muscle cell bending during contraction to determine cell contraction forces under fluidic conditions[134]. In another case, the Wheeler group capitalized on the automated capabilities of their droplet digital microfluidic (DMF) systems, pioneering a platform that downsizes standard mammalian cell culture techniques to the microscale utilizing droplets[135]. This system effectively supported the growth of mammalian cells, frequently introducing new generations into fresh media. An image of their DMF device, constructed from an array of electrodes for manipulating the discrete fluidic system, is depicted in **Figure 1.4.3**.

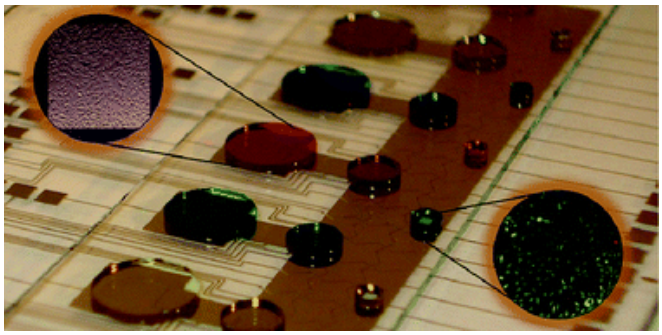

Figure 1.4. 3 Droplet-based digital microfluidics (DMF) was used by the Wheeler group to automate multi-step cell culture at the microscale. Adapted from Ref. [135] with permission from the Royal Society of Chemistry, Copyright 2010.

1.4.10 Organs-on-Chips or Microchip-Based Bioreactors

In the past decade, there has been a notable rise in the development of organ-on-a-chip systems, which has led to substantial research efforts focused on engineering devices for in vitro cell and tissue cultivation. Some experts consider the terms "Organ-on-a-chip" and "Micro-Bioreactor" as interchangeable, as both aim to create finely tailored microfluidic environments that are optimized for specific cell types[136]. These systems are highly regarded as advanced tools in biotechnology and find applications in various domains, including the study of human physiology, drug development, and bioprocess development[131, 137].

One effective approach for outlining the fundamental functional elements essential for designing such systems is through Hubka-Eder mapping[138], which allows for the exploration of how the various integrated functions can be configured[136]. While the specific use and outcomes of these devices may vary, the underlying connections between biological modules tend to exhibit similarities. For instance, configurations may encompass an array of small micro-bioreactors, each equipped with optical sensors at the base, compact artificial liver bioreactors featuring liquid and gas exchange, or small channels incorporating core membranes for measuring transepithelial

electrical resistance (TEER) to study drug diffusion[136]. Additional noteworthy examples come from the work of the Eddington group, who have demonstrated the ability to establish stable oxygen gradients across cells or tissues by capitalizing on diffusion through polydimethylsiloxane (PDMS) membranes[139, 140]. Their systems have been employed to explore hypoxia-induced activation of transcription factors in human endothelial cells[139] (**Figure 1.4.4**) and the impact of hypoxia on encapsulated pancreatic islets from rats and humans[140]. Continuous bioreactor designs can be engineered for the constant replenishment of media and the utilization of feedback control for regulating variables like temperature, pH, and nutrient levels, resulting in the creation of mammalian cell chemostats[141]. Several analogous systems have been developed and reviewed in other sources, but these are beyond the scope of the present study.

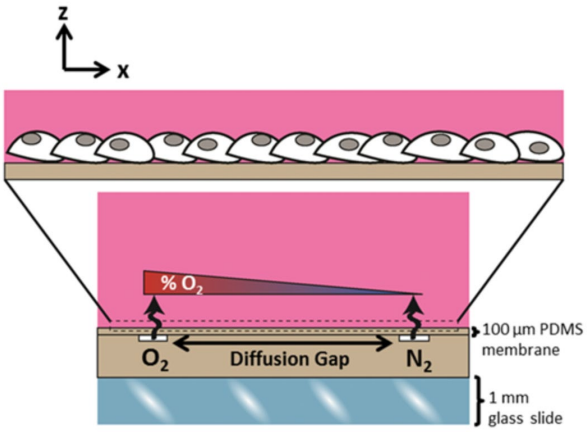

Figure 1.4. 4 The Eddington group has used constant perfusion of compressed oxygen and nitrogen gases into microchannels separated by a diffusion gap, which allows precise control of spatial gradients of oxygen. Hypoxia-induced effects on cell or tissue function can be studied in this way. Adapted from Ref. [139] with permission from the Royal Society of Chemistry, Copyright 2017.

1.4.11 Human Cell Derived Tissues On-Chip

In recent times, microfluidic systems have found application in the culture, processing, and manipulation of stem cells, offering capabilities that encompass trapping, sorting, categorizing, and analyzing these cells[142]. Notably, there have been various approaches to stem cell trapping. For instance, geometry-based methods have utilized polyethylene glycol microstructures to ensnare mouse embryonic stem cells[143]. Similarly, predictable laminar flow, when combined with microfabricated geometric obstacles, has allowed the precise pairing of two different cell types in close proximity, facilitating the fusion of embryonic stem cells[144]. With this approach, defined pairing of two cell types in close proximity was accomplished and used for the fusion of embryonic stem cells[144]. Moreover, microfluidic devices designed for single-cell analysis have incorporated innovative features such as 2048 single-cell traps, which can be efficiently assessed using automated image cytometry[145]. Another notable contribution by Zhang et al.[146] introduced a cell separation device where rigid cells are retained within micro-barriers, while more deformable stem-cell-like cells, including metastatic cancer cells, can pass through the sorting device. Additionally, the utilization of water-in-oil droplets has been employed to encapsulate cells, enabling their long-term culture[147]. Further elaboration on this methodology will be provided in subsequent sections.

1.4.12 Ex-Vivo Tissue Culture On-Chip

Measurements or experiments conducted with tissue removed from an organism, placed in an external environment with minimal alterations to its natural conditions, fall under the category of ex-vivo tissue culture. Ex-vivo studies offer distinct advantages over in-vivo experiments, including the ability to investigate fully developed multi-cellular tissues, organs, or micro-organs in their native in vivo environment before experimentation. To establish an adequate number of

cells for culture and experiments, ex-vivo methods involve surgically extracting living cells or tissues from a living organism, followed by their cultivation in a microdevice under sterile conditions that closely mimic the tissue's natural surroundings. Notably, microfluidic systems featuring continuous perfusion have demonstrated their remarkable utility for ex-vivo tissue experiments in contrast to conventional static culture systems that lack continuous media exchange, especially in the context of extended culture periods[148-150]. In vivo experiments are considerably more technically challenging and are typically incapable of maintaining consistent nutrient, oxygen, or other solution delivery rates due to reliance on environmental and physiological variables like stress, exercise, and diet. Conversely, ex vivo tissue culture can benefit from continuous media perfusion, ensuring a steady composition of media and consistent provision of nutrients while facilitating waste removal[148, 151].

Recently Xiao et al.[149] introduced a device composed of interconnected modular culture chambers. In this system, tissue explants were linked via microfluidic channels and electromagnetically actuated micropumps to drive media flow and physiological hormones. This innovative setup (illustrated in Figure 1.4.5) enabled the sequential co-culture of ovary, fallopian tube, uterus, cervix, and liver explant tissues, fostering hormonal and cellular communication between the tissue chambers. Of significance, murine ovarian follicles were shown to produce the hormone profile of the human 28-day menstrual cycle, successfully influencing the dynamics of the human female reproductive tract and peripheral tissues. Such ex-vivo culture systems exemplify the immense potential of microfluidics in extending culture durations, enhancing viability, and improving the functionality of complex tissue and organ modules while advancing our comprehension of physiological systems.

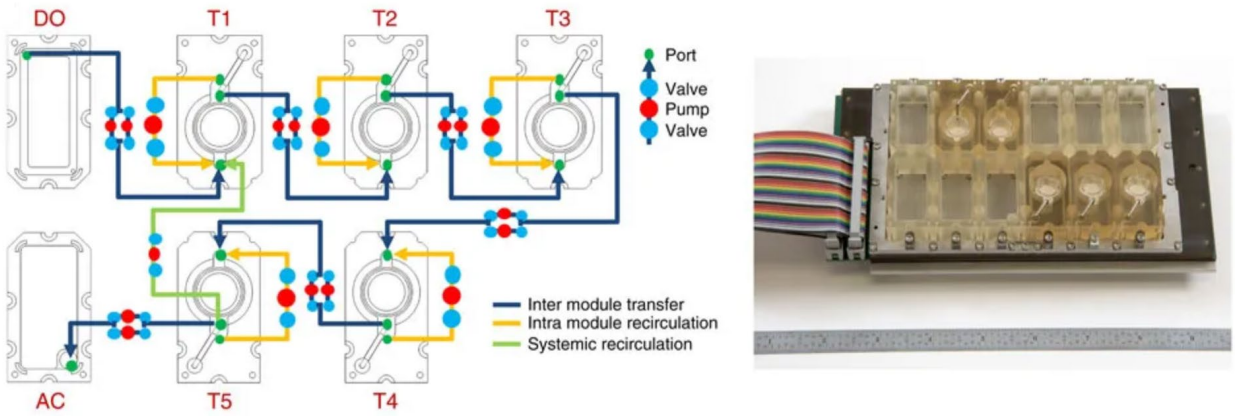

Figure 1.4. 5 Explants of ovary, fallopian tube, uterus, cervix, and liver tissues were cultured and connected in series using microfluidic modules. This interconnected system of tissues was shown to recapitulate function of the human reproductive tract and exhibited a 28-day menstrual cycle. Adapted from Ref. [149] with permission from Springer Nature, Copyright 2017.

1.4.13 Droplet Enabled Cell and Tissue Culture

While this section predominantly focuses on the droplet-enabled analysis of cells and tissues, several noteworthy studies have demonstrated the utility of microfluidic droplet formation as a distinct preparative technique in cell biology. Xu et al. [152] harnessed microfabrication techniques to create droplet arrays that solidified into columns within a microdevice, resulting in a sandwich-like structure with a liquid top, cells housed in the central columns, and gas exchange channels at the bottom. This user-friendly system exhibited remarkable cell viability and holds promise for high-throughput investigations. Agarwal and coworkers [153] showcased the one-step generation of microcapsules containing mouse embryonic stem cells using a droplet-based microfluidic system. These microcapsules featured an alginate hydrogel shell and an aqueous core filled with cells (as depicted in Figure 1.4.6). Notably, the encapsulated cells displayed high viability, and their cardiac differentiation was compared to conventional hanging drop models[153].

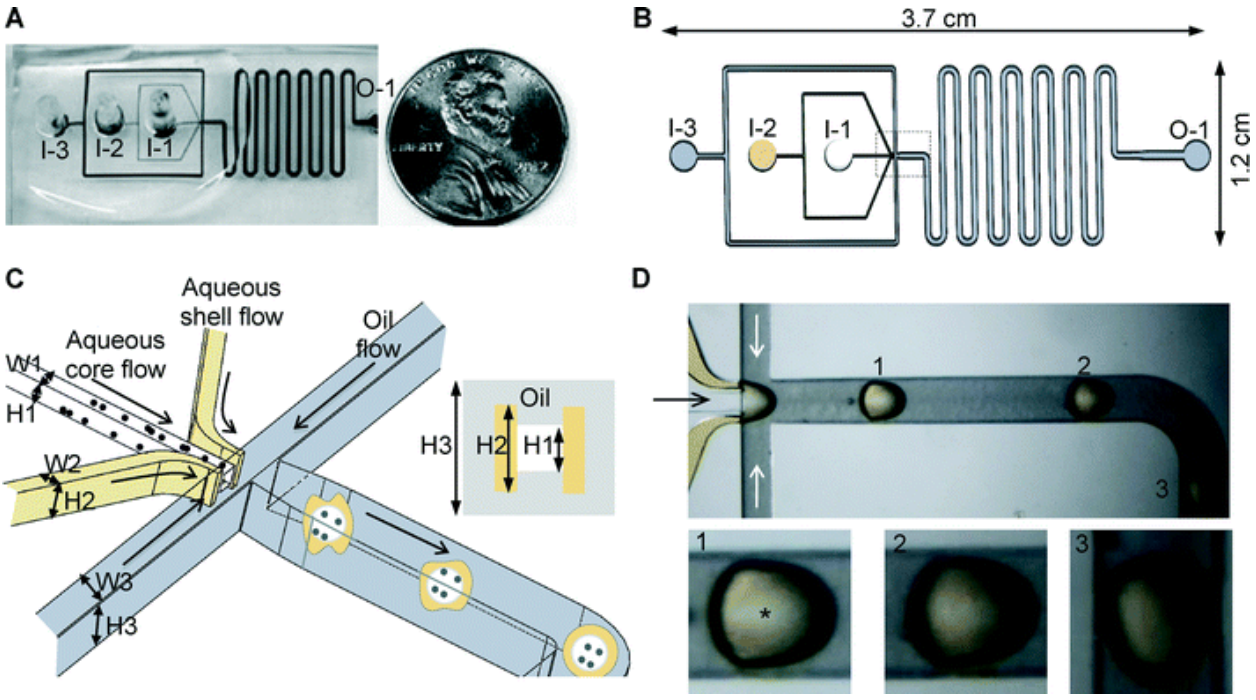

Figure 1.4. 6 Droplet-based microdevice enabled fabrication of alginate hydrogel shells with an aqueous liquid core of cells with a simple, one-step workflow. The internal cells showed high viability and their cardiac differentiation was similar to conventional hanging drop models. (A) Device overview, (B) schematic, (C) 3D depiction of flow-focusing junction, and (D) typical images of droplets showing gradual formation of the shell. Adapted from Ref. [153] with permission from the Royal Society of Chemistry, Copyright 2013.

Water-in-oil droplets, combined with distinctive, photopolymerizable material properties, have been employed for the prolonged culture of encapsulated cells. Oakey and coworkers[147] demonstrated that human lung adenocarcinoma epithelial cells (A549s) could be maintained in a viable state for several weeks within microfluidically generated polyethylene glycol norbornene (PEGNB) droplets. These droplets were polymerized through UV light exposure following on-chip emulsification. This droplet microencapsulation method was proven to yield cell-laden hydrogel microspheres at high rates, with uniform size distributions and exceptional long-term cell viability, surpassing the performance of existing materials In a similar vein, our recent research

involved the encapsulation of 3T3-L1 adipocytes (fat cells) within agarose droplets using a valve-controlled droplet generator. Subsequently, we employed these adipocyte spheroids as biological controls to compare cell line functionality with ex vivo murine adipose tissue explants[96]. These investigations collectively underscore that microfluidic droplet formation serves as an innovative tool for cell culture by enabling the creation of micrometer-scale containers laden with cells or tissue.

1.4.14 Small-Volume Bioanalysis

When dealing with cells and tissues cultured on microfluidic devices, the available analytical methods become more limited. To be effective, any suitable bioanalytical approach must initially be compatible with minute sample volumes, typically ranging from picoliters to nanoliters. Furthermore, specific applications may require on-chip analysis for optimal outcomes. For instance, the real-time quantification of cell and tissue secretions greatly benefits from rapid, on-chip analysis to minimize diffusional spreading. In this section, we will provide an overview of the general strategies employed by researchers to conduct analyses on such small volumes. Subsequently, we will shift our focus towards droplet-based microfluidic techniques for achieving similar goals[84, 95, 96].

1.4.15 Modular Analysis with Droplet-Based Techniques

Droplet microfluidics has revolutionized the ability to conduct millions of independent nanoliter/picoliter reactions and high-throughput screenings[154]. Presently, droplet-based microfluidic technology is widely recognized as a swift and precise tool for the cultivation, isolation, and assessment of cells and their secretions, with several systems available in the

commercial market[155]. However, when it comes to intricate cell or gene analyses requiring multiple processes such as high-temperature heating, sample manipulation, sorting, amplification, and extended incubation, these tasks cannot be executed on a single microfluidic device[156] An effective strategy is to integrate multiple distinct microchips in a modular fashion to facilitate the complete workflow of complex biological analyses[157]. For example, in the automated measurement of single-cell miRNA on a high-throughput scale, Chen and colleagues integrated two droplet-based microchips, as depicted in **Figure 1.4.7**.[155] In this automated system, two separate microdevices were created – one for generating and one for detecting target droplets containing individual cells and reagents for miRNA analysis. These devices were interconnected through extended tubing. Occasionally, a combination of a few droplet-based microfluidic devices may not entirely meet the research requirements. This is particularly true when several off-chip operations are necessary to process and analyze the sample, such as multiple thermal cycles and inactivating specific enzymes[158]. In such scenarios, the integration of multiple on- and off-chip manipulations becomes indispensable for complex cellular analysis. The Abate group has introduced a method for single-cell genome sequencing that integrates numerous microscale and bulk steps together, illustrated in **Figure 1.4.8**.[154]

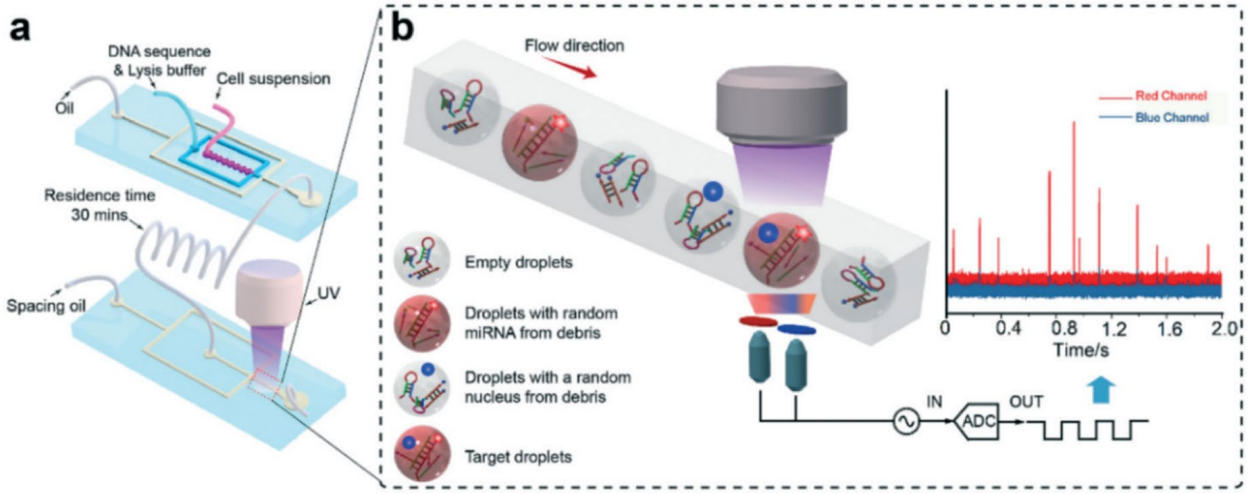

Figure 1.4. 7 Single-cell miRNA screening was accomplished by integrating multicolour fluorescence detection with isothermal nucleic acid analysis. (a) Modular system with one chip generating droplets for cell encapsulation, a long tube for 30-min incubation, and the second chip spacing and optically detecting the droplets for readout. (b) Multiple fluorescence filters and a photomultiplier tube (PMT) were used for detection. Adapted from Ref. [155] with permission from the Royal Society of Chemistry, Copyright 2018.

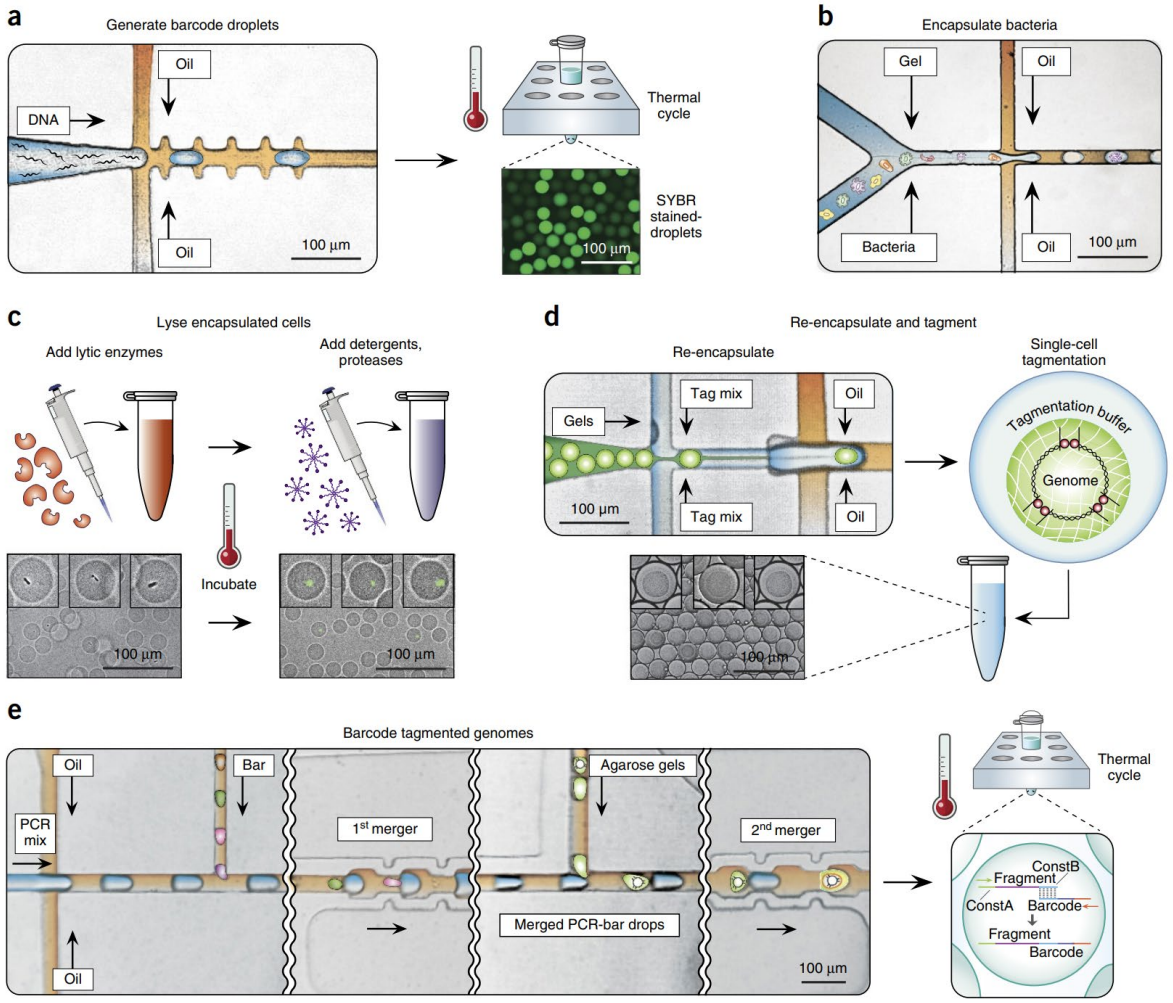

Figure 1.4. 8 Integrating a combined workflow between on-chip microfluidic droplet methods and off-chip biochemical methods for single-cell genomic sequencing (SiC-seq). (a) Encapsulation of random DNA oligo and in-droplet PCR to generate barcode droplets. (b) Formation of single-cell

containing agarose microgels. (c) Off-chip steps of enzymatic and detergent lysis were conducted to purify the single-cell genomes. (d) Using another chip, tagmentation reagents were encapsulated again with the microgel droplets. (e) The droplets of PCR reagents and barcodes were sequentially merged with droplets having tagmented genomes at 1:1 ratio on-chip, then barcodes were spliced to genomic fragments by another off-chip PCR step. Adapted from Ref. [154] with permission from Springer Nature, Copyright 2017.

While droplet-based approaches excel in high-throughput cell culture and analysis, certain challenges remain, including the need for internal/external pumping, sensitive readout equipment, and advanced droplet-control techniques for tasks like generation, flowing, merging, sorting, etc. As an alternative to flowing systems for digital assays via droplet formation, there's a powerful concept centered around well-based workflows for digital methods. This methodology involves segregating bulk samples into ultra-small clusters of containers, allowing microfluidic well-based techniques to detect nucleic acids, proteins, enzyme activity, or even single-cell genotypes and phenotypes with exceptional sensitivity[159-161]. Among these, the SlipChip developed by the Ismagilov group stands out as an automated, versatile digital platform that operates without the need for pumps and valves. This device employs a bottom plate containing preloaded ducts and a top plate equipped with wells serving as a lid with fluidic pathways. By aligning and sliding (or "slipping") the plates, solution contact enables diffusional reactions to occur, as depicted in **Figure 1.4.9**[162, 163]. These devices have been employed for various applications, including the quantification of methicillin-resistant Staphylococcus aureus (MRSA) through digital PCR amplification on SlipChips with uniform-size wells[164, 165]. Furthermore, for clinical diagnosis, the limit of detection (LOD) for viral HIV and hepatitis C virus (HCV) was enhanced to 2.0×102 molecules mL-1 by employing real-time quantitative digital RT-PCR on the rotational multivolume-well SlipChips[163].

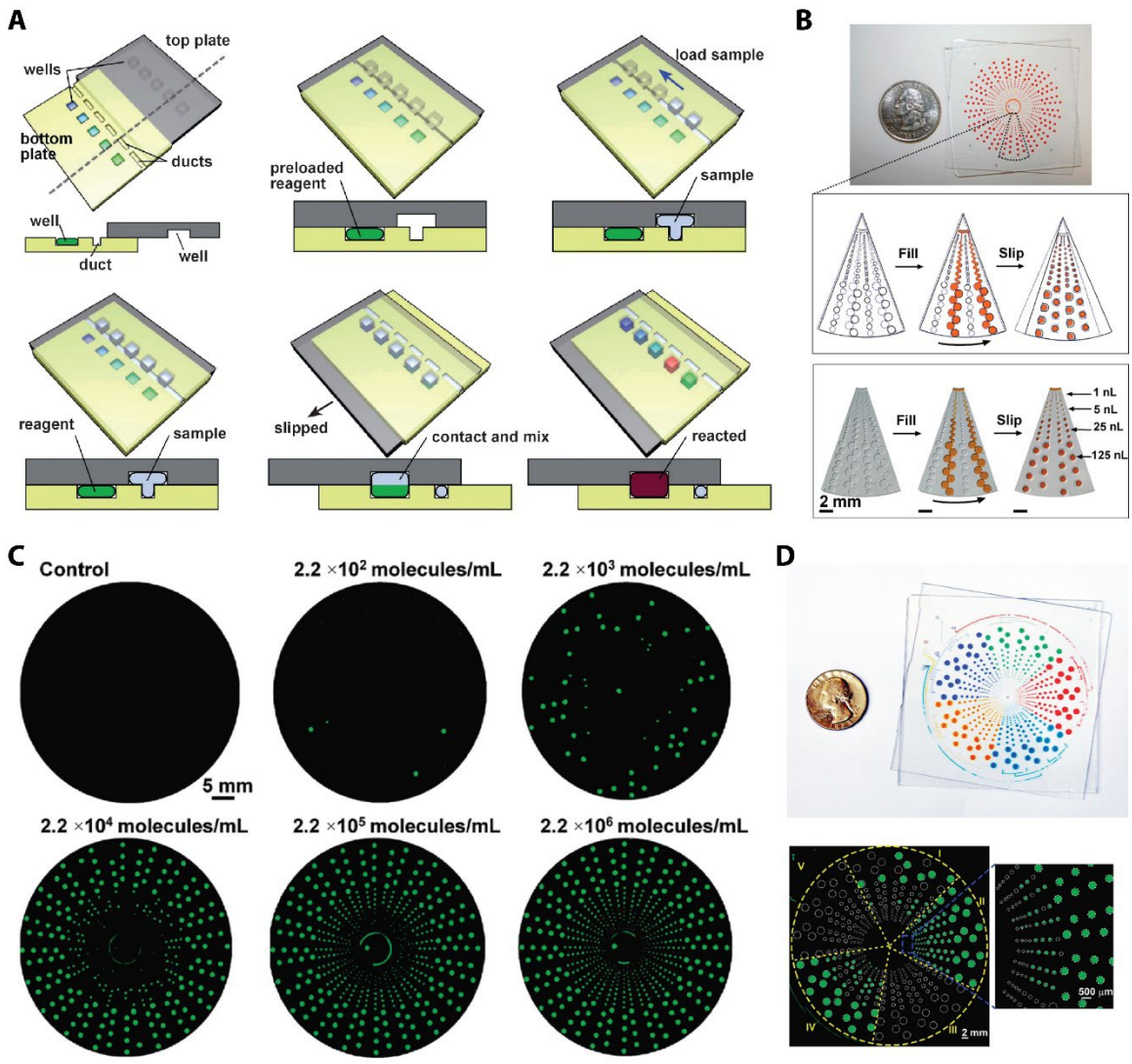

Figure 1.4. 9 SlipChips for digital assays without valves or pumps. (A) Sequential operation steps. Adapted from Ref. [162] with permission from the Royal Society of Chemistry, Copyright 2009. (B) Image and schematic of rotational multivolume SlipChip with 640 wells of varying volumes. (C) Fluorescence imaging after thermal cycling of RNA template varied concentrations using SlipChips from part B. (D) High dynamic SlipChip for multiplexed, multivolume digital RT-PCR. B-D were adapted from Ref. [163] with permission from the American Chemical Society, Copyright 2011.

1.4.16 Fully Integrated Analysis On-Chip

As forecasted by Manz and coworkers in 1990[166], microfluidic systems have demonstrated their capacity for complete integration, culminating in a sample-in-answer-out workflow. The pursuit of seamlessly merging multiple sample processing and analytical steps into a single device has been a central goal of microfluidic systems from the outset, offering substantial advantages, including material and cost efficiencies, shortened reaction times, high-throughput capabilities, and enhanced portability. It is essential to acknowledge that this endeavor was not devoid of challenges, including the need for trained personnel, the heightened risk of contamination during analyte transfers, unexpected cost escalations, and prolonged analytical processes that introduced certain complexities during the development of integrated microdevices[167]. After years of diligent effort, the Landers group has notably achieved the publication of the first fully integrated microfluidic genetic analysis system. This system enables the sensitive and rapid detection of genetic signatures of B. anthracis directly from whole blood samples by integrating solid-phase DNA extraction, PCR, and electrophoretic separation on a single chip[94] (**Figure 1.4.10A**). More recently, the Woolley research group has introduced an integrated microdevice designed for the concurrent quantification of two protein markers associated with preterm birth (lactoferrin and ferritin) in human serum. This feat was accomplished through integrated immunoaffinity extraction and microchip electrophoresis[168] (**Figure 1.4.10B**). For the analysis of cellular secretions and interactions between various endocrine tissues (adipocytes and pancreatic islets), the Kennedy group has ingeniously merged co-culture with on-chip competitive immunoassays and electrophoretic separations[87] (**Figure 1.4.10C**). Additionally, the Roper lab has devised a temperature-controlled system that provides precise control over input glucose patterns imposed on pancreatic islet tissue. This is followed by an online fluorescence anisotropy-based immunoassay to monitor insulin secretion dynamics using a mix-and-read assay downstream[112]

(**Figure 1.4.10D**). These innovative devices underscore the remarkable potential of microfluidic systems to consolidate conventional techniques within a single, miniaturized platform. In the subsequent sections of this chapter, we explore methodologies for incorporating droplet microfluidics into both the sampling and analysis phases, thereby expanding the array of bioanalytical tools available at the microscale.

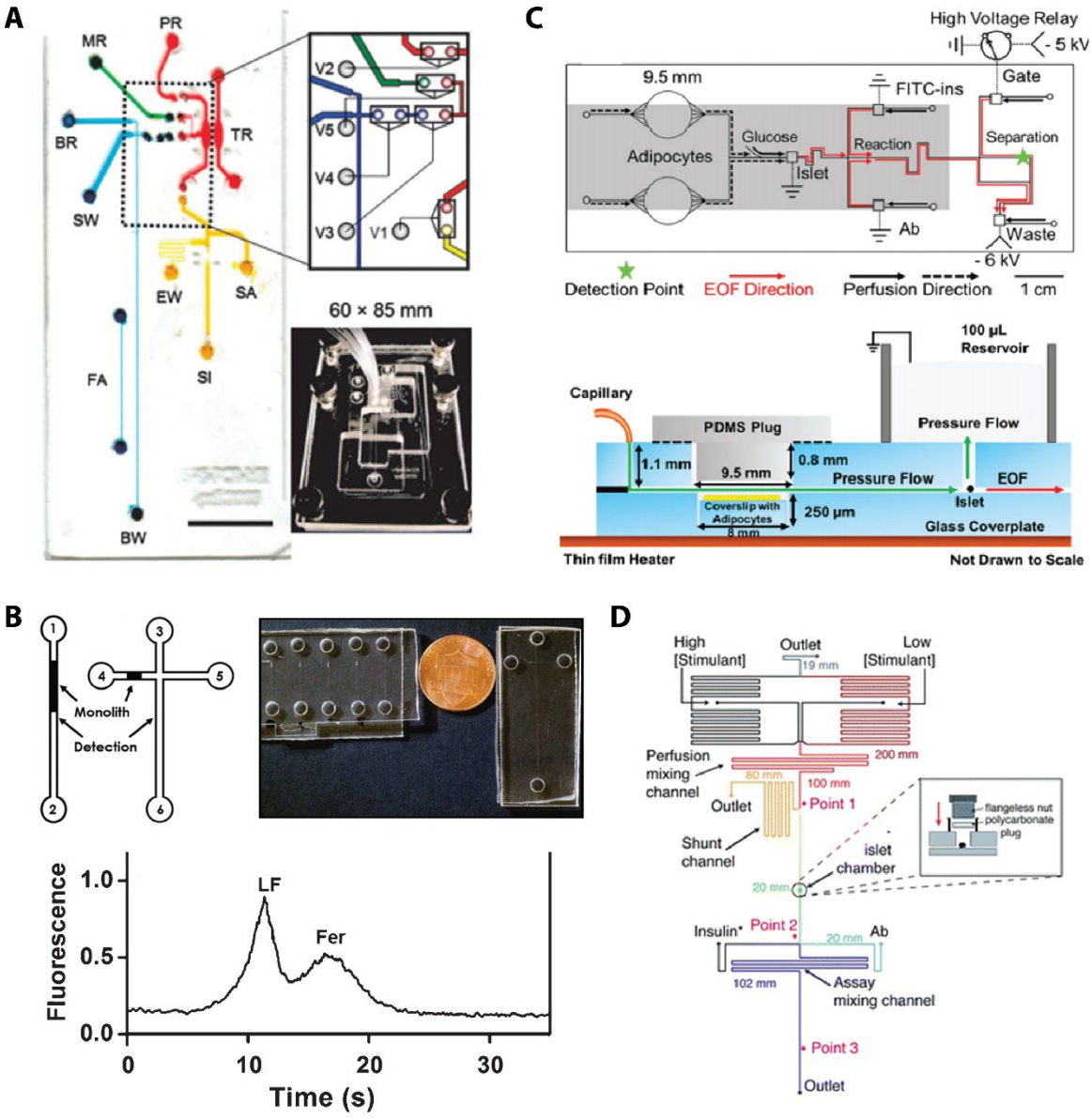

Figure 1.4. 10 Integration of sample processing, cell culture, and analysis on microfluidic devices. (A) Sample-in-answer-out capability for genetic analysis directly from blood or nasal aspirates in

<30 min by Easley et al. Adapted from Ref. [94] with permission from the National Academy of Sciences of the United States of America, Copyright 2006. (B) Integration of microchip immunoaffinity extraction and microchip electrophoresis for analysis of preterm birth biomarkers in serum. Adapted from Ref. [168] with permission from the Royal Society of Chemistry, Copyright 2018. (C) Integration of tissue co-culture with electrophoretic immunoassays. Adapted from Ref. [87] with permission form the American Chemical Society, Copyright 2018. (D) On-chip integration of input stimulant patterns, tissue culture, secretion sampling, and homogeneous immunoassays based on fluorescence anisotropy. Adapted from Ref. [112] with permission from the Royal Society of Chemistry, Copyright 2017.

1.4.17 Integrated Droplet-Based Analysis of Cells and Tissues

Our research group, in addition to other scientific endeavors, has established the efficacy of continuous-flow microfluidic sampling as a potent method for investigating the dynamic changes in various metabolites like insulin, glucose, glycerol, and fatty acids within pancreas, liver, and adipose tissues[82, 83, 87, 88, 112, 169]. Nevertheless, a significant challenge remains in the form of longitudinal broadening, primarily caused by dispersion and laminar diffusion within the microchannels, which significantly hampers the temporal resolution in the sampling and analysis of cells and tissues. This limitation can lead to the loss of crucial, intricate details concerning biological activities. Furthermore, conducting single-cell analyses in a continuous-flow setting is constrained by the minuscule amount of starting material available. Although droplet microfluidics has already garnered recognition as a potent tool for single-cell analysis, limited research has been devoted to the dynamics of single-cell behaviors, including processes such as single-cell-like breakdown, nutrient absorption, and metabolite uptake/release[84, 118]. In this domain, we contend that droplet microfluidics holds the potential to offer distinct analytical solutions. Notably, droplet sampling has been shown to preserve temporal chemical information[84, 95, 96], even at a millisecond

time scale if thoughtfully designed[117]. Moreover, skillful manipulation of time- and frequency-domain chemical information encapsulated within droplets has been demonstrated to substantially enhance analytical sensitivity[118, 170, 171].

Leveraging these enhancements in analytical sensitivity, our laboratory recently employed a droplet-based microfluidic system, combined with lock-in analysis, to quantify the uptake of labeled free fatty acids (FFA*) by individual 3T3-L1 adipocytes[118]. Precise nanoliter flow control was enabled by active, pneumatic push-up valves (Quake style[172]), allowing droplet formation to be strictly phase-locked to the fluorescence emission detector at narrow bandwidth (±0.04 Hz) for droplets generated at 3.50 Hz. Using this "μChopper" concept[170], alternative generation of sample and reference droplets (**Figure 1.4.11A**) allows real-time detector drift correction, permitting very low signals to be recovered from noise. Compared to conventional single droplet fluorescence detection, the noise magnitude was reduced by more than 50-fold (**Figure 1.4.11B**). Rather than averaging the cell population, this μChopper system could precisely quantify single-cell FFA* uptake rates in 3T3-L1 adipocytes to be $3.5 \pm 0.2 \times 10^{-15}$ mol cell^{-1} for the first time (**Figure 1.4.11C**). Overall, the μChopper was able to reduce limits of detection (LODs) in absorbance[170] and fluorescence[118] by as much as 200-fold and 50-fold, respectively. We propose that significant performance enhancements should be achievable in various other detection modes, whether using optical readout, electrochemical detection, mass spectrometry, etc.

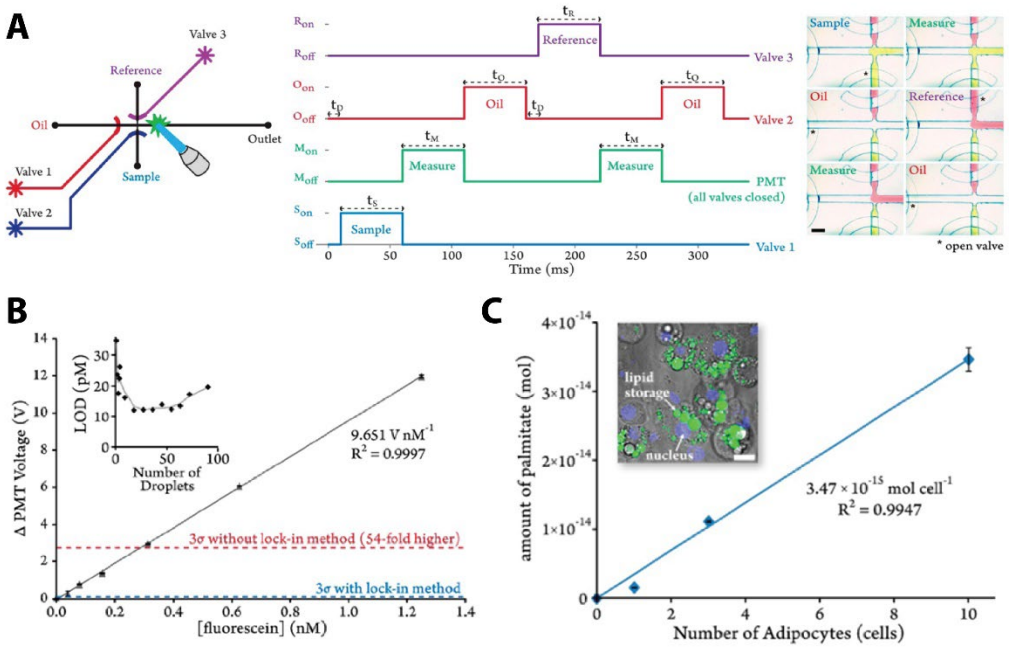

Figure 1.4. 11 Lock-in detection with the μChopper device concept. (A) Automated device with valve-controlled segmentation of sample, oil, and reference liquids. (B) With noise reduced by more than 50-fold, an LOD of 12 pM fluorescein was achieved with standard microscope optics. (C) Single-cell fatty acid uptake by 3T3-L1 adipocytes was quantified for the first time with the μChopper system. Adapted from Ref. [118] with permission from the American Chemical Society, Copyright 2017.

Recognizing the critical need to improve temporal resolution for the examination of tissue secretions, Easley et al.[95] developed a novel passive droplet-based microfluidic sampling method to monitor glucose-stimulated secretion of zinc ions from pancreatic islets with high temporal resolution (**Figure 1.4.12**). Zn^{2+} secretion sampled and stored into a continuous stream of small droplets (~0.5 nL) preserved the temporal information and allowed reconstruction of the secretory time record through downstream analysis (**Figure 1.4.12A-C**). Bursts in Zn^{2+} secretion as high as ~800 fg $islet^{-1}$ min^{-1} were captured and quantified, and two major classes of rapid and slow oscillations (~20-40 s and ~5-10 min) were observed. In later work from our group, we showed

that automation of the secretion sampling μChopper with pneumatic valves could be combined with a customized, mix-and-read immunoassay to monitor insulin secretion directly at high temporal resolution[84] (**Figure 1.4.12D-H**). During secretion sampling of single pancreatic islets, bursts in glucose-stimulated insulin secretion were captured into droplets at 15-second temporal resolution, revealing fast insulin secretion oscillations (~20-30 s) which matched with the timing of well-known calcium signals within islets.[173]

These systems unequivocally affirm the effectiveness of droplet-based sampling for high-resolution analysis of cells and tissues. By integrating passive[95] or automated[84] droplet sampling with on-chip tissue culture, reagent mixing, on-chip homogeneous assay incubation, and optical readout through lock-in detection, these pioneering analytical systems have shed light on previously unquantified bursts in secreted ions or hormones from tissue.

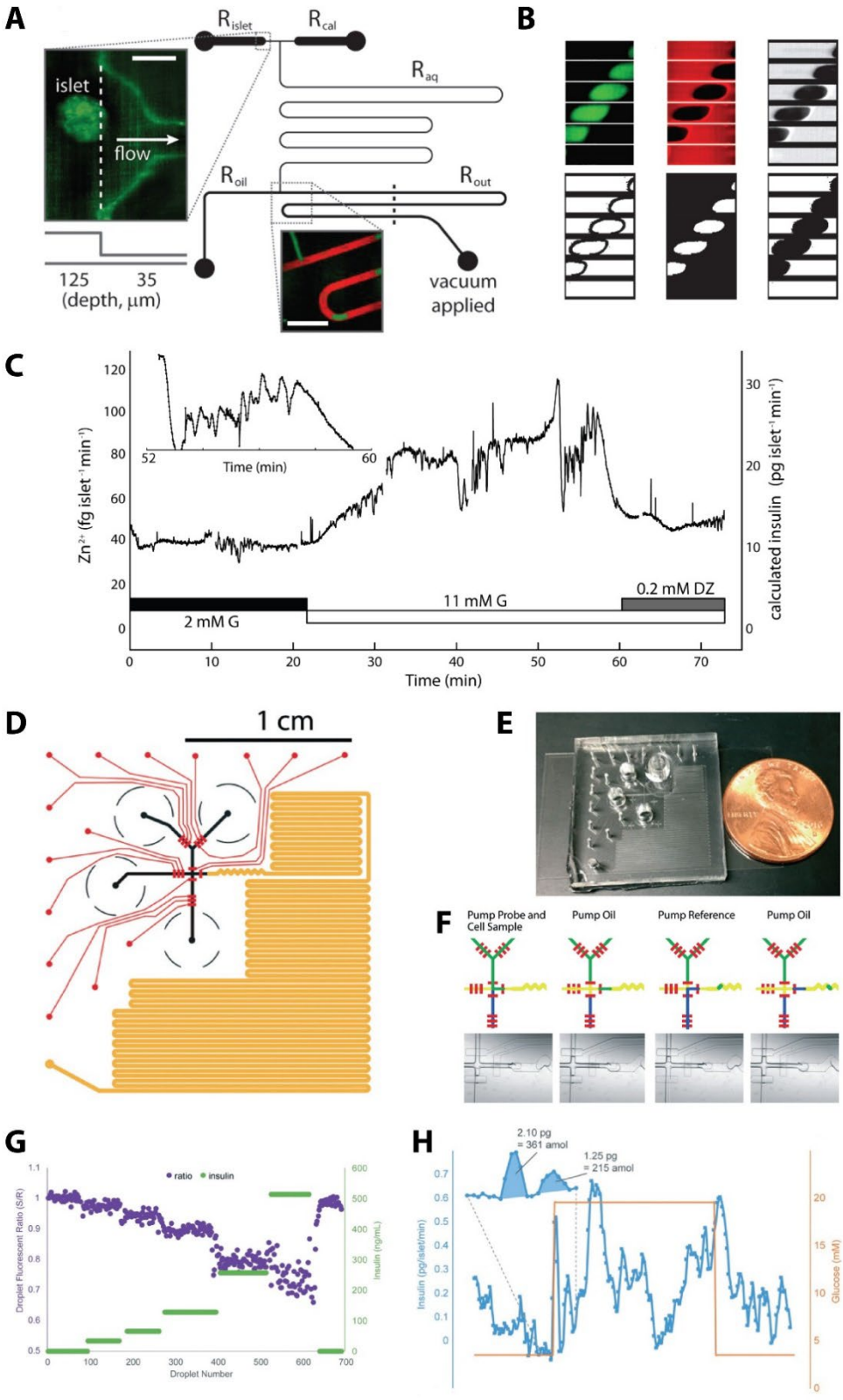
A
B
C
D
E
F
G
H
islet
flow
R_{islet}
R_{cal}
R_{aq}
R_{oil}
R_{out}
125
35
(depth, μm)
vacuum
applied
Zn^{2+} (fg islet^{-1} min^{-1})
calculated insulin (pg islet^{-1} min^{-1})
Time (min)
2 mM G
11 mM G
0.2 mM DZ
1 cm
Pump Probe and
Cell Sample
Pump Oil
Pump Reference
Pump Oil
ratio
insulin
Droplet Fluorescent Ratio (S/R)
Insulin (ng/mL)
Droplet Number
2.10 pg
= 361 amol
1.25 pg
= 215 amol
Insulin (pg/islet/min)
Glucose (mM)

Figure 1.4. 12 Droplet-based secretion sampling at high temporal resolution with μChopper devices. (A) Device layout for passive sampling. (B) Novel image analysis for phase-locking droplet signals to oil signals. (C) Zn^{2+} secretion from pancreatic islet tissue was sampled into droplets and quantified by lock-in analysis, allowing the capture of bursts of secretion under showing both rapid and slow oscillations (~20-40 s and ~5-10 min). Parts A – C adapted from Ref. [95] with permission from the American Chemical Society, Copyright 2009. (D) Device layout for automated secretion sampling and lock-in analysis. (E) Image of complete device. (F) Automation of μChopper workflow. (G) Homogeneous immunoassays showed predictable sample-to-reference ratios (S/R) as a function of insulin concentration, with an LOD of 10 amol in a single droplet. (H) Single-islet insulin secretion rates shown in pg $islet^{-1}$ min^{-1} (blue) along with imposed glucose waveforms (orange). This device gave 15 second resolution and observed both fast and slow insulin oscillations, with burst on the order of hundreds of attomoles. Parts D – H adapted from Ref. [84] with permission from the Royal Society of Chemistry, Copyright 2018.

1.4.18 Recent Applications in Tissue Engineering and Analysis with Droplet Microfluidics

In this part, we review recent applications of droplet-based microfluidic devices to explore and interrogate cells and tissues. These applications are organized based on the cells or tissues studied, and coverage includes the bioanalysis of hepatocytes, pancreatic islets, adipose tissue, and neuronal cells.

1.4.18.1 Hepatocytes

Hepatocytes comprise a significant portion, ranging from 70% to 85% of liver tissue and are responsible for the majority of metabolic and biosynthetic processes in the liver. However, there has been limited exploration into how insulin and glucagon affect hepatic metabolism[60, 85]. The Roper group designed a modular microfluidic system to observe the growth and function of HepG2 cells, which are derived from human hepatocarcinoma[85]. This innovative bioreactor featured a cell

culture incubator for HepG2 cell growth, automated delivery of glucose and insulin stimulants, droplet-based sampling and mixing with enzymatic assay reagents, and real-time optical detection for measuring HepG2 cell glucose consumption (**Figure 1.4.13A**). The Revzin group introduced another modular bioanalysis platform, which combined a cell culture device and a droplet-generating device to enable multiplexed analysis of injury responses in hepatocyte spheroids[157]. In this automated droplet-based microfluidic system, three types of secretions—glucose, total bile acids, and lactate dehydrogenase (LDH)—were concurrently monitored using colorimetric and fluorescence detection methods (**Figure 1.4.13B**). To study cell-to-cell communication within the liver, the Revzin lab presented a device for creating microcapsules with liquid cores and polyethylene glycol (PEG) shells, allowing for the assembly and culture of rat hepatocyte spheroids[174] (**Figure 1.4.13C**). This work showcased the functionality of encapsulated hepatocytes, hepatic gene expression, and the interaction between 3T3-J2 fibroblasts and hepatocytes. Likewise, the Weitz group recently published a method that employed biocompatible 3D core-shell hydrogel scaffolds to create tissue-in-droplets[175]. Highly permeable water-water-oil (w/w/o) double emulsions were used to create hepatocyte cores with fibroblast shells, resulting in the formation of "artificial liver" spheroids that were employed to investigate cell-cell interactions (**Figure 1.4.13D**). The Wheeler group adopted an alternative approach using digital microfluidics (DMF) devices and developed a microfluidic organoid culture device for drug screening, known as MODS[176]. This platform facilitated the generation and on-chip culture of individual, free-floating, and 3D hydrogel-based liver organoids. These organoids were used to study cytochrome P450 enzyme activity and hepatotoxicity (**Figure 1.4.13E**). By co-culturing HepG2 and NIH-3T3 cells in droplets, the resulting hepatic organoids demonstrated fibroblast-dependent contractile behavior as well as favorable albumin and cytochrome P450 secretion activities.

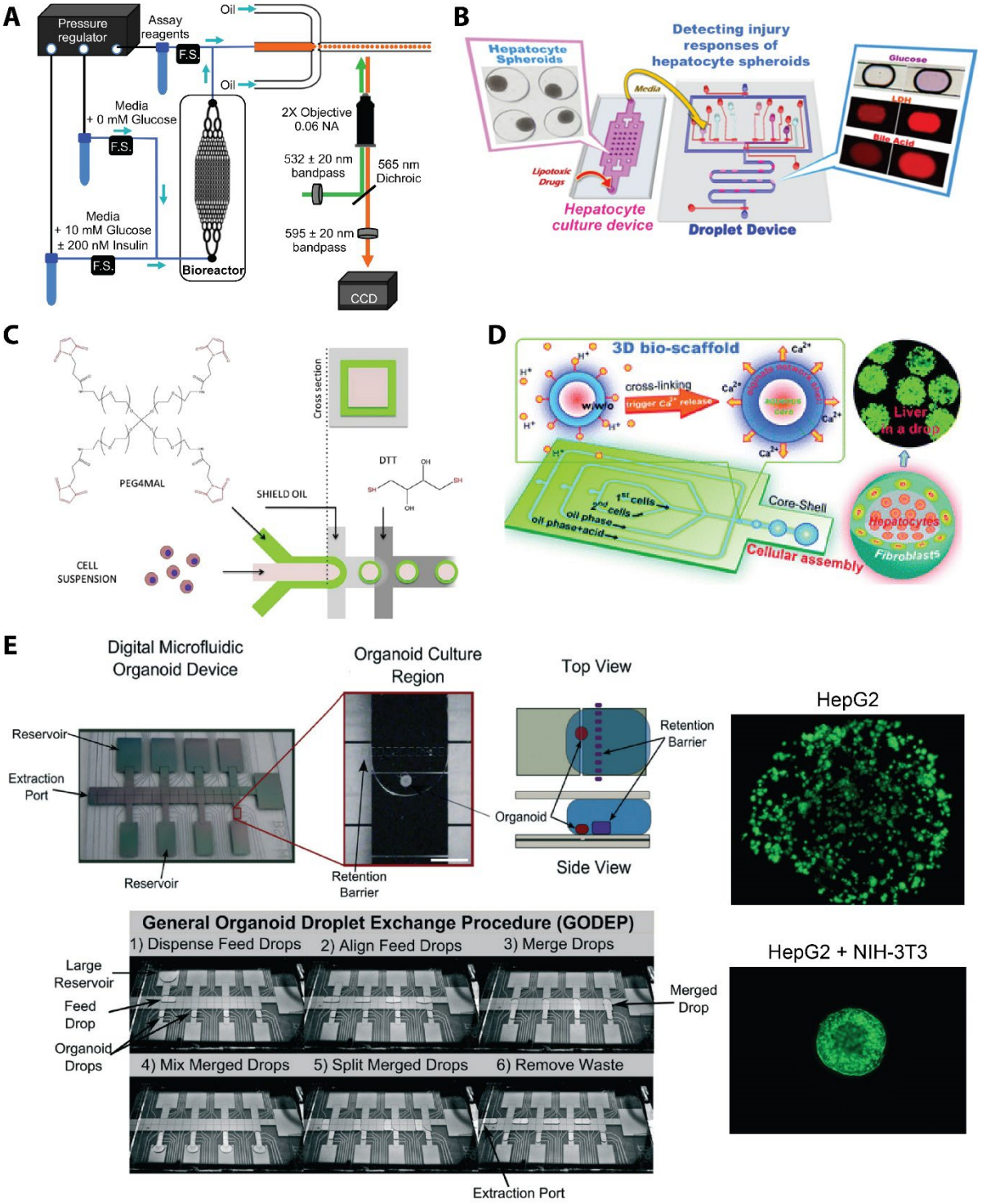
A
Pressure regulator
Assay reagents
F.S.
Oil
Oil
Media
+ 0 mM Glucose
F.S.
Media
+ 10 mM Glucose
± 200 nM Insulin
F.S.
Bioreactor
2X Objective
0.06 NA
532 ± 20 nm bandpass
565 nm Dichroic
595 ± 20 nm bandpass
CCD
B
Hepatocyte Spheroids
Detecting injury responses of hepatocyte spheroids
Media
Glucose
LDH
Bile Acid
Lipotoxic Drugs
Hepatocyte culture device
Droplet Device
C
Cross section
PEG4MAL
DTT
SHIELD OIL
CELL SUSPENSION
D
3D bio-scaffold
cross-linking
trigger Ca2+ release
w/w/o
Liver in a drop
1st cells
2nd cells
oil phase
oil phase+acid
Core-Shell
Cellular assembly
Hepatocytes
Fibroblasts
E
Digital Microfluidic Organoid Device
Organoid Culture Region
Top View
Reservoir
Extraction Port
Reservoir
Retention Barrier
Organoid
Retention Barrier
Side View
HepG2
General Organoid Droplet Exchange Procedure (GODEP)
1) Dispense Feed Drops
2) Align Feed Drops
3) Merge Drops
Large Reservoir
Feed Drop
Organoid Drops
Merged Drop
4) Mix Merged Drops
5) Split Merged Drops
6) Remove Waste
Extraction Port
HepG2 + NIH-3T3

Figure 1.4. 13 Hepatocyte culture and analysis with droplet-based microfluidics. (A) Schematic of integrated system for perfusion, droplet sampling, and online glucose consumption analysis of HepG2 cells. Adapted from Ref. [85] with permission from the American Chemical Society, Copyright 2019. (B) Multianalyte secretory analysis (glucose, total bile acids, lactate dehydrogenase) with a modular system of cell culture device coupled to a droplet sampling and analysis device. Adapted from Ref. [157] with permission from the American Chemical Society, Copyright 2019. (C) Device used to fabricate PEG/hepatocyte spheroids. Adapted from Ref. [174] with permission from Elsevier, Copyright 2017. (D) Multicellular core-shell capsules were generated using droplet-based microfluidics to make artificial liver spheroids. Adapted from Ref. [175] with permission from the Royal Society of Chemistry, Copyright 2016. (E) Microfluidic organoids for drug screening (MODS) were made with digital microfluidics (DMF) automation. Adapted from Ref. [176], with permission from the Royal Society of Chemistry, Copyright 2014.

1.4.18.2 Pancreatic Islets

The exocrine pancreas is responsible for the production and release of digestive enzymes, which aid in nutrient digestion and absorption, while the endocrine pancreas, comprising the islets of Langerhans, plays a crucial role in the endocrine system by regulating glucose homeostasis. Consequently, the pancreas is a vital organ in both the digestive and endocrine systems. This discussion will primarily focus on the pancreatic islets. The significance of comprehending this relatively small organ for research and clinical purposes has been well-established[177]. In recent decades, droplet-based microfluidics have gained recognition as a valuable tool for investigating the function and characteristics of pancreatic islets on a microscale. Indeed, various microdevices have been presented and discussed for studying islets (see **Figure 1.4.2**[129]; **Figure 1.4.10A**[94], 9-10C [87], and **1.4.10D** [112]; and **Figure 1.4.12** [84, 95]). Several research groups active in this field, including our own, have been examined. In other work, Chen et al.[178] developed a droplet device designed to encapsulate rat islets with an oxygen-sensitive dye. They quantified the secretion of

ATP and insulin under varying protocols, demonstrating the impact of oxygen consumption rate on the metabolism and function of islets within hydrogel microcapsules. Hai-Tao Liu et al.[179] introduced an innovative biocompatible water-in-water droplet system, controlled by valves, for encapsulating and culturing rat pancreatic cell lines (β-TC6). In this system, PEG and dextran were employed as the continuous and dispersed phases, respectively, and insulin secretion was measured, highlighting its strong potential for tissue engineering applications. In earlier research aimed at examining the dynamics of stimulated islets with high temporal resolution, Ismagilov and colleagues developed the "chemistrode,"[180], a droplet-based microfluidic system coupled with offline detection instruments such as fluorescence correlation spectroscopy, MALDI-MS, fluorescence microscopy, and ELISA.

1.4.18.3 Adipose Tissue

Adipose tissue is a multifaceted, indispensable, and dynamic metabolic and endocrine organ that emits and reacts to signals involved in regulating various factors, including appetite, energy expenditure, insulin sensitivity, bone metabolism, inflammation, and immunity. It constitutes a significant proportion, ranging from 5 to 50% of an individual's body weight and is categorized into two primary types: white adipose tissue (WAT) and brown adipose tissue[181-183]. While our comprehension of adipose tissue has advanced significantly over recent decades, certain functions and mechanisms of this organ remain enigmatic to researchers due to the limitations of conventional bioanalytical techniques. Droplet microfluidics provides unique platforms for investigating adipose tissue on a microscale, offering cost-effective, low-volume, high spatial resolution methods. In one approach, Sakai and colleagues introduced a microfluidic flow-focusing system employing gelatin, known for its high cell adhesiveness, non-toxicity, and

biodegradability, for tissue engineering[184]. This device facilitated the continuous generation of small droplets, within which adipose-derived cells were encapsulated (**Figure 1.4.14A**). In contrast, Deveza and co-workers developed a droplet-based microfluidic device to create biodegradable PEG-based microspheres, aimed at controlling the release of growth factors and DNA nanoparticles (**Figure 1.4.14B**)[185]. This work examined the mesh size and degradation rate of the droplets at varying concentrations of PEG polymer, ranging from 7.5% to 15% (w/v), which determined the release rate of encapsulated proteins and DNA. The study also investigated the effects of released growth factors on adipose-derived stem cells (ADSCs).

In research employing droplets for high-resolution analysis of adipose tissue, our laboratory recently enhanced our automated μChopper concept to achieve an unprecedented resolution of 3.5 seconds. This improved device was employed for sampling secretions from primary murine adipose explants[96] (**Figure 1.4.14C**). In this study, both the peaks and valleys of glycerol secreted from cells and tissues of wild-type, aged, and obese mice were captured. By sampling ex vivo epididymal white adipose tissue (eWAT) explants from mice, the study unveiled previously unreported rapid oscillations in glycerol secretion occurring at frequencies of 0.2 to 2.0 minutes-1 (corresponding to periods of approximately 30 to 300 seconds), made possible by the device's high temporal resolution. These oscillations were absent in clustered cell lines. This research represents the first report of cell-to-cell communication in adipose tissue resembling that of pancreatic endocrine tissue, with glycerol secretion spectrographs presented in **Figure 1.4.14D** as an example of the distinctive insights offered by this technology-enabled analysis.

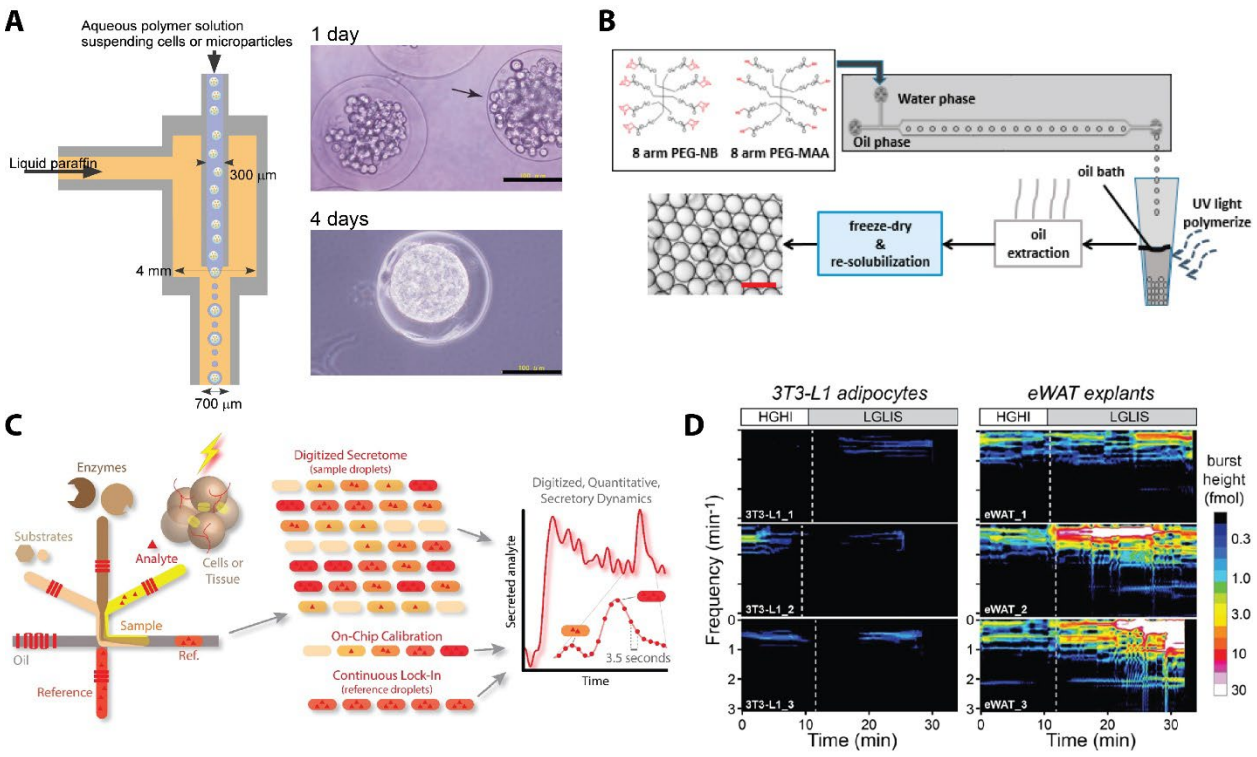

Figure 1.4. 14 Adipose tissue culture and analysis with droplet-based microfluidics. (A) Schematic of a microfluidic flow-focusing device for adipose-derived cell encapsulation. Adapted from Ref. [184] with permission from AIP Publishing, Copyright 2011. (B) Droplet formation was also used to form biodegradable microspheres for controlled release of growth factors to adipose cells. Adapted from Ref. [185] with permission from the American Chemical Society, Copyright 2015. (C) High-resolution, automated sampling with an improved μChopper device enabled 3.5-second resolution measurement of glycerol secretion from adipose tissue. This valve-automated device integrated tissue culture, enzyme and reagent mixing, droplet-based sampling, and downstream optical analysis with lock-in detection. (D) Unique oscillation analysis of glycerol release (FFT spectrograms) was enabled by the microfluidic tools developed in this work, where previously unreported lipolytic oscillations were observed from the eWAT tissue. Parts C – D were adapted from Ref. [96] with permission from the Royal Society of Chemistry, Copyright 2020.

1.4.18.4 Neuronal Tissue

Neuronal tissue engineering has garnered significant attention in recent decades due to its fundamental role in physiological processes. Nonetheless, the intricacies of the nervous system pose formidable challenges that traditional cell culture and tissue engineering methods struggle to address[186]. Microfluidic techniques offer considerable promise in the realm of microscale tissue engineering, offering benefits such as high-resolution in situ imaging, simultaneous performance of multiple assays, and the creation of integrated systems that mimic cellular interactions with the extracellular matrix (ECM)[187-189]. Alessandri and colleagues introduced a 3D-printed microfluidic device designed for the generation of functionalized microcapsules used in incubating and differentiating human neuronal stem cells (hNSC)[190]. These encapsulated neuronal stem cells, along with a reconstituted micro-thick ECM layer and a protective alginate shell, resulted in the formation of hollow micro-hydrogels (**Figure 1.4.15A**). In a separate effort, Jianhua Qin's research group combined a floatage-based trap array with a tapered immobilization channel array, incorporated into a droplet-based microfluidic device, to investigate various responses of individual C. elegans organisms to a neurotoxin, 6-hydroxydopamine (6-OHDA)[191]. This integrated system handled all processes, including droplet generation, trapping, immobilization, worm encapsulation, behavior assessment, and image analysis (**Figure 1.4.15B**). This study particularly demonstrated the feasibility of conducting whole-animal assays and high-throughput drug screening for neurodegenerative diseases at a single-animal resolution, highlighting the ingenuity of tissue engineering and droplet-based device development in achieving these outcomes.

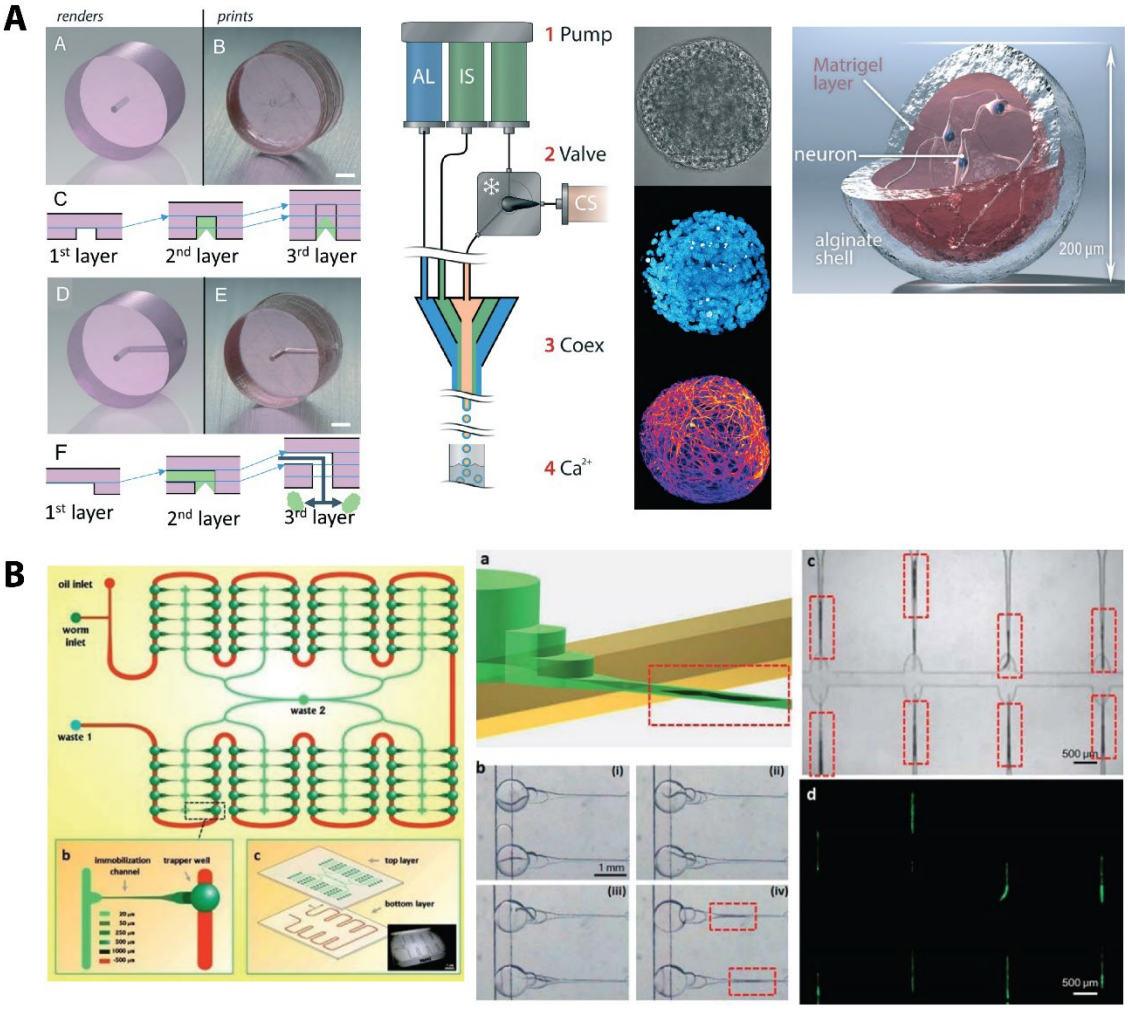

Figure 1.4. 15 Neuronal tissue culture and analysis with droplet-based microfluidics. (A) Combining 3D printing with droplet-based devices allowed production of functionalized microcapsules for incubating and differentiating human neuronal stem cells. Adapted from Ref. [190] with permission from the Royal Society of Chemistry, Copyright 2016. (B) Schematic and photograph of an integrated microfluidic system for individual *C. elegans* assays, using a tapered immobilization channel array for immobilizing and imaging the worms to study neurotoxicity. Adapted from Ref. [191] with permission from the Royal Society of Chemistry, Copyright 2010.

1.5 Summary, challenges, and future outlook of this chapter

Herein we have discussed tissue engineering and microfluidics, with a particular focus on droplet-based microfluidics. Droplet-based microfluidics has been proven highly useful for both

cell and tissue engineering on-chip, but also for many useful applications in analysing cellular function. This technology enables generation of monodispersed, micrometer-sized droplets that can be viewed as individual bioreactors for culture, delivery, and analysis of cells and tissue. We have shown examples in which unique architectures of cells and tissues can be created through encapsulation at high throughput, in which particles can be created for controlled release of various factors onto cells, and in which droplets can be continuously sampled from cells and tissues to provide high temporal resolution and on-chip analysis, among others. Alongside these capabilities, the accompanying microfluidic systems can permit the biological and biophysical microenvironments to be adjusted to mimic the physiological microenvironments, enabling studies that match more closely to the respective *in vivo* biology. Considering these and other similar developments in materials science, bioanalytical chemistry, and tissue engineering, it is clear that droplet-based microfluidics is well-poised for continued, transformative impacts on our understanding of biology and physiology in the coming future.

While considerable efforts have been invested with many positive impacts realised, there remain several challenges to be addressed in the future. For instance, much of the current studies are focused on single tissue-on-a-chip systems. However, the activities of individual tissues on these devices may differ significantly from that in the living body, since communication and physical contact with other tissues is removed. Furthermore, stimulants and media are often obtained as purified materials from commercial sources, often differing greatly from the complex mixtures present *in vivo*. In the future, continued emphasis should be placed on multi-tissue-on-a-chip systems, and creative solutions should be explored to more closely mimic in vivo media. One example would be for more investigators to use whole blood where appropriate, rather than minimal cell media. Indeed, a more realistic microenvironment for many tissues should contain

branched vascular networks to supply such blood, yet this remains challenging for many to incorporate into their tissue chips.

In terms of analysis, multiplexing of current techniques is a continued need. More generalizable, microscale-compatible methods should be sought after to allow real-time, quantitative detection of multiple biologically relevant analytes, each with the requisite sensitivity. A multi-analyte readout in real-time would allow a much more comprehensive view of the functions of cells and tissues as they are being analysed. Automation is another area that could be improved in many of these systems. Unless the end-use of the device is intended for point-of-care, many of the systems presented herein could benefit from, for example, valve-based automation that can help remove user error from the equation. Interestingly, droplet-based microfluidics is well-positioned for improvements in automation, since each container can be segregated and individualized, much like digital data in computing. We contend that there is a need for a more formalized treatment of droplets as packets of information, and we hope to see more of these types of studies in the future. Finally, it is important for users to carefully evaluate the volumes of cells and tissues that are examined in their devices, since the scaling of tissues should differ depending on their true physiological scale. Tissue scaling can have profound impacts on the function under study, and this issue may pose limitations on the temporal resolutions or analyte sensitivities that are accessible to the researcher.

While it is true that various challenges remain, it is apparent from the work presented in this chapter that the various capabilities of forming and manipulating droplets on microfluidic devices should be considered as a vitally important tools to aid in our understanding of the function of biological cells and tissues.

1.6 References

1. Puska, P.; Nishida, C.; Porter, D.; Organization, W. H., Obesity and overweight. *World Health Organization* **2003**, 1-2.
2. Collaboration, N. R. F., Trends in adult body-mass index in 200 countries from 1975 to 2014: a pooled analysis of 1698 population-based measurement studies with 19.2 million participants. *The lancet* **2016,** *387* (10026), 1377-1396.
3. Zheng, Y.; Manson, J. E.; Yuan, C.; Liang, M. H.; Grodstein, F.; Stampfer, M. J.; Willett, W. C.; Hu, F. B., Associations of weight gain from early to middle adulthood with major health outcomes later in life. *Jama* **2017,** *318* (3), 255-269.
4. Luppino, F. S.; de Wit, L. M.; Bouvy, P. F.; Stijnen, T.; Cuijpers, P.; Penninx, B. W.; Zitman, F. G., Overweight, obesity, and depression: a systematic review and meta-analysis of longitudinal studies. *Archives of general psychiatry* **2010,** *67* (3), 220-229.
5. Apovian, C. M., Obesity: definition, comorbidities, causes, and burden. **2016**.
6. Guh, D. P.; Zhang, W.; Bansback, N.; Amarsi, Z.; Birmingham, C. L.; Anis, A. H., The incidence of co-morbidities related to obesity and overweight: a systematic review and meta-analysis. *BMC public health* **2009,** *9*, 1-20.
7. Ralston, J.; Brinsden, H.; Buse, K.; Candeias, V.; Caterson, I.; Hassell, T.; Kumanyika, S.; Nece, P.; Nishtar, S.; Patton, I., Time for a new obesity narrative. *The Lancet* **2018,** *392* (10156), 1384-1386.
8. Swinburn, B. A.; Kraak, V. I.; Allender, S.; Atkins, V. J.; Baker, P. I.; Bogard, J. R.; Brinsden, H.; Calvillo, A.; De Schutter, O.; Devarajan, R., The global syndemic of obesity, undernutrition, and climate change: the Lancet Commission report. *The lancet* **2019,** *393* (10173), 791-846.
9. Ogden, C. L.; Fryar, C. D.; Martin, C. B.; Freedman, D. S.; Carroll, M. D.; Gu, Q.; Hales, C. M., Trends in obesity prevalence by race and Hispanic origin—1999-2000 to 2017-2018. *Jama* **2020,** *324* (12), 1208-1210.
10. Organization, W. H., *Global action plan on physical activity 2018-2030: more active people for a healthier world*. World Health Organization: 2019.
11. Rosen, E. D.; Spiegelman, B. M., What we talk about when we talk about fat. *Cell* **2014,** *156* (1), 20-44.
12. Hirschhorn, J. N.; Daly, M. J., Genome-wide association studies for common diseases and complex traits. *Nature reviews genetics* **2005,** *6* (2), 95-108.
13. Wellen, K. E.; Hotamisligil, G. S., Inflammation, stress, and diabetes. *The Journal of clinical investigation* **2005,** *115* (5), 1111-1119.
14. Gregor, M. F.; Hotamisligil, G. S., Inflammatory mechanisms in obesity. *Annual review of immunology* **2011,** *29*, 415-445.
15. Arner, E.; Westermark, P. O.; Spalding, K. L.; Britton, T.; Rydén, M.; Frisén, J.; Bernard, S.; Arner, P., Adipocyte turnover: relevance to human adipose tissue morphology. *Diabetes* **2010,** *59* (1), 105-109.
16. Mathis, D., Immunological goings-on in visceral adipose tissue. *Cell metabolism* **2013,** *17* (6), 851-859.
17. Whittle, A. J.; Carobbio, S.; Martins, L.; Slawik, M.; Hondares, E.; Vázquez, M. J.; Morgan, D.; Csikasz, R. I.; Gallego, R.; Rodriguez-Cuenca, S., BMP8B increases brown

adipose tissue thermogenesis through both central and peripheral actions. *Cell* **2012,** *149* (4), 871-885.
18. Nagrath, S.; Sequist, L. V.; Maheswaran, S.; Bell, D. W.; Irimia, D.; Ulkus, L.; Smith, M. R.; Kwak, E. L.; Digumarthy, S.; Muzikansky, A., Isolation of rare circulating tumour cells in cancer patients by microchip technology. *Nature* **2007,** *450* (7173), 1235-1239.
19. Forbes, L.; Ebsworth-Mojica, K.; DiDone, L.; Li, S.-G.; Freundlich, J. S.; Connell, N.; Dunman, P. M.; Krysan, D. J., A high throughput screening assay for anti-mycobacterial small molecules based on adenylate kinase release as a reporter of cell lysis. *PLoS One* **2015,** *10* (6), e0129234.
20. Taylor, A. M.; Rhee, S. W.; Tu, C. H.; Cribbs, D. H.; Cotman, C. W.; Jeon, N. L., Microfluidic multicompartment device for neuroscience research. *Langmuir* **2003,** *19* (5), 1551-1556.
21. Altintas, Z.; Akgun, M.; Kokturk, G.; Uludag, Y., A fully automated microfluidic-based electrochemical sensor for real-time bacteria detection. *Biosensors and Bioelectronics* **2018,** *100*, 541-548.
22. Huh, D.; Matthews, B. D.; Mammoto, A.; Montoya-Zavala, M.; Hsin, H. Y.; Ingber, D. E., Reconstituting organ-level lung functions on a chip. *Science* **2010,** *328* (5986), 1662-1668.
23. Kim, K. M.; Choi, Y. J.; Hwang, J.-H.; Kim, A. R.; Cho, H. J.; Hwang, E. S.; Park, J. Y.; Lee, S.-H.; Hong, J.-H., Shear stress induced by an interstitial level of slow flow increases the osteogenic differentiation of mesenchymal stem cells through TAZ activation. *PloS one* **2014,** *9* (3), e92427.
24. Song, H.; Chen, D. L.; Ismagilov, R. F., Reactions in droplets in microfluidic channels. *Angewandte chemie international edition* **2006,** *45* (44), 7336-7356.
25. Whitesides, G. M., The origins and the future of microfluidics. *nature* **2006,** *442* (7101), 368-373.
26. Squires, T. M.; Quake, S. R., Microfluidics: Fluid physics at the nanoliter scale. *Reviews of modern physics* **2005,** *77* (3), 977.
27. Becker, H.; Gärtner, C., Polymer microfabrication technologies for microfluidic systems. *Analytical and bioanalytical chemistry* **2008,** *390*, 89-111.
28. Cabodi, M.; Choi, N. W.; Gleghorn, J. P.; Lee, C. S.; Bonassar, L. J.; Stroock, A. D., A microfluidic biomaterial. *Journal of the American Chemical Society* **2005,** *127* (40), 13788-13789.
29. Au, A. K.; Bhattacharjee, N.; Horowitz, L. F.; Chang, T. C.; Folch, A., 3D-printed microfluidic automation. *Lab on a Chip* **2015,** *15* (8), 1934-1941.
30. Alves, G.; Rodrigues, M.; Fortuna, A.; Falcão, A.; Queiroz, J., A critical review of microextraction by packed sorbent as a sample preparation approach in drug bioanalysis. *Bioanalysis* **2013,** *5* (11), 1409-1442.
31. Ding, Y.; Li, J.; Xiao, W.; Xiao, K.; Lee, J.; Bhardwaj, U.; Zhu, Z.; Digiglio, P.; Yang, G.; Lam, K. S., Microfluidic-enabled print-to-screen platform for high-throughput screening of combinatorial chemotherapy. *Analytical chemistry* **2015,** *87* (20), 10166-10171.
32. Wang, H.; Li, Y.-j.; Wei, J.-f.; Xu, J.-r.; Wang, Y.-h.; Zheng, G.-x., based three-dimensional microfluidic device for monitoring of heavy metals with a camera cell phone. *Analytical and bioanalytical chemistry* **2014,** *406*, 2799-2807.
33. Renardy, Y., The effects of confinement and inertia on the production of droplets. *Rheologica acta* **2007,** *46*, 521-529.

34. Wu, Z.; Nguyen, N.-T., Hydrodynamic focusing in microchannels under consideration of diffusive dispersion: theories and experiments. *Sensors and Actuators B: Chemical* **2005,** *107* (2), 965-974.
35. Martinez, A. W.; Phillips, S. T.; Butte, M. J.; Whitesides, G. M., Patterned paper as a platform for inexpensive, low-volume, portable bioassays. *Angewandte Chemie* **2007,** *119* (8), 1340-1342.
36. Kim, M. S.; Yeon, J. H.; Park, J.-K., A microfluidic platform for 3-dimensional cell culture and cell-based assays. *Biomedical microdevices* **2007,** *9*, 25-34.
37. Huh, D.; Hamilton, G. A.; Ingber, D. E., From 3D cell culture to organs-on-chips. *Trends in cell biology* **2011,** *21* (12), 745-754.
38. Gawad, S.; Schild, L.; Renaud, P., Micromachined impedance spectroscopy flow cytometer for cell analysis and particle sizing. *Lab on a Chip* **2001,** *1* (1), 76-82.
39. Tan, W.-H.; Takeuchi, S., A trap-and-release integrated microfluidic system for dynamic microarray applications. *Proceedings of the national academy of sciences* **2007,** *104* (4), 1146-1151.
40. Zhang, B.; Radisic, M., Organ-on-a-chip devices advance to market. *Lab on a Chip* **2017,** *17* (14), 2395-2420.
41. Kim, K.-T.; Lee, H. W.; Lee, H.-O.; Song, H. J.; Jeong, D. E.; Shin, S.; Kim, H.; Shin, Y.; Nam, D.-H.; Jeong, B. C., Application of single-cell RNA sequencing in optimizing a combinatorial therapeutic strategy in metastatic renal cell carcinoma. *Genome biology* **2016,** *17* (1), 1-17.
42. Mazutis, L.; Gilbert, J.; Ung, W. L.; Weitz, D. A.; Griffiths, A. D.; Heyman, J. A., Single-cell analysis and sorting using droplet-based microfluidics. *Nature protocols* **2013,** *8* (5), 870-891.
43. Gui, M.; Song, W.; Zhou, H.; Xu, J.; Chen, S.; Xiang, Y.; Wang, X., Cryo-electron microscopy structures of the SARS-CoV spike glycoprotein reveal a prerequisite conformational state for receptor binding. *Cell research* **2017,** *27* (1), 119-129.
44. Dendukuri, D.; Gu, S. S.; Pregibon, D. C.; Hatton, T. A.; Doyle, P. S., Stop-flow lithography in a microfluidic device. *Lab on a Chip* **2007,** *7* (7), 818-828.
45. Nobre, T. M.; Martynowycz, M. W.; Andreev, K.; Kuzmenko, I.; Nikaido, H.; Gidalevitz, D., Modification of Salmonella lipopolysaccharides prevents the outer membrane penetration of novobiocin. *Biophysical journal* **2015,** *109* (12), 2537-2545.
46. Xia, Y.; Whitesides, G. M., Soft lithography. *Annual review of materials science* **1998,** *28* (1), 153-184.
47. Darhuber, A. A.; Valentino, J. P.; Davis, J. M.; Troian, S. M.; Wagner, S., Microfluidic actuation by modulation of surface stresses. *Applied Physics Letters* **2003,** *82* (4), 657-659.
48. Guo, M. T.; Rotem, A.; Heyman, J. A.; Weitz, D. A., Droplet microfluidics for high-throughput biological assays. *Lab on a Chip* **2012,** *12* (12), 2146-2155.
49. Teh, S.-Y.; Lin, R.; Hung, L.-H.; Lee, A. P., Droplet microfluidics. *Lab on a Chip* **2008,** *8* (2), 198-220.
50. Wojtovich, A. P.; Wei, A. Y.; Sherman, T. A.; Foster, T. H.; Nehrke, K., Chromophore-assisted light inactivation of mitochondrial electron transport chain complex II in Caenorhabditis elegans. *Scientific reports* **2016,** *6* (1), 29695.
51. Hess, D.; Yang, T.; Stavrakis, S., Droplet-based optofluidic systems for measuring enzyme kinetics. *Analytical and bioanalytical chemistry* **2020,** *412*, 3265-3283.

52. Lou, X.; Hong, Y.; Chen, S.; Leung, C. W. T.; Zhao, N.; Situ, B.; Lam, J. W. Y.; Tang, B. Z., A selective glutathione probe based on AIE fluorogen and its application in enzymatic activity assay. *Scientific reports* **2014,** *4* (1), 4272.
53. Kim, J. W.; Utada, A. S.; Fernández-Nieves, A.; Hu, Z.; Weitz, D. A., Fabrication of monodisperse gel shells and functional microgels in microfluidic devices. *Angewandte chemie international edition* **2007,** *46* (11), 1819-1822.
54. Smith, J. D.; Ferris, A. E.; Heise, G. D.; Hinrichs, R. N.; Martin, P. E., Oscillation and reaction board techniques for estimating inertial properties of a below-knee prosthesis. *JoVE (Journal of Visualized Experiments)* **2014,** (87), e50977.
55. Kang, J. H.; Super, M.; Yung, C. W.; Cooper, R. M.; Domansky, K.; Graveline, A. R.; Mammoto, T.; Berthet, J. B.; Tobin, H.; Cartwright, M. J., An extracorporeal blood-cleansing device for sepsis therapy. *Nature medicine* **2014,** *20* (10), 1211-1216.
56. Macosko, E. Z.; Basu, A.; Satija, R.; Nemesh, J.; Shekhar, K.; Goldman, M.; Tirosh, I.; Bialas, A. R.; Kamitaki, N.; Martersteck, E. M., Highly parallel genome-wide expression profiling of individual cells using nanoliter droplets. *Cell* **2015,** *161* (5), 1202-1214.
57. Li, L.; Ismagilov, R. F., Protein crystallization using microfluidic technologies based on valves, droplets, and SlipChip. *Annual review of biophysics* **2010,** *39*, 139-158.
58. Takmakov, P.; Zachek, M. K.; Keithley, R. B.; Bucher, E. S.; McCarty, G. S.; Wightman, R. M., Characterization of local pH changes in brain using fast-scan cyclic voltammetry with carbon microelectrodes. *Analytical chemistry* **2010,** *82* (23), 9892-9900.
59. Khademhosseini, A.; Langer, R.; Borenstein, J.; Vacanti, J. P., Microscale technologies for tissue engineering and biology. *Proceedings of the National Academy of Sciences* **2006,** *103* (8), 2480-2487.
60. Andersson, H.; Van Den Berg, A., Microfabrication and microfluidics for tissue engineering: state of the art and future opportunities. *Lab on a Chip* **2004,** *4* (2), 98-103.
61. Lanza, R.; Langer, R.; Vacanti, J. P., *Principles of tissue engineering*. Academic press: 2011.
62. Khademhosseini, A.; Langer, R., A decade of progress in tissue engineering. *Nature protocols* **2016,** *11* (10), 1775.
63. Karageorgiou, V.; Kaplan, D., Porosity of 3D biomaterial scaffolds and osteogenesis. *Biomaterials* **2005,** *26* (27), 5474-5491.
64. Oladapo, B. I.; Zahedi, S.; Adeoye, A., 3D printing of bone scaffolds with hybrid biomaterials. *Composites Part B: Engineering* **2019,** *158*, 428-436.
65. Wu, J.; Brazile, B.; McMahan, S. R.; Liao, J.; Hong, Y., Heart valve tissue-derived hydrogels: Preparation and characterization of mitral valve chordae, aortic valve, and mitral valve gels. *Journal of Biomedical Materials Research Part B: Applied Biomaterials* **2019,** *107* (5), 1732-1740.
66. Poddar, S.; Agarwal, P. S.; Mahto, S. K., Preparation of psyllium husk powder based microporous composite scaffolds for tissue engineering. *Engineering of Biomaterials* **2018,** *21* (147).
67. Chen, C.; Mehl, B. T.; Sell, S. A.; Martin, R. S., Use of electrospinning and dynamic air focusing to create three-dimensional cell culture scaffolds in microfluidic devices. *Analyst* **2016,** *141* (18), 5311-5320.
68. Mehl, B. T.; Martin, R. S., Integrating 3D cell culture of PC12 cells with microchip-based electrochemical detection. *Analytical Methods* **2019,** *11* (8), 1064-1072.

69. Chen, C.; Townsend, A. D.; Sell, S. A.; Martin, R. S., Microchip-based 3D-cell culture using polymer nanofibers generated by solution blow spinning. *Analytical Methods* **2017,** *9* (22), 3274-3283.
70. Raeisdasteh Hokmabad, V.; Davaran, S.; Ramazani, A.; Salehi, R., Design and fabrication of porous biodegradable scaffolds: a strategy for tissue engineering. *Journal of Biomaterials science, Polymer edition* **2017,** *28* (16), 1797-1825.
71. Mellati, A.; Fan, C. M.; Tamayol, A.; Annabi, N.; Dai, S.; Bi, J.; Jin, B.; Xian, C.; Khademhosseini, A.; Zhang, H., Microengineered 3D cell-laden thermoresponsive hydrogels for mimicking cell morphology and orientation in cartilage tissue engineering. *Biotechnology and bioengineering* **2017,** *114* (1), 217-231.
72. Khademhosseini, A.; Langer, R., Microengineered hydrogels for tissue engineering. *Biomaterials* **2007,** *28* (34), 5087-5092.
73. Bertassoni, L. E.; Cecconi, M.; Manoharan, V.; Nikkhah, M.; Hjortnaes, J.; Cristino, A. L.; Barabaschi, G.; Demarchi, D.; Dokmeci, M. R.; Yang, Y., Hydrogel bioprinted microchannel networks for vascularization of tissue engineering constructs. *Lab on a Chip* **2014,** *14* (13), 2202-2211.
74. Novosel, E. C.; Kleinhans, C.; Kluger, P. J., Vascularization is the key challenge in tissue engineering. *Advanced drug delivery reviews* **2011,** *63* (4-5), 300-311.
75. Sekine, H.; Shimizu, T.; Sakaguchi, K.; Dobashi, I.; Wada, M.; Yamato, M.; Kobayashi, E.; Umezu, M.; Okano, T., In vitro fabrication of functional three-dimensional tissues with perfusable blood vessels. *Nature communications* **2013,** *4*, 1399.
76. Auger, F. A.; Gibot, L.; Lacroix, D., The pivotal role of vascularization in tissue engineering. *Annual review of biomedical engineering* **2013,** *15*, 177-200.
77. Chang, H.-I.; Wang, Y., Cell responses to surface and architecture of tissue engineering scaffolds. In *Regenerative medicine and tissue engineering-cells and biomaterials*, InTechOpen: 2011.
78. Gaspar, D. A.; Gomide, V.; Monteiro, F. J., The role of perfusion bioreactors in bone tissue engineering. *Biomatter* **2012,** *2* (4), 167-175.
79. Sung, J. H.; Esch, M. B.; Prot, J.-M.; Long, C. J.; Smith, A.; Hickman, J. J.; Shuler, M. L., Microfabricated mammalian organ systems and their integration into models of whole animals and humans. *Lab on a Chip* **2013,** *13* (7), 1201-1212.
80. Godwin, L. A.; Pilkerton, M. E.; Deal, K. S.; Wanders, D.; Judd, R. L.; Easley, C. J., Passively operated microfluidic device for stimulation and secretion sampling of single pancreatic islets. *Anal Chem* **2011,** *83* (18), 7166-72.
81. Godwin, L. A.; Brooks, J. C.; Hoepfner, L. D.; Wanders, D.; Judd, R. L.; Easley, C. J., A microfluidic interface for the culture and sampling of adiponectin from primary adipocytes. *Analyst* **2015,** *140* (4), 1019-25.
82. Brooks, J. C.; Ford, K. I.; Holder, D. H.; Holtan, M. D.; Easley, C. J., Macro-to-micro interfacing to microfluidic channels using 3D-printed templates: application to time-resolved secretion sampling of endocrine tissue. *Analyst* **2016,** *141* (20), 5714-5721.
83. Li, X.; Brooks, J. C.; Hu, J.; Ford, K. I.; Easley, C. J., 3D-templated, fully automated microfluidic input/output multiplexer for endocrine tissue culture and secretion sampling. *Lab Chip* **2017,** *17* (2), 341-349.
84. Li, X.; Hu, J.; Easley, C. J., Automated microfluidic droplet sampling with integrated, mix-and-read immunoassays to resolve endocrine tissue secretion dynamics. *Lab Chip* **2018,** *18* (19), 2926-2935.

85. Adams, A. G.; Bulusu, R. K. M.; Mukhitov, N.; Mendoza-Cortes, J. L.; Roper, M. G., Online measurement of glucose consumption from HepG2 cells using an integrated bioreactor and enzymatic assay. *Analytical chemistry* **2019,** *91* (8), 5184-5190.
86. Bandak, B.; Yi, L.; Roper, M. G., Microfluidic-enabled quantitative measurements of insulin release dynamics from single islets of Langerhans in response to 5-palmitic acid hydroxy stearic acid. *Lab on a Chip* **2018,** *18* (18), 2873-2882.
87. Lu, S.; Dugan, C. E.; Kennedy, R. T., Microfluidic Chip with Integrated Electrophoretic Immunoassay for Investigating Cell–Cell Interactions. *Analytical chemistry* **2018,** *90* (8), 5171-5178.
88. Dugan, C. E.; Grinias, J. P.; Parlee, S. D.; El-Azzouny, M.; Evans, C. R.; Kennedy, R. T., Monitoring cell secretions on microfluidic chips using solid-phase extraction with mass spectrometry. *Anal Bioanal Chem* **2017,** *409* (1), 169-178.
89. Kaestli, A. J.; Junkin, M.; Tay, S., Integrated platform for cell culture and dynamic quantification of cell secretion. *Lab on a Chip* **2017,** *17* (23), 4124-4133.
90. Lin, J.; Jordi, C.; Son, M.; Van Phan, H.; Drayman, N.; Abasiyanik, M. F.; Vistain, L.; Tu, H.-L.; Tay, S., Ultra-sensitive digital quantification of proteins and mRNA in single cells. *Nature communications* **2019,** *10* (1), 1-10.
91. Dettinger, P.; Frank, T.; Etzrodt, M.; Ahmed, N.; Reimann, A.; Trenzinger, C.; Loeffler, D.; Kokkaliaris, K. D.; Schroeder, T.; Tay, S., Automated Microfluidic System for Dynamic Stimulation and Tracking of Single Cells. *Anal Chem* **2018,** *90* (18), 10695-10700.
92. Loskill, P.; Sezhian, T.; Tharp, K. M.; Lee-Montiel, F. T.; Jeeawoody, S.; Reese, W. M.; Zushin, P. H.; Stahl, A.; Healy, K. E., WAT-on-a-chip: a physiologically relevant microfluidic system incorporating white adipose tissue. *Lab Chip* **2017,** *17* (9), 1645-1654.
93. Zhao, Y.; Rafatian, N.; Feric, N. T.; Cox, B. J.; Aschar-Sobbi, R.; Wang, E. Y.; Aggarwal, P.; Zhang, B.; Conant, G.; Ronaldson-Bouchard, K.; Pahnke, A.; Protze, S.; Lee, J. H.; Davenport Huyer, L.; Jekic, D.; Wickeler, A.; Naguib, H. E.; Keller, G. M.; Vunjak-Novakovic, G.; Broeckel, U.; Backx, P. H.; Radisic, M., A Platform for Generation of Chamber-Specific Cardiac Tissues and Disease Modeling. *Cell* **2019,** *176* (4), 913-927.e18.
94. Easley, C. J.; Karlinsey, J. M.; Bienvenue, J. M.; Legendre, L. A.; Roper, M. G.; Feldman, S. H.; Hughes, M. A.; Hewlett, E. L.; Merkel, T. J.; Ferrance, J. P., A fully integrated microfluidic genetic analysis system with sample-in–answer-out capability. *Proceedings of the National Academy of Sciences* **2006,** *103* (51), 19272-19277.
95. Easley, C. J.; Rocheleau, J. V.; Head, W. S.; Piston, D. W., Quantitative measurement of zinc secretion from pancreatic islets with high temporal resolution using droplet-based microfluidics. *Analytical chemistry* **2009,** *81* (21), 9086-9095.
96. Hu, J.; Li, X.; Judd, R. L.; Easley, C. J., Rapid Lipolytic Oscillations in Ex-Vivo Adipose Tissue Explants Revealed Through Microfluidic Droplet Sampling at High Temporal Resolution. *Lab Chip* **2020,** *under revision*.
97. Sciambi, A.; Abate, A. R., Accurate microfluidic sorting of droplets at 30 kHz. *Lab on a Chip* **2015,** *15* (1), 47-51.
98. Sahore, V.; Doonan, S. R.; Bailey, R. C., Droplet microfluidics in thermoplastics: device fabrication, droplet generation, and content manipulation using integrated electric and magnetic fields. *Analytical methods* **2018,** *10* (35), 4264-4274.
99. Clark, I. C.; Thakur, R.; Abate, A. R., Concentric electrodes improve microfluidic droplet sorting. *Lab on a Chip* **2018,** *18* (5), 710-713.

100. Zhang, P.; Chen, C.; Guo, F.; Philippe, J.; Gu, Y.; Tian, Z.; Bachman, H.; Ren, L.; Yang, S.; Zhong, Z., Contactless, programmable acoustofluidic manipulation of objects on water. *Lab on a Chip* **2019**.
101. Tian, Z.; Yang, S.; Huang, P.-H.; Wang, Z.; Zhang, P.; Gu, Y.; Bachman, H.; Chen, C.; Wu, M.; Xie, Y., Wave number–spiral acoustic tweezers for dynamic and reconfigurable manipulation of particles and cells. *Science advances* **2019,** *5* (5), eaau6062.
102. Doonan, S. R.; Lin, M.; Bailey, R. C., Droplet CAR-Wash: continuous picoliter-scale immunocapture and washing. *Lab on a Chip* **2019,** *19* (9), 1589-1598.
103. Gilliland Jr, W. M.; Mellors, J. S.; Ramsey, J. M., Coupling microchip electrospray ionization devices with high pressure mass spectrometry. *Analytical chemistry* **2017,** *89* (24), 13320-13325.
104. Steyer, D. J.; Kennedy, R. T., High-Throughput Nanoelectrospray Ionization-Mass Spectrometry Analysis of Microfluidic Droplet Samples. *Analytical chemistry* **2019**.
105. Wang, X.; Yi, L.; Roper, M. G., Microfluidic device for the measurement of amino acid secretion dynamics from murine and human islets of Langerhans. *Analytical chemistry* **2016,** *88* (6), 3369-3375.
106. Jin, S.; Furtaw, M. D.; Chen, H.; Lamb, D. T.; Ferguson, S. A.; Arvin, N. E.; Dawod, M.; Kennedy, R. T., Multiplexed Western blotting using microchip electrophoresis. *Analytical chemistry* **2016,** *88* (13), 6703-6710.
107. Reid, K. R.; Kennedy, R. T., Continuous operation of microfabricated electrophoresis devices for 24 hours and application to chemical monitoring of living cells. *Analytical chemistry* **2009,** *81* (16), 6837-6842.
108. Yi, L.; Wang, X.; Dhumpa, R.; Schrell, A. M.; Mukhitov, N.; Roper, M. G., Integrated perfusion and separation systems for entrainment of insulin secretion from islets of Langerhans. *Lab Chip* **2015,** *15* (3), 823-32.
109. Zhu, Y.; Fang, Q., Analytical detection techniques for droplet microfluidics—A review. *Analytica chimica acta* **2013,** *787*, 24-35.
110. Chiu, D. T.; Lorenz, R. M.; Jeffries, G. D., Droplets for ultrasmall-volume analysis. ACS Publications: 2009.
111. Zheng, F.; Fu, F.; Cheng, Y.; Wang, C.; Zhao, Y.; Gu, Z., Organ-on-a-Chip Systems: Microengineering to Biomimic Living Systems. *Small* **2016,** *12* (17), 2253-2282.
112. Schrell, A. M.; Mukhitov, N.; Yi, L.; Adablah, J. E.; Menezes, J.; Roper, M. G., Online fluorescence anisotropy immunoassay for monitoring insulin secretion from islets of Langerhans. *Analytical Methods* **2017,** *9* (1), 38-45.
113. Tang, M. Y.; Shum, H. C., One-step immunoassay of C-reactive protein using droplet microfluidics. *Lab on a Chip* **2016,** *16* (22), 4359-4365.
114. Gao, R.; Cheng, Z.; deMello, A. J.; Choo, J., Wash-free magnetic immunoassay of the PSA cancer marker using SERS and droplet microfluidics. *Lab on a Chip* **2016,** *16* (6), 1022-1029.
115. Chaipan, C.; Pryszlak, A.; Dean, H.; Poignard, P.; Benes, V.; Griffiths, A. D.; Merten, C. A., Single-virus droplet microfluidics for high-throughput screening of neutralizing epitopes on HIV particles. *Cell chemical biology* **2017,** *24* (6), 751-757. e3.
116. Huang, M.; Bai, Y.; Sjostrom, S. L.; Hallström, B. M.; Liu, Z.; Petranovic, D.; Uhlén, M.; Joensson, H. N.; Andersson-Svahn, H.; Nielsen, J., Microfluidic screening and whole-genome sequencing identifies mutations associated with improved protein secretion by yeast. *Proceedings of the National Academy of Sciences* **2015,** *112* (34), E4689-E4696.

117. Song, H.; Ismagilov, R. F., Millisecond kinetics on a microfluidic chip using nanoliters of reagents. *J Am Chem Soc* **2003,** *125* (47), 14613-9.
118. Negou, J. T.; Avila, L. A.; Li, X.; Hagos, T. M.; Easley, C. J., Automated Microfluidic Droplet-Based Sample Chopper for Detection of Small Fluorescence Differences Using Lock-In Analysis. *Anal Chem* **2017,** *89* (11), 6153-6159.
119. Cole, R. H.; Tang, S.-Y.; Siltanen, C. A.; Shahi, P.; Zhang, J. Q.; Poust, S.; Gartner, Z. J.; Abate, A. R., Printed droplet microfluidics for on demand dispensing of picoliter droplets and cells. *Proceedings of the National Academy of Sciences* **2017,** *114* (33), 8728-8733.
120. Klein, A. M.; Mazutis, L.; Akartuna, I.; Tallapragada, N.; Veres, A.; Li, V.; Peshkin, L.; Weitz, D. A.; Kirschner, M. W., Droplet barcoding for single-cell transcriptomics applied to embryonic stem cells. *Cell* **2015,** *161* (5), 1187-1201.
121. Del Ben, F.; Turetta, M.; Celetti, G.; Piruska, A.; Bulfoni, M.; Cesselli, D.; Huck, W. T.; Scoles, G., A Method for Detecting Circulating Tumor Cells Based on the Measurement of Single-Cell Metabolism in Droplet-Based Microfluidics. *Angewandte Chemie International Edition* **2016,** *55* (30), 8581-8584.
122. Segaliny, A. I.; Li, G.; Kong, L.; Ren, C.; Chen, X.; Wang, J. K.; Baltimore, D.; Wu, G.; Zhao, W., Functional TCR T cell screening using single-cell droplet microfluidics. *Lab on a Chip* **2018,** *18* (24), 3733-3749.
123. Honegger, P., Overview of cell and tissue culture techniques. *Curr Protoc Pharmacol* **2001,** *Chapter 12*, Unit12 1.
124. Sittinger, M.; Bujia, J.; Rotter, N.; Reitzel, D.; Minuth, W. W.; Burmester, G. R., Tissue engineering and autologous transplant formation: practical approaches with resorbable biomaterials and new cell culture techniques. *Biomaterials* **1996,** *17* (3), 237-42.
125. Al-Lamki, R. S.; Bradley, J. R.; Pober, J. S., Human Organ Culture: Updating the Approach to Bridge the Gap from In Vitro to In Vivo in Inflammation, Cancer, and Stem Cell Biology. *Front Med (Lausanne)* **2017,** *4*, 148.
126. Phelan, K.; May, K. M., Mammalian Cell Tissue Culture Techniques. *Curr Protoc Mol Biol* **2017,** *117*, A 3F 1-A 3F 23.
127. Carter, M.; Shieh, J. C., *Guide to Research Techniques in Neuroscience*. Elsevier Academic Press Inc: San Diego, 2010; p 1-375.
128. Klaunig, J. E.; Goldblatt, P. J.; Hinton, D. E.; Lipsky, M. M.; Trump, B. F., Mouse liver cell culture. II. Primary culture. *In Vitro* **1981,** *17* (10), 926-34.
129. Benninger, R. K.; Zhang, M.; Head, W. S.; Satin, L. S.; Piston, D. W., Gap junction coupling and calcium waves in the pancreatic islet. *Biophys J* **2008,** *95* (11), 5048-61.
130. Ulrich, A. B.; Schmied, B. M.; Standop, J.; Schneider, M. B.; Pour, P. M., Pancreatic cell lines: a review. *Pancreas* **2002,** *24* (2), 111-20.
131. Bhatia, S. N.; Ingber, D. E., Microfluidic organs-on-chips. *Nat Biotechnol* **2014,** *32* (8), 760-72.
132. Whitesides, G. M., The origins and the future of microfluidics. *Nature* **2006,** *442* (7101), 368-73.
133. Young, E. W.; Beebe, D. J., Fundamentals of microfluidic cell culture in controlled microenvironments. *Chem Soc Rev* **2010,** *39* (3), 1036-48.
134. Agarwal, A.; Goss, J. A.; Cho, A.; McCain, M. L.; Parker, K. K., Microfluidic heart on a chip for higher throughput pharmacological studies. *Lab Chip* **2013,** *13* (18), 3599-608.
135. Barbulovic-Nad, I.; Au, S. H.; Wheeler, A. R., A microfluidic platform for complete mammalian cell culture. *Lab Chip* **2010,** *10* (12), 1536-42.

136. Mandenius, C. F., Conceptual Design of Micro-Bioreactors and Organ-on-Chips for Studies of Cell Cultures. *Bioengineering (Basel)* **2018,** *5* (3).
137. Hemmerich, J.; Noack, S.; Wiechert, W.; Oldiges, M., Microbioreactor Systems for Accelerated Bioprocess Development. *Biotechnol J* **2018,** *13* (4), e1700141.
138. Hubka, V.; Eder, W. E., *Design Science: Introduction to the Needs, Scope and Organization of Engineering Design Knowledge*. Springer-Verlag London: London, UK, 1996; p XVI, 251.
139. Rexius-Hall, M. L.; Rehman, J.; Eddington, D. T., A microfluidic oxygen gradient demonstrates differential activation of the hypoxia-regulated transcription factors HIF-1alpha and HIF-2alpha. *Integr Biol (Camb)* **2017,** *9* (9), 742-750.
140. Nourmohammadzadeh, M.; Lo, J. F.; Bochenek, M.; Mendoza-Elias, J. E.; Wang, Q.; Li, Z.; Zeng, L.; Qi, M.; Eddington, D. T.; Oberholzer, J.; Wang, Y., Microfluidic Array with Integrated Oxygenation Control for Real-Time Live-Cell Imaging: Effect of Hypoxia on Physiology of Microencapsulated Pancreatic Islets. *Analytical Chemistry* **2013,** *85* (23), 11240-11249.
141. Lee, K. S.; Boccazzi, P.; Sinskey, A. J.; Ram, R. J., Microfluidic chemostat and turbidostat with flow rate, oxygen, and temperature control for dynamic continuous culture. *Lab Chip* **2011,** *11* (10), 1730-9.
142. Ertl, P.; Sticker, D.; Charwat, V.; Kasper, C.; Lepperdinger, G., Lab-on-a-chip technologies for stem cell analysis. *Trends Biotechnol* **2014,** *32* (5), 245-53.
143. Khademhosseini, A.; Yeh, J.; Jon, S.; Eng, G.; Suh, K. Y.; Burdick, J. A.; Langer, R., Molded polyethylene glycol microstructures for capturing cells within microfluidic channels. *Lab Chip* **2004,** *4* (5), 425-30.
144. Skelley, A. M.; Kirak, O.; Suh, H.; Jaenisch, R.; Voldman, J., Microfluidic control of cell pairing and fusion. *Nat Methods* **2009,** *6* (2), 147-52.
145. Kobel, S. A.; Burri, O.; Griffa, A.; Girotra, M.; Seitz, A.; Lutolf, M. P., Automated analysis of single stem cells in microfluidic traps. *Lab Chip* **2012,** *12* (16), 2843-9.
146. Zhang, W.; Kai, K.; Choi, D. S.; Iwamoto, T.; Nguyen, Y. H.; Wong, H.; Landis, M. D.; Ueno, N. T.; Chang, J.; Qin, L., Microfluidics separation reveals the stem-cell-like deformability of tumor-initiating cells. *Proc Natl Acad Sci U S A* **2012,** *109* (46), 18707-12.
147. Jiang, Z.; Xia, B.; McBride, R.; Oakey, J., A microfluidic-based cell encapsulation platform to achieve high long-term cell viability in photopolymerized PEGNB hydrogel microspheres. *J Mater Chem B* **2017,** *5* (1), 173-180.
148. Atac, B.; Wagner, I.; Horland, R.; Lauster, R.; Marx, U.; Tonevitsky, A. G.; Azar, R. P.; Lindner, G., Skin and hair on-a-chip: in vitro skin models versus ex vivo tissue maintenance with dynamic perfusion. *Lab Chip* **2013,** *13* (18), 3555-61.
149. Xiao, S.; Coppeta, J. R.; Rogers, H. B.; Isenberg, B. C.; Zhu, J.; Olalekan, S. A.; McKinnon, K. E.; Dokic, D.; Rashedi, A. S.; Haisenleder, D. J.; Malpani, S. S.; Arnold-Murray, C. A.; Chen, K.; Jiang, M.; Bai, L.; Nguyen, C. T.; Zhang, J.; Laronda, M. M.; Hope, T. J.; Maniar, K. P.; Pavone, M. E.; Avram, M. J.; Sefton, E. C.; Getsios, S.; Burdette, J. E.; Kim, J. J.; Borenstein, J. T.; Woodruff, T. K., A microfluidic culture model of the human reproductive tract and 28-day menstrual cycle. *Nat Commun* **2017,** *8*, 14584.
150. McLean, I. C.; Schwerdtfeger, L. A.; Tobet, S. A.; Henry, C. S., Powering ex vivo tissue models in microfluidic systems. *Lab Chip* **2018,** *18* (10), 1399-1410.

151. Halldorsson, S.; Lucumi, E.; Gomez-Sjoberg, R.; Fleming, R. M. T., Advantages and challenges of microfluidic cell culture in polydimethylsiloxane devices. *Biosens Bioelectron* **2015,** *63*, 218-231.
152. Xu, B. Y.; Hu, S. W.; Qian, G. S.; Xu, J. J.; Chen, H. Y., A novel microfluidic platform with stable concentration gradient for on chip cell culture and screening assays. *Lab Chip* **2013,** *13* (18), 3714-20.
153. Agarwal, P.; Zhao, S.; Bielecki, P.; Rao, W.; Choi, J. K.; Zhao, Y.; Yu, J.; Zhang, W.; He, X., One-step microfluidic generation of pre-hatching embryo-like core-shell microcapsules for miniaturized 3D culture of pluripotent stem cells. *Lab Chip* **2013,** *13* (23), 4525-33.
154. Lan, F.; Demaree, B.; Ahmed, N.; Abate, A. R., Single-cell genome sequencing at ultra-high-throughput with microfluidic droplet barcoding. *Nature biotechnology* **2017,** *35* (7), 640.
155. Guo, S.; Lin, W. N.; Hu, Y.; Sun, G.; Phan, D.-T.; Chen, C.-H., Ultrahigh-throughput droplet microfluidic device for single-cell miRNA detection with isothermal amplification. *Lab on a Chip* **2018,** *18* (13), 1914-1920.
156. Kim, S. C.; Clark, I. C.; Shahi, P.; Abate, A. R., Single-cell RT-PCR in microfluidic droplets with integrated chemical lysis. *Analytical chemistry* **2018,** *90* (2), 1273-1279.
157. Cedillo-Alcantar, D. F.; Han, Y. D.; Choi, J.; Garcia-Cordero, J. L.; Revzin, A., Automated Droplet-Based Microfluidic Platform for Multiplexed Analysis of Biochemical Markers in Small Volumes. *Analytical chemistry* **2019,** *91* (8), 5133-5141.
158. Abatemarco, J.; Sarhan, M. F.; Wagner, J. M.; Lin, J.-L.; Liu, L.; Hassouneh, W.; Yuan, S.-F.; Alper, H. S.; Abate, A. R., RNA-aptamers-in-droplets (RAPID) high-throughput screening for secretory phenotypes. *Nature communications* **2017,** *8* (1), 332.
159. Wang, J.; Ramakrishnan, R.; Tang, Z.; Fan, W.; Kluge, A.; Dowlati, A.; Jones, R. C.; Ma, P. C., Quantifying EGFR alterations in the lung cancer genome with nanofluidic digital PCR arrays. *Clinical chemistry* **2010,** *56* (4), 623-632.
160. Rissin, D. M.; Kan, C. W.; Campbell, T. G.; Howes, S. C.; Fournier, D. R.; Song, L.; Piech, T.; Patel, P. P.; Chang, L.; Rivnak, A. J., Single-molecule enzyme-linked immunosorbent assay detects serum proteins at subfemtomolar concentrations. *Nature biotechnology* **2010,** *28* (6), 595.
161. Basu, A. S., Digital assays part I: partitioning statistics and digital PCR. *SLAS TECHNOLOGY: Translating Life Sciences Innovation* **2017,** *22* (4), 369-386.
162. Du, W.; Li, L.; Nichols, K. P.; Ismagilov, R. F., SlipChip. *Lab on a Chip* **2009,** *9* (16), 2286-2292.
163. Shen, F.; Sun, B.; Kreutz, J. E.; Davydova, E. K.; Du, W.; Reddy, P. L.; Joseph, L. J.; Ismagilov, R. F., Multiplexed quantification of nucleic acids with large dynamic range using multivolume digital RT-PCR on a rotational SlipChip tested with HIV and hepatitis C viral load. *Journal of the American Chemical Society* **2011,** *133* (44), 17705-17712.
164. Shen, F.; Du, W.; Davydova, E. K.; Karymov, M. A.; Pandey, J.; Ismagilov, R. F., Nanoliter multiplex PCR arrays on a SlipChip. *Analytical chemistry* **2010,** *82* (11), 4606-4612.
165. Shen, F.; Davydova, E. K.; Du, W.; Kreutz, J. E.; Piepenburg, O.; Ismagilov, R. F., Digital isothermal quantification of nucleic acids via simultaneous chemical initiation of recombinase polymerase amplification reactions on SlipChip. *Analytical chemistry* **2011,** *83* (9), 3533-3540.
166. Manz, A.; Graber, N.; Widmer, H. M., Miniaturized total chemical analysis systems: A novel concept for chemical sensing. *Sensors and Actuators B: Chemical* **1990,** *1* (1), 244-248.

167. Le Roux, D.; Root, B. E.; Hickey, J. A.; Scott, O. N.; Tsuei, A.; Li, J.; Saul, D. J.; Chassagne, L.; Landers, J. P.; De Mazancourt, P., An integrated sample-in-answer-out microfluidic chip for rapid human identification by STR analysis. *Lab on a Chip* **2014,** *14* (22), 4415-4425.
168. Sonker, M.; Parker, E. K.; Nielsen, A. V.; Sahore, V.; Woolley, A. T., Electrokinetically operated microfluidic devices for integrated immunoaffinity monolith extraction and electrophoretic separation of preterm birth biomarkers. *Analyst* **2018,** *143* (1), 224-231.
169. Skardal, A.; Murphy, S. V.; Devarasetty, M.; Mead, I.; Kang, H.-W.; Seol, Y.-J.; Zhang, Y. S.; Shin, S.-R.; Zhao, L.; Aleman, J., Multi-tissue interactions in an integrated three-tissue organ-on-a-chip platform. *Scientific reports* **2017,** *7* (1), 8837.
170. Deal, K. S.; Easley, C. J., Self-regulated, droplet-based sample chopper for microfluidic absorbance detection. *Anal Chem* **2012,** *84* (3), 1510-6.
171. Negou, J. T.; Hu, J.; Li, X.; Easley, C. J., Advancement of analytical modes in a multichannel, microfluidic droplet-based sample chopper employing phase-locked detection. *Anal Methods* **2018,** *10* (28), 3436-3443.
172. Unger, M. A.; Chou, H.-P.; Thorsen, T.; Scherer, A.; Quake, S. R., Monolithic microfabricated valves and pumps by multilayer soft lithography. *Science* **2000,** *288* (5463), 113-116.
173. Gilon, P.; Ravier, M. A.; Jonas, J.-C.; Henquin, J.-C., Control mechanisms of the oscillations of insulin secretion in vitro and in vivo. *Diabetes* **2002,** *51* (suppl 1), S144-S151.
174. Siltanen, C.; Diakatou, M.; Lowen, J.; Haque, A.; Rahimian, A.; Stybayeva, G.; Revzin, A., One step fabrication of hydrogel microcapsules with hollow core for assembly and cultivation of hepatocyte spheroids. *Acta biomaterialia* **2017,** *50*, 428-436.
175. Chen, Q.; Utech, S.; Chen, D.; Prodanovic, R.; Lin, J.-M.; Weitz, D. A., Controlled assembly of heterotypic cells in a core–shell scaffold: organ in a droplet. *Lab on a Chip* **2016,** *16* (8), 1346-1349.
176. Au, S. H.; Chamberlain, M. D.; Mahesh, S.; Sefton, M. V.; Wheeler, A. R., Hepatic organoids for microfluidic drug screening. *Lab on a Chip* **2014,** *14* (17), 3290-3299.
177. Cabrera, O.; Berman, D. M.; Kenyon, N. S.; Ricordi, C.; Berggren, P.-O.; Caicedo, A., The unique cytoarchitecture of human pancreatic islets has implications for islet cell function. *Proceedings of the National Academy of Sciences* **2006,** *103* (7), 2334-2339.
178. Chen, W.; Shu, Z.; Gao, D.; Shen, A. Q., Sensing and Sensibility: Single-Islet-based Quality Control Assay of Cryopreserved Pancreatic Islets with Functionalized Hydrogel Microcapsules. *Advanced healthcare materials* **2016,** *5* (2), 223-231.
179. Liu, H. T.; Wang, H.; Wei, W. B.; Liu, H.; Jiang, L.; Qin, J. H., A Microfluidic Strategy for Controllable Generation of Water-in-Water Droplets as Biocompatible Microcarriers. *Small* **2018,** *14* (36), 1801095.
180. Chen, D.; Du, W.; Liu, Y.; Liu, W.; Kuznetsov, A.; Mendez, F. E.; Philipson, L. H.; Ismagilov, R. F., The chemistrode: a droplet-based microfluidic device for stimulation and recording with high temporal, spatial, and chemical resolution. *Proceedings of the National Academy of Sciences* **2008,** *105* (44), 16843-16848.
181. Fantuzzi, G., Adipose tissue, adipokines, and inflammation. *Journal of Allergy and clinical immunology* **2005,** *115* (5), 911-919.
182. Kershaw, E. E.; Flier, J. S., Adipose tissue as an endocrine organ. *Journal of Clinical Endocrinology & Metabolism* **2004,** *89* (6), 2548-2556.

183. Li, X.; Easley, C. J., Microfluidic systems for studying dynamic function of adipocytes and adipose tissue. *Anal Bioanal Chem* **2018,** *410* (3), 791-800.
184. Sakai, S.; Ito, S.; Inagaki, H.; Hirose, K.; Matsuyama, T.; Taya, M.; Kawakami, K., Cell-enclosing gelatin-based microcapsule production for tissue engineering using a microfluidic flow-focusing system. *Biomicrofluidics* **2011,** *5* (1), 013402.
185. Deveza, L.; Ashoken, J.; Castaneda, G.; Tong, X.; Keeney, M.; Han, L.-H.; Yang, F., Microfluidic synthesis of biodegradable polyethylene-glycol microspheres for controlled delivery of proteins and DNA nanoparticles. *ACS Biomaterials Science & Engineering* **2015,** *1* (3), 157-165.
186. Karimi, M.; Bahrami, S.; Mirshekari, H.; Basri, S. M. M.; Nik, A. B.; Aref, A. R.; Akbari, M.; Hamblin, M. R., Microfluidic systems for stem cell-based neural tissue engineering. *Lab on a Chip* **2016,** *16* (14), 2551-2571.
187. Shin, Y.; Han, S.; Jeon, J. S.; Yamamoto, K.; Zervantonakis, I. K.; Sudo, R.; Kamm, R. D.; Chung, S., Microfluidic assay for simultaneous culture of multiple cell types on surfaces or within hydrogels. *Nature protocols* **2012,** *7* (7), 1247.
188. Harink, B.; Le Gac, S.; Truckenmüller, R.; van Blitterswijk, C.; Habibovic, P., Regeneration-on-a-chip? The perspectives on use of microfluidics in regenerative medicine. *Lab on a Chip* **2013,** *13* (18), 3512-3528.
189. Ghorbanian, S.; Qasaimeh, M. A.; Akbari, M.; Tamayol, A.; Juncker, D., Microfluidic direct writer with integrated declogging mechanism for fabricating cell-laden hydrogel constructs. *Biomedical microdevices* **2014,** *16* (3), 387-395.
190. Alessandri, K.; Feyeux, M.; Gurchenkov, B.; Delgado, C.; Trushko, A.; Krause, K.-H.; Vignjević, D.; Nassoy, P.; Roux, A., A 3D printed microfluidic device for production of functionalized hydrogel microcapsules for culture and differentiation of human Neuronal Stem Cells (hNSC). *Lab on a Chip* **2016,** *16* (9), 1593-1604.
191. Shi, W.; Wen, H.; Lu, Y.; Shi, Y.; Lin, B.; Qin, J., Droplet microfluidics for characterizing the neurotoxin-induced responses in individual Caenorhabditis elegans. *Lab on a Chip* **2010,** *10* (21), 2855-2863.

Chapter 2

Microfluidic digital-to-analog converter (μDAC) to rapidly stimulate *ex vivo* tissue explants and quantify non-esterified fatty acid (NEFA) uptake rates

This chapter is adopted from the in-preparation publication "Microfluidic digital-to-analog converter (μDAC) to rapidly stimulate ex vivo tissue explants and quantify nonesterified fatty acid (NEFA) uptake rates" (Md Moniruzzaman,[a] Nan Shi,[a] and Christopher J. Easley[a])*

2.1 Introduction

The rising prevalence of obesity[1] has drawn attention to the importance of understanding the biology of adipose tissues (fat tissues). Adipose tissues, comprising 5% to 50% of human bodyweight, play a pivotal role in energy homeostasis. According to recent research, adipose tissue is a crucial and multifaceted metabolic and endocrine organ with significant systemic impacts, potentially disrupting the operation of almost all other organ systems[2]. Alterations in the uptake dynamics of lipids, such as glycerol and noon-esterified free fatty acids (NFFA), can occur in various physiological and pathological conditions due to the inactivation of their stimulating enzymes. Changes in NFFA uptake dynamics can activate different pathologies, such as cardiac hypoxia[3], intestinal malabsorption[4] and brown adipose tissue (BAT)[5] might happen in metabolic processes due to change in NFFA uptake dynamics. Adipocytes naturally absorb and store excess energy obtained from ingested food, including glucose and NFFA, and transform them into

triacylglycerol during lipogenesis for long-term storage, which is used for regulating other body tissues. Excessive intake of energy from food or the bloodstream increases the uptake amount of NFFA by lipogenesis, leading to insulin resistance in skeleton muscle[6], pancreatic β-cells[7], liver[8], hepatosteatosis[9], cardiac myopathies[10], and lipotoxicity[11] in heart. Pharmacological interventions, such as the anti-cancer drug doxorubicin, cause cardiac metabolic transformation[12], which also contributes to the changes in NFFA uptake dynamics. The localization and quantification of NFFA uptake and lipid flux have various implications for basic biological research as well as disease diagnosis and drug discovery.

Adipose tissue has been shown to be closely related to various diseases, including diabetes, Alzheimer's disease, and compromised immunity[13-15]. Although our understanding of adipose tissue has improved significantly in recent decades, the specific functions and mechanisms related to its metabolism and nutrient uptake still remain a mystery due to the limitations of traditional bioanalytical methodology. For instance, conventional techniques used for tissue analysis have a temporal resolution ranging from minutes to hours, which may cause loss of important biological information[16]. Furthermore, traditional tube- or well-based sampling requires a large number of tissues and cells, and the results obtained from static culture systems are significantly different from those obtained in vivo[17]. The challenges caused by the buoyancy of adipocytes also limit the development of conventional tools for adipose tissue analysis[18].

Currently, limited techniques and methods exist to investigate the dynamic function of adipose tissue in small amounts. In recent years, microfluidics has emerged as an effective tool for cell and tissue culture and bioanalysis[19-24]. Microfluidic chips provide an ideal platform for cellular growth, proliferation, and response to stimuli in conjunction with material and 3D printing technology[24,

[25]. The microscale channels and reservoirs not only offer a large surface-to-volume ratio but also closely mimic the in vivo environment[26]. The main advantage of microfluidics is the ability to collect and access metabolites from cells or single cells, which are typically present at ultra-low volumes and concentrations. This technology significantly improves our understanding of the metabolic activities of cells and organs under different conditions[1, 27]. To investigate the dynamic changes of specific metabolites such as glucose, insulin, glycerol, and fatty acids in the liver, pancreas, and adipose tissue, microfluidic systems integrating multiplexed functions like cellular culture, sampling, and monitoring have been developed by various research groups, including ours[1, 16, 20, 24, 28-30]. Our group, along with the Kennedy and Roper group, has made significant efforts in developing high-resolution sampling in continuous-flow systems and automated droplet-based microfluidics, accurately revealing several secretion dynamics of adipose tissue and pancreatic islets[1, 16, 18, 31, 32].

The metabolism of adipose tissue has garnered significant attention in recent years, and microfluidics have demonstrated usefulness in this field. Researchers are keen to explore whether nutrient uptake can be accurately monitored using this micro-technology. Recent work has indicated that fatty acid uptake can be visualized and quantified using fluorescence imaging and encapsulated droplets, respectively, via the use of bodipy-modified free fatty acids (NFFA)[1, 33]. Recent advances in cellular co-culture and organs-on-chips platforms have demonstrated that microfluidic analysis systems can simulate physiology at the single-cell, tissue, and even organ level. Previously, our group developed a fully automated, 16-channel microfluidic input/output multiplexer (μMUX) for endocrine tissue culture and secretion sampling. Shi et al. discuss the development of microfluidic-based analog-to-digital converters (μADCs) and digital-to-analog

converters (μDACs). These devices are critical components for signal processing in microfluidic systems, allowing for precise and reliable control of fluidic flow rates and volumes. μADCs and μDACs have the potential to greatly enhance the capabilities of microfluidic systems, enabling precise and dynamic control of fluidic flow rates and volumes which can be used in a wide range of applications, including chemical and biological analysis, drug discovery, and lab-on-a-chip systems[34]. Stimulating tissues in microfluidic devices poses several challenges. One of the main challenges is ensuring the accuracy and consistency of the applied stimulus. The microfluidic system must be designed to allow for precise control of the stimulus, such as electrical, mechanical, or chemical, and to prevent interference from other stimuli[35]. Another challenge is achieving a physiologically relevant environment for the tissue. This involves maintaining the necessary temperature, humidity, and oxygen and carbon dioxide levels, as well as providing the appropriate nutrient and waste exchange[36]. Additionally, the compatibility of the materials used in the microfluidic device with the tissue being stimulated must be considered to avoid any toxicity or damage to the tissue[37]. Finally, the design of the microfluidic device must consider the specific requirements of the tissue being studied, such as its size, shape, and mechanical properties, in order to ensure accurate and relevant results. Another challenge of these devices is interfacing the tissue to keep the high temporal resolution. In this study, we present a novel 4-input microfluidic digital-to-analog converter (μDAC), equipped with automated control through pneumatic valving to stimulate tissues at higher resolution with the help pf a 3D printed tissue trap template, which allows for the quantification of NFFA from white adipose tissue (WAT) through downstream fluorescence imaging.

2.2 Experimental Design

2.2.1 General materials and reagents

All buffers used for this study were prepared with deionized, ultrafiltered water collected from BarnsteadTM MicroPureTM Water Purification system (Thermo Fisher Scientific, serial No. 42034239). The following reagents were used without further purification: Polydimethylsiloxane (PDMS) precursors (Sylgard 184, Dow Corning, Midland, MD); SU-8 2015 photoresist (Microchem, Newton, MA); AZ-40-XT photoresist (MicroChem, Westborough, MA); insulin, D-glucose, 4-2-hydroxyethyl-1-piperazineethanesulfonicacid (HEPES), (3-Aminopropyl)trimethoxysilane, trimethylsilyl chloride (Me3SiCl), sodium dodecanoate, fluorescein isothiocyanate (FITC), KH2PO4, NaH2PO4, and NaOH were all obtained from Sigma-Aldrich (St. Louis, Missouri); Bovine serum albumin (BSA), fetal bovine serum (FBS), NaCl, CaCl2·s2H2O, EtOH, MeOH, and DMF were purchased from VWR (West Chester, PA). 4,4-difluoro-5,7-dimethyl-4-bora-3a,4a-diaza-s-indacene-3-dodecanoic acid (BODIPY FL C12, FFA*; 'bodipy-laurate'), minimal Essential Media (MEM) non-essential amino acids solution 100x, collagenase P, collagenase type I, Dulbecco's Modified Eagle Medium (DMEM), and MgSO4·7H2O were purchased from ThermoFisher Scientific (Grand Island, New York). Fatty acid free bovine serum albumin (FAF-BSA) was purchased from Akron Biotech (Boca Raton, FL). Dimethylformamide (DMF), dicyclohexylcarbodiimide (DCC), N-Hydroxy-sulfosuccinimide sodium salt (NHS-SO3Na), and Diethyl ether (Et2O) were purchased from Sigma-Aldrich (St. Louis, MO). Penicillin-streptomycin, sodium pyruvate, L-glutamine, and Dulbecco's phosphate-buffered saline (DPBS) were purchased from Thermo Fisher Scientific (Grand Island, New York). 4,4-Difluoro-5,7-Dimethyl-4-Bora-3a,4a-Diaza-s-Indacene-3-Dodecanoic Acid (BODIPY-FL-

C12, 505/512 nm), and 4,4-Difluoro-5-(2-Thienyl)-4-Bora-3a,4,a-Diaza-s-Indacene-3-Dodecanoic Acid (BODIPY-558/586-C12, 558/586 nm) were purchased from Thermo Fisher Scientific (Grand Island, New York).

2.2.2 Microfluidic Master Wafer Fabrication

The study utilized standard multilayer soft lithography methods with 3D-printed templating for tissue culture interfaces to fabricate two-layer microfluidic devices. To create the fluidic channel and pneumatic valve control channels, two master wafers were first made using soft lithography. The channel design was created using Adobe Illustrator and printed by Fineline Imaging (Colorado Spring, CO) at 50800 dpi resolution to serve as the photolithographic mask. For the control channel (thin lower layer), a silicon wafer was spin-coated with 30-μm thick negative photoresist (SU-8 2015) and baked at 105 °C for 5 min. UV exposure through the mask was done at ~330 mJ/cm2 on an in-house built UV LED exposure unit, followed by hard baking for 5 min at 105 °C and development in the SU-8 developer solution for 5 min. For the fluidic channel layer, a 50-μm thick positive photoresist (AZ 40 XT) was spun onto the silicon wafer, baked at 105 °C for 5 min, and exposed to UV at ~330 mJ/cm2. After hard baking at 105 °C for 5 min and developing the wafer in AZ developer for about 5 min, the master wafer was annealed at 115 °C for 10 min to round out the cross-section of the fluidic channel template. Prior to use, the silicon wafers were exposed to trimethylsilyl chloride vapor for 30 min to enhance PDMS removal. The channels were later characterized by imaging the channel cross section after slicing an assembled PDMS device.

2.2.3 3D-printed interface templates for tissue culture regions

3D printed templates were used for culture the tissue in 96 well plate and to hold the tissue in the tissue trap inlet of this μDAC. Both 3D-printed templates were designed in SketchUp 3D modeling software and printed on a MakerBot Replicator 2 (100 μm layer resolution in the z direction) with polylactic acid filament (PLAF, 1.75 mm diameter).

2.2.4 Microchip Fabrication

The upper layer of the microfluidic device was fabricated by pouring 36 g of a mixed PDMS precursor mixture (with a 5:1 ratio of monomer to curing agent) onto a flowing channel wafer. Meanwhile, 7.5 g of PDMS precursor (with a 20:1 ratio of monomer to curing agent) were spin-coated onto a separate silicon wafer, which served as the lower pneumatic membrane, at 2100 rpm for 45 s. Both layers were baked in an oven at 60℃ for approximately 30 minutes.

Next, the thick fluidic layer was peeled off, cut, punched, and washed before being aligned to the valve channel. The assembled layers were then baked overnight in the oven at 60℃. To irreversibly bind the PDMS to a glass slide, plasma oxidization was used after the PDMS was peeled from the wafer, diced, and punched. Finally, the microfluidic device was assembled and ready to use, and it was stored at room temperature.

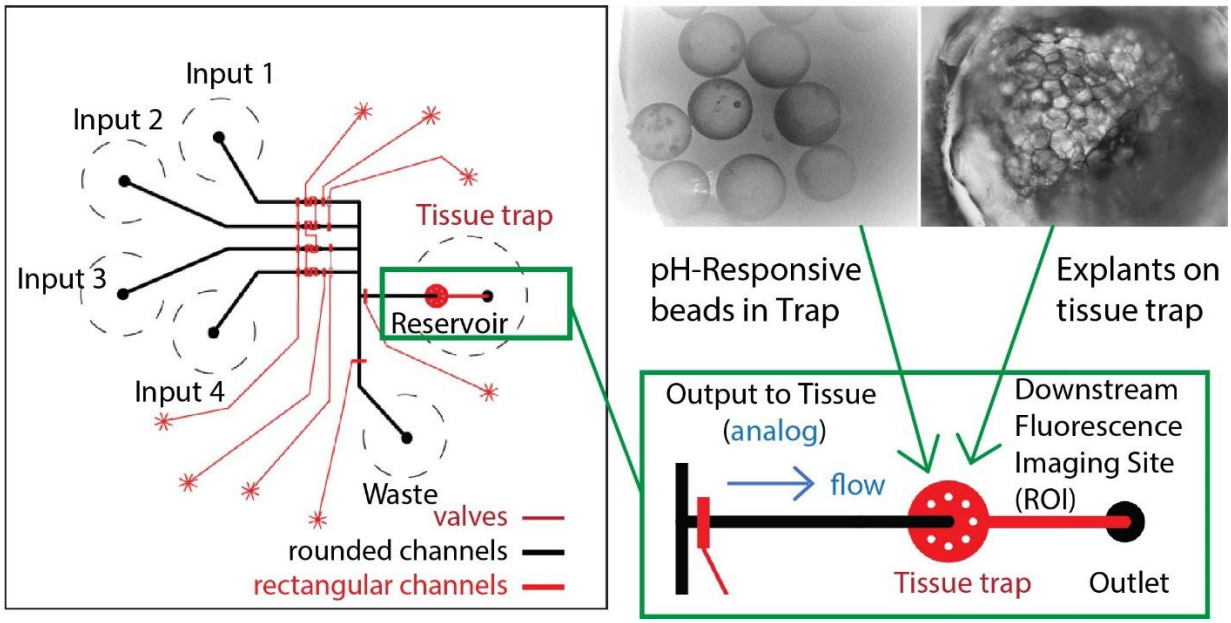

Figure 2. 1 Chip design: Adobe Illustrator design of chip including valves layer; pH- responsive glass beads (top middle) and adipose tissue (top right) in the tissue trap reservoir and the zoomed image of the fluidic channel of tissue trap

2.2.5 Extraction of Murine Epidydimal Adipose Tissue (eWAT)

In this study, male C57BL/6J mice were used, and all animal experiments were conducted in accordance with relevant laws and institutional guidelines. The protocols of 2017-3101 were approved by the institutional animal care and use committee (IACUC) of Auburn University. Epididymal white adipose tissue (eWAT) pads were extracted from the mice as previously described in published papers[1, 24]. After extraction, the pads were placed in a 60 mm Petri dish with 10 mL phosphate-HEPES buffer (10 mM HEPES, 135.3 mM NaCl, 2.2 mM CaCl2·2H2O, 1.2 mM MgSO4·7H2O, 0.4 mM KH2PO4, 2.2 mM Na2HPO4, 0.4 mM D-glucose, 2% BSA, pH 7.4), and excess vasculature was removed using Iris micro-dissecting scissors. Next, 2-mm diameter explants were punched from the fat pads with a sterile disposable biopsy punch and

placed in a glass tube containing 4 mL phosphate-HEPES buffer. The explants were washed three times with the buffer, and after each centrifugation at 1000 rpm for 3 min, 3 mL of buffer was removed using a syringe and replaced with 3 mL of fresh buffer. The phosphate-HEPES buffer was then replaced with fat serum media (DMEM + low glucose and phenol red with 12% fetal bovine serum, 120 units/mL Nystatin, 120 units/mL Penicillin-Streptomycin and 1.2X MEM NEAA), and the explants were washed twice more in the serum media. Once washed, they were stored in a sterile 96-well plate containing 200 µL fat serum media. Specific 3D-printed anchors were used to prevent the buoyancy of the fat tissue, and each explant was placed in a separate well. The explants were cultured at 37 °C in a 5% CO_2 incubator and could survive for up to 7-10 days with the serum media being refreshed twice daily. Prior to loading the explant on the microchip, it was washed and pretreated with on-demand media without serum for 30 min.

2.2.6 Quantification of Free Fatty Acid Uptake by eWAT

Ex vivo adipose tissue explants were extracted from C57BL/6J mice and cultured for up to 5 days until ready for transfer to tissue traps on the microfluidic devices. Free fatty acid (FFA) uptake on this automated device was quantified using fluorescence imaging of a labeled FFA molecule (BODIPY FL C16; green emission), at a region-of-interest (ROI) downstream of the tissue. By using a LabVIEW application to automate valves on the µDAC device, we alternatively pulsed 2 µM labelled FFAs in either high-glucose/high-insulin solution (HGHI) or low-glucose/low-insulin with isoproterenol (LGLIS), mimicking feeding and fasting states, respectively. Since the trapped tissue is minimally disturbed during flow, fluorescence emission at the downstream ROI can be calibrated for quantitative FFA uptake analysis. As an imaging control, TAMRA-labeled DNA

(orange/red emission) was spiked into all solutions at 2 μM, and we confirmed that this labeled DNA was not absorbed by the adipose tissue.

To serve as tissue mimics during characterization, glass beads were made pH-responsive by modifying with fluorescein, which has higher fluorescence quantum yield in slightly basic solutions (pH = 8) compared to acidic solutions (pH = 4).

2.2.7 FFA Uptake Dynamic Study at Varying Treatments

To prepare the explants for the experiment, they were washed three times with fresh serum-free media and then treated with a pretreatment solution for 30 minutes in a 96-well plate. To ensure that the explants were fully immersed in the solution, 3D-printed anchors were used. After the 30-minute off-chip culture, the tissue was removed, and a 0.50 mm explant was punched out and placed in a 3D printed tissue trap. The trap was then carefully inserted into the tissue inlet. Two different solutions, HGHI (25 mM glucose and 2 nM insulin in DMEM without glucose, glutamine, or phenol red, with 0.2% FF-BSA) and LGLIS (3 mM glucose, 50 pM insulin, and 20 μM isoproterenol in DMEM without glucose, glutamine, or phenol red, with 0.2% FF-BSA) mixed with 2 μM labeled fatty acid were combined to examine the dependence of adipose tissue FFA uptake dynamics on the treatments.

2.2.8 Fatty acid uptake analysis

Real time fatty acid uptake by adipose tissue explants was measured with a kit with a custom fluorescence quenching assay.[37] Each method used bodipy-labelled laurate (cell permeable fatty acid analogue, FFA*) and a cell-impermeable fluorescent quencher. The μDAC device was mounted within a microscope stage-top incubator (Tokai Hit, Japan) held at 37 °C, and input channels were filled with two different solutions, HGHI and LGLIS with 2 μM of labelled FFA*.

The treatment buffer consisted of serum free DMEM, either 2 μM of FFA* or unlabeled free fatty acid (FFA). The waste channel was attached to vacuum via a syringe. 2 mm diameter adipose tissue explants were removed from storage serum media, washed 3× with fresh serum free media, and pre-treated in serum free DMEM buffer with 3 mM glucose, 0.5 nM insulin and 2.0 μM FFA for 30 min. After the 30-minute off-chip culture, the tissue was removed, and a 0.50 mm explant was punched out and placed in a 3D printed tissue trap which can hold the explant in place. The trap was then carefully inserted into the tissue inlet. In this instance, the μDAC device inlet was filled with new solutions, filled all the channels with fresh solutions with nutrient using the vacuum connected to the waste channel. All solutions with FFA* or FFA were held at 37 °C and alternatively pulsed onto adipose explants as fluorescent videos were collected downstream using a 20× objective and FITC filter continuously for 8 minutes. Videos were analyzed using NIS-Elements, ImageJ, Microsoft Excel and MATLAB.

2.3 Results and discussion

2.3.1 Microfluidic Chip Design and Modes of Operation

The μDAC device has four fluidic inputs with one waste output, another final output reservoir for collecting fluids after tissue stimulation and a tissue reservoir (**Figure 2. 2)**. All fluidic channels and reservoirs are black in color in **Figure 2. 3**. All red channels are fluidic controls layer made with SU-8 photoresists where all fluidic channels are made with AZ photoresists. Fluidic flow layer ~ 35-micron depth, 150-micron width with round shape but all control layers are ~20-micron depth with 100-micron width. All control layers are connected with external pressure (~20 psi) via tube to control the fluid flow as the valves can be precisely controlled by LabVIEW program. The μDAC device was operated as: First input 1 fluidic channel is responsible for HGHI flowing to

the waste channel for 5 s to wash the whole channel, then the fluid will go to tissue trap region by opening the respective valves, then HGHI with other fluids will stimulate tissue for 55 s then finally solution will be stored at final output reservoir. After completion of this cycle the first input will automatically stop the fluid flow by closing the valves on this channel and will start pumping the second input. The second input will start circulation of the fluid flow as valves start pumping on this channel. This one also follows the similar path as first fluidic channel, and this reservoir is filled with LGLIS with 2 μM FFA and 2 μM Tamara-labeled DNA. The third and fourth fluidic input are filled with same fluids as first and second input respectively and these fluidic channels also follow a similar path of fluid flow as first and second channel respectively. 2 μM Tamara-labeled DNA solution is used as reference solution as this solution does not interact with the adipose explants. All the FFA uptake quantification by the tissue measured consider 2 μM Tamara-labeled DNA as references. Thus, this μDAC device was operated to stimulate the explants and quantify the FFA uptake by the explants. The LabVIEW program helps the device to precisely control the valves operation as when the specific valves should be open and close to continue the fluid flow as we want it to flow.

2.3.2 Device Characterization with pH responsive glass beads

To characterize this μDAC device, pH-responsive glass beads were used as mimicking the tissue. Glass beads were modified with fluorophore to make them pH-responsive. Glass beads experiments and Fluorescein/food dye solution were used to find out the device resolution. To evaluate the solution exchange times, we examined the fluorescence output from pH-responsive glass beads with dimensions ranging from approximately 100 to 200 μm, which were placed in the tissue trap reservoir. This analysis was conducted as two different pH solutions were introduced

(**Figure 2. 4**) to the glass beads. The pH-responsive beads were synthesized as described in previous research[1]. Initially, 100 mg glass beads were subjected to a series of washes, including 1 M NaOH (1 mL, 3×), deionized H_2O (1 mL, 3×), and MeOH (1 mL, 3×), followed by drying at 65 °C. Subsequently, the beads were treated with 5.0% (3-aminopropyl)trimethoxysilane in EtOH (281778, Sigma-Aldrich) to introduce the amine functional group on the glass surface by silanization. The amine-glass beads were then washed with EtOH three times to eliminate unreacted silane and dried at 65 °C. Following this, the amine-glass beads were exposed to FITC in DMF solution (0.1%, 1 mL) at room temperature for a 2-hour incubation. The beads were subsequently washed with DMF and EtOH, and they were stored in EtOH at 4 °C until utilization. The fluorescence images of the beads during automated pH switching were captured using a Nikon Ti-E microscope, and the obtained images were subjected to analysis using ImageJ and Microsoft Excel.

The resolution was measured of this device using both the pH- responsive glass beads on tissue trap region and with alternating a fluorescent solution. Then two different pH solutions were used to fill all fluidic input. Then, the LabVIEW program was used to run the device in a way that high and low pH solution stimulated the glass beads in certain time (2 minutes for each pH solution) periods back and forth for 16 minutes. In these experiments the microscope was focused on the pH-responsive glass beads. Similar experiments were performed with fluorescein solution in first and third fluidic inputs and buffer in second and fourth inputs. But for these experiments, microscope was focused on our region of interest which after the tissue trap region but before the final output. **Figure 2. 5 A** shows the data for two different pH solutions experiments. Here, we noticed that as the solution changed from high pH to low pH fluorescence intensity decreased

sharply, and if the solution changed from low pH to high pH the fluorescence intensity increased sharply in a short period of time. We focused our analysis on the changing part of our data. We took 40 s lapse (**Figure 2. 6 B & C**) data for further analysis considering the changes in fluorescence intensity in the middle of this time period to find out how fast actually the solution can be changed with fluorescence intensity. Considering all up and down in fluorescence intensity we can come up with a reasonable resolution of this μDAC which is average of 4.1 s for low pH to high pH (**Figure 2. 7 B**)and 3.2 s for high pH to low pH (**Figure 2. 8 C**). The average resolution of this μDAC with glass beads experiments for high pH and low pH is measured as 3.6 s (**Figure 2. 9 A** inset figure). To confirm this resolution, we did a similar experiment with fluorescein and buffer solution instead of high pH and low pH. The tissue trap was also filled with the same glass beads, but the microscope was focused after the trap region as fluorescein and buffer does not affect the glass beads. This experiment also showed similar numbers as the resolution (**Figure 2. 10 A**, top right). Thus, this μDAC resolution can be confidently stated as ~5.0 seconds, which means within this time the explants in each future experiment experienced changes in different nutrients within 5.0 seconds.

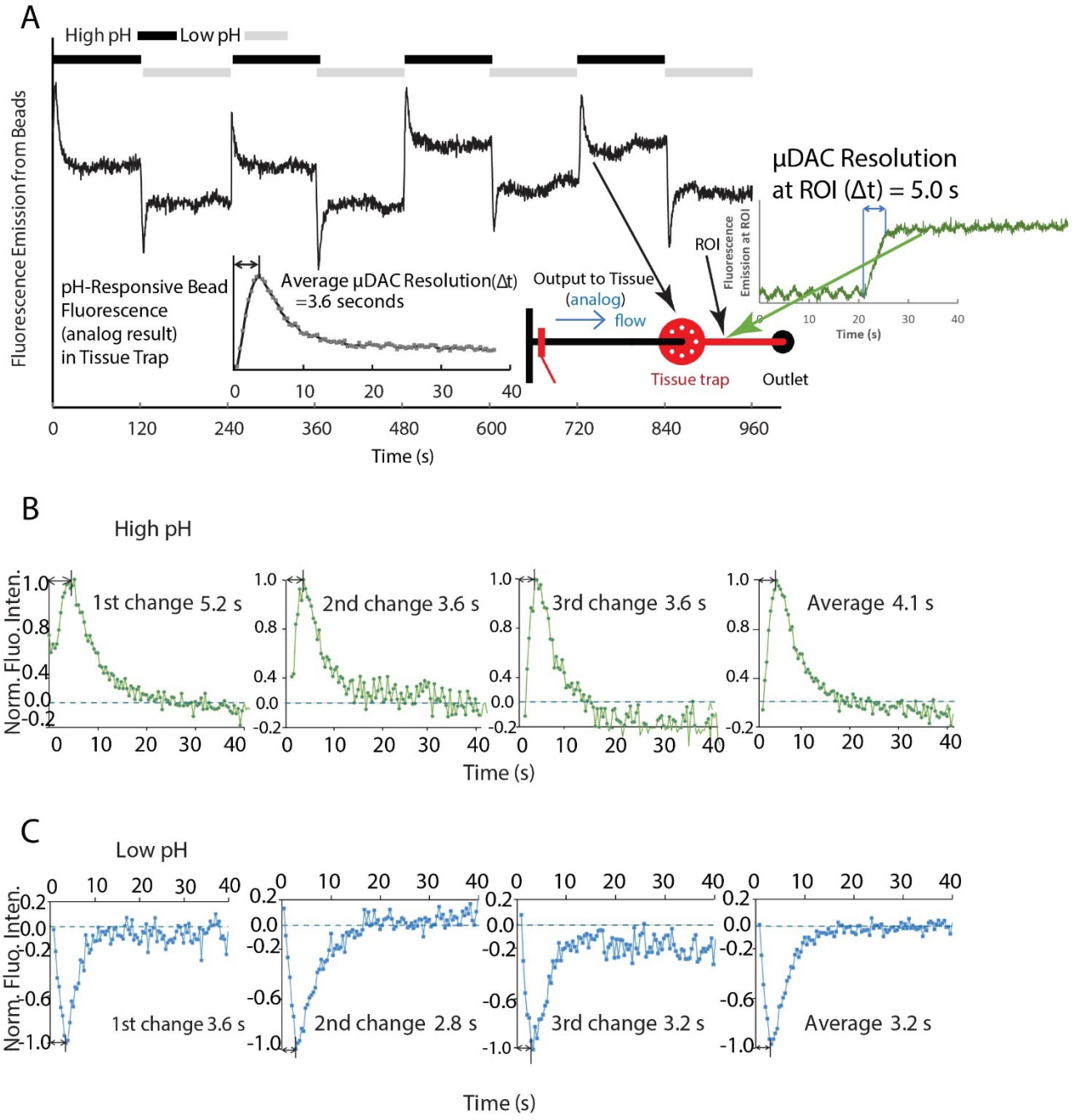
A
High pH
Low pH
Fluorescence Emission from Beads
pH-Responsive Bead Fluorescence (analog result) in Tissue Trap
Average µDAC Resolution(Δt) =3.6 seconds
Output to Tissue (analog)
flow
ROI
Fluorescence Emission at ROI
µDAC Resolution at ROI (Δt) = 5.0 s
Tissue trap
Outlet
Time (s)
B
High pH
Norm. Fluo. Inten.
1st change 5.2 s
2nd change 3.6 s
3rd change 3.6 s
Average 4.1 s
Time (s)
C
Low pH
Norm. Fluo. Inten.
1st change 3.6 s
2nd change 2.8 s
3rd change 3.2 s
Average 3.2 s
Time (s)

Figure 2. 11 Characterization of device with pH-responsive glass beads and device resolution. **A.** Fluorescence emission of pH-responsive glass beads over the 16 minutes (2 minutes each cycle including 5 s washing time) time where high pH gives higher intensity and low pH gives low intensity. Inside plot is the average resolution of this device with glass beads and outsider plot is the average resolution of this device with fluorescent and buffer solution instead of high pH and low pH. **B.** Each plot is the final 40-s (20 s before changing the solution and 20 s after changed the solution) cycle for high pH to find out the resolution of this µDAC **C.** Same plot as in B with low pH to see how fast beads can change the intensity as the solution changes from high pH to low pH.

2.3.3 Montage of green and red data in µDAC channel

In **Figure 2. 12 A** is the data for the first explants used for FFA uptake with this µDAC. The first and third fluidic input were filled with labeled FFA and Tamara-labeled DNA in HGHI where second and fourth fluidic input were filled with labeled FFA and Tamara-labeled DNA in LGLIS. The microscope collects the data for both Fluorescein isothiocyanate (FITC) and Tetramethyl rhodamine (TRITC). For the analysis shown in **Figure 2. 13 A,** we selected three different time points to see the changes in fluorescence intensity for both FITC and TRITC emission. For FITC, the intensity increases as the time passes but for TRITC the intensity remained relatively constant for the whole time period during the experiments. From these analyses we conclude that labeled FFA was taken up at the very beginning of the explants were stimulated by the fluids, and as the time passes the uptake rate was decreasing, so the fluorescence intensity was increasing. But for the labeled DNA intensity did not change significantly as expected since the DNA was used as reference for the project. The ratio metric approach of green and red emission (I_{green} and I_{red}) thus helps us to determine the NFFA uptake rate during the experiment.

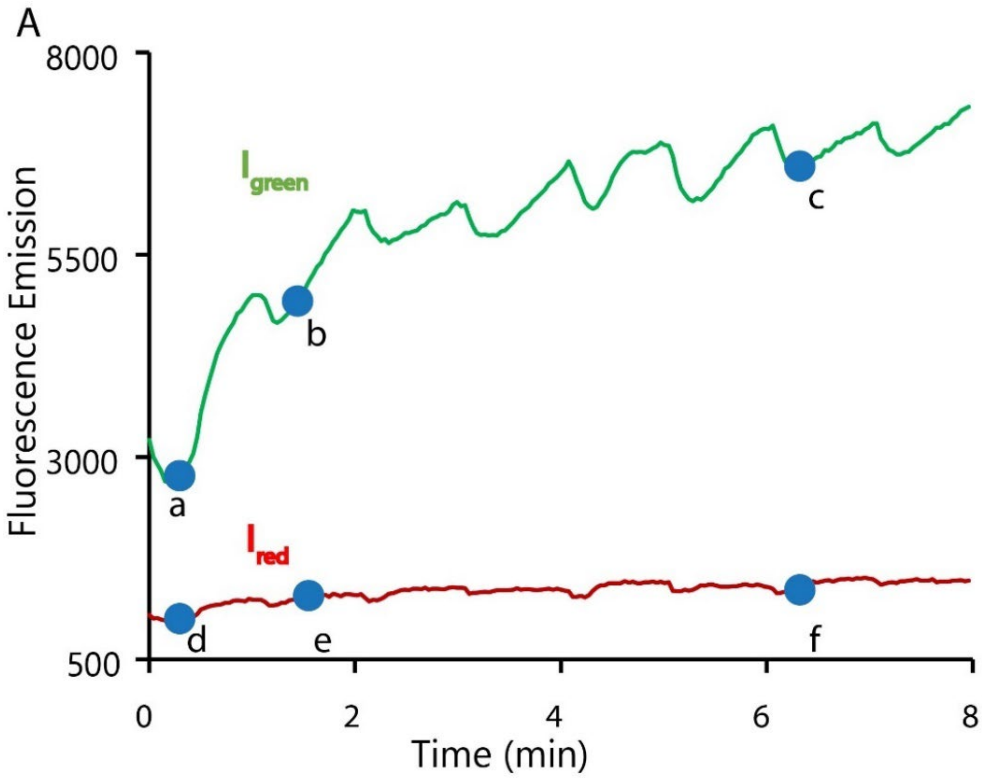

Figure 2. 14 Example NEFA uptake data over time. **A.** Fluorescence emission from green NEFA and red DNA, where green emission shows significant intensity change as the explant was stimulated with HGHI and LGLIS, alternatively. Selected points a, b, c in green emission and d, e, f in red emission chose in specific times.

2.3.4 Stimulation of explants and FFA uptake

Explants were placed in the tissue reservoir with 3D printed tissue holder very carefully with minimal disturbance. Then two different fluids HGHI and LGLIS was used to stimulate the tissue. 2 µM labeled NFFA and 2 µM labeled TAMRA-labeled DNA was added to both fluids, HGHI and LGLIS. The µDAC device was designed in the way so that it can stimulate with one nutrient and automatically starting the other fluids from next fluidic input by stopping the previous fluid

with the help of LabVIEW program. The μDAC device was used to introduce square-wave pulses of feeding (black) or fasting conditions (gray) (**Figure 2. 15**) to the adipose tissue while quantifying leftover FFA downstream. 60-s pulses of each treatment were introduced during continuous flow with on-chip pneumatic pumps. Green emission from labeled NFFA (green trace) was corrected with orange/red emission from labeled DNA (red trace) via a ratio metric approach, allowing dynamic and quantitative NFFA absorption measurements from *ex vivo* tissue (black trace). NFFA uptake rates could then be quantitatively determined in units of pmol min^{-1}. Some unique dynamic trends were observed. When any new treatment was introduced (first ~15 s of 60-s pulse), tissue initially absorbed NFFA with similar positive rate changes (+4.60 ± 0.94 fmol min^{-2}), independent of glucose or insulin. However, FFA uptake rate changes appeared to be insulin/glucose dependent during the sustained region of uptake (last ~30 s of 60-s pulse), with a slower rate reduction of -1.35 ± 0.55 fmol min^{-2} under postprandial or feeding conditions (HGHI), but a more rapid rate reduction of -2.38 ± 0.71 fmol min^{-2} under fasting conditions (LGLIS). In **Figure 2. 16** explants 1, 2 & 3 shows the data for fluorescence emission in ratio metric approach of I_{green} and I_{red}. Inset data shows the fluorescence intensity for green and red emission for FFA and DNA. Each right figure actually shows the FFA uptake rate by the explants. This was calculated by considering the flow rate of this device. Flow rate was calculated by considering the channel width, depth, and the valves area which actually the only responsible component to flow the fluid into the μDAC.

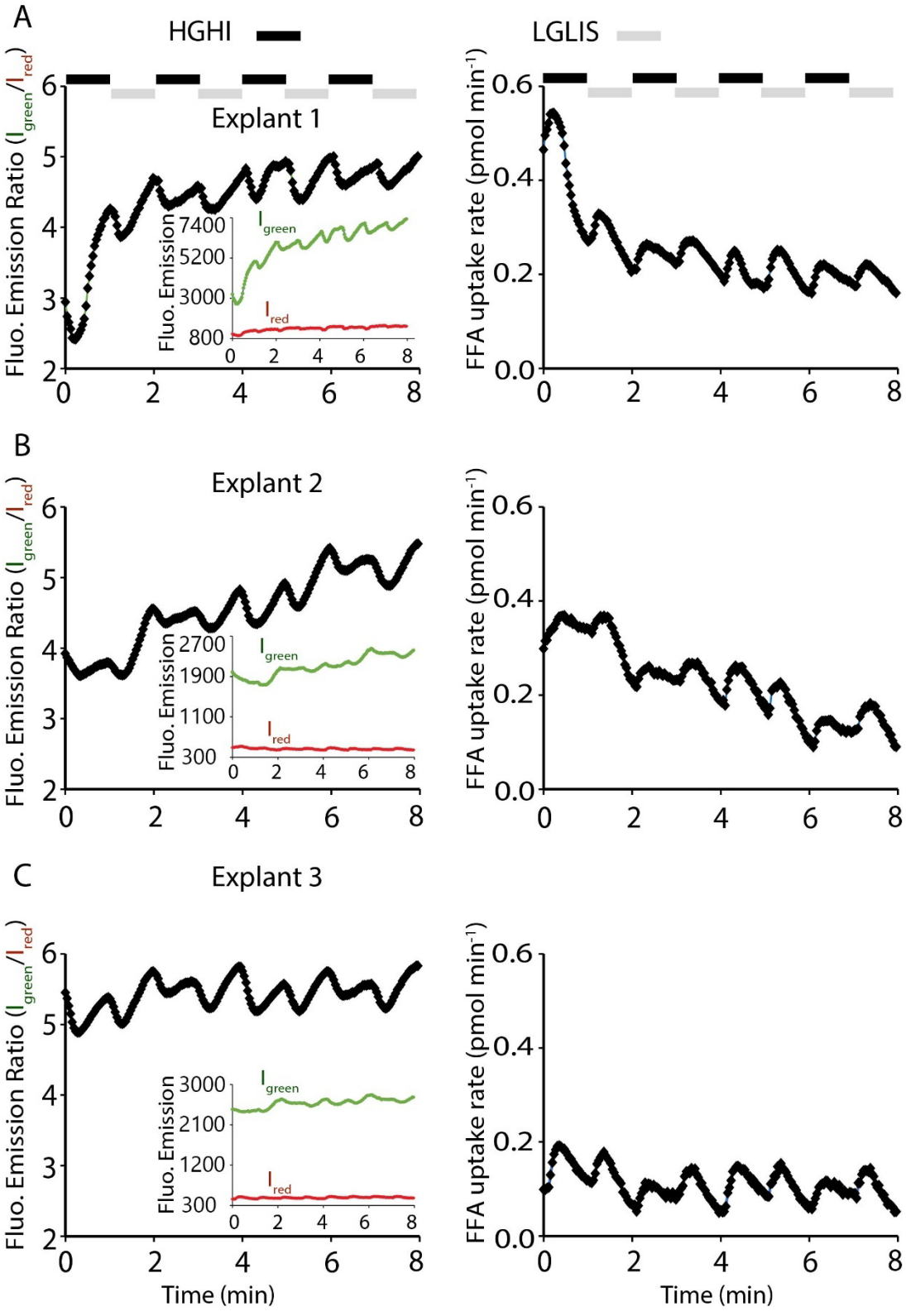
A
HGHI
LGLIS
Explant 1
Fluo. Emission Ratio (I_green/I_red)
FFA uptake rate (pmol min-1)
Fluo. Emission
I_green
I_red
B
Explant 2
C
Explant 3
Time (min)

Figure 2. 17 Explants stimulation with HGHI and LGLIS for FFA uptake. **A.** Explant 1 shows significant change in intensity ratio over 8 minutes time period as the HGHI and LGLIS stimulates the explants in 60 s cycle (including 5 s washing time) back and forth (left figure). Right plot exactly represents how much FFA was uptake by the explants in $pmolmin^{-1}$ unit where FFA uptake rate decreases as the time goes up because the explants become full FFAs over the time. Inset figure shows both green and red emission where green FFA emission increasing, and red DNA emission remains same for whole time. **B** and **C** are the similar data for two other explants representing the similar result as explant 1.

2.3.5 Insulin and glucose dependency of FFA uptake rate

All explants stimulation experiments show some unique dynamic trends in terms of FFA uptake. When any new treatment of either LGLIS or HGHI was introduced, tissue initially absorbed NFFA with similar positive rate changes around $+4.60 \pm 0.94$ fmol min^{-2} for first ~15 s of 60-s pulse, which means this change was independent of glucose or insulin levels. However, FFA uptake rate changes appeared to be insulin/glucose dependent during the sustained region of uptake (last ~30 s of 60-s pulse), with a slower rate reduction of -1.35 ± 0.55 fmol min^{-2} under postprandial or feeding conditions (HGHI), but a more rapid rate reduction of -2.38 ± 0.71 fmol min^{-2} under fasting conditions (LGLIS). Three different explants showed a significant dependency of glucose and insulin levels on FFA uptake rate. **Figure 2. 18** shows the ~30 s time period for first piece of explants, in feeding state shifted curves (LGLIS to HGHI) are not changing abruptly which means FFA uptake rates are higher, on the other hand, in fasting state shifted curve (HGHI to LGLIS) are being changed very abruptly which indicates that lower amount of FFA absorbed by the tissue. The box plot also represents the similar effect of levels of glucose and insulin on FFA uptake rate. In **Figure 2. 19** (right) box plot clearly shows that under HGHI the change in FFA uptake rate is higher than LGLIS. We hypothesize that at HGHI conditions, since there are more CD 36 (FFA

transporter) ready to use, the FFA uptake rate "deceleration" was minimized, thus the slope is less negative in **Figure 2. 20** box plot. But at LGLIS conditions there are few FFA transporters (CD 36) ready to use, so the FFA uptake rate "deceleration" was higher than HGHI, and the slope is more negative in **Figure 2. 21** box plot.

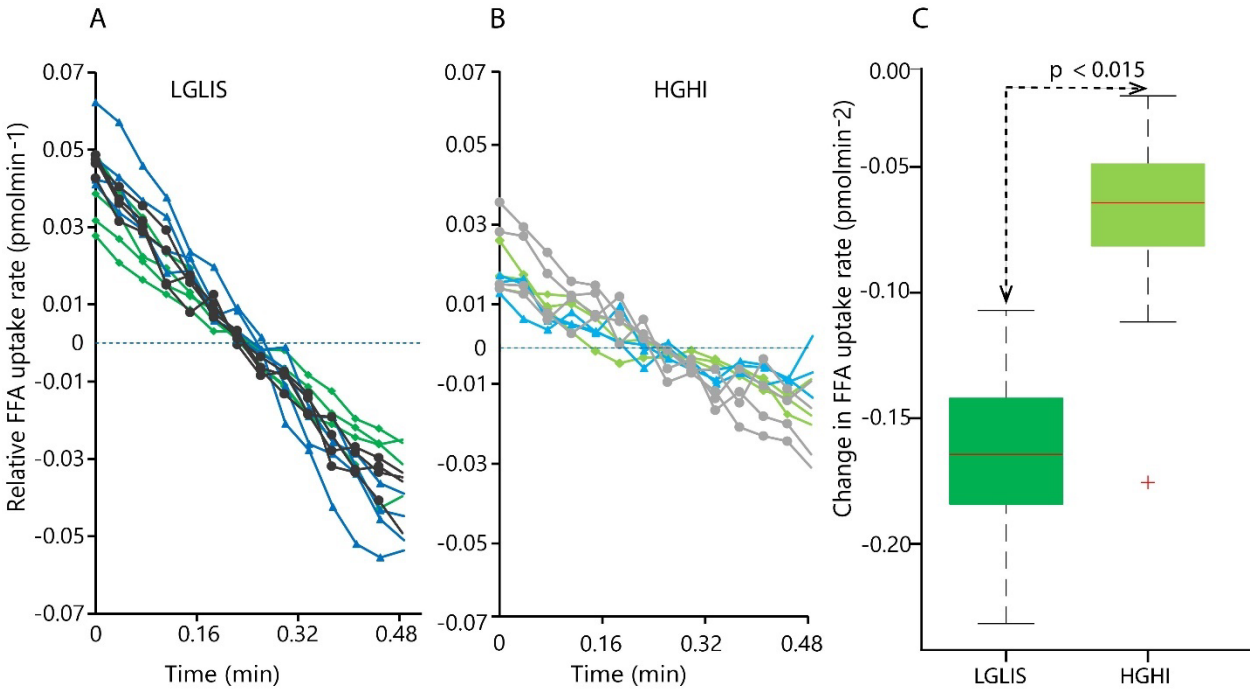

Figure 2. 22 Insulin and glucose dependency of FFA uptake. **A**. Relative FFA uptake rate in LGLIS for all explants are less shallow which means changes in FFA uptake in LGLIS for all explants are less in amount. **B.** In HGHI, FFA uptake rate is shallower for all explants expressing the high uptake of FFA by the tissue. **C.** Box plot also clearly represents the insulin and glucose dependency in FFA uptake rate considering all explants data. These data calculate a p value less than 0.015 which means data are experimentally significant.

2.3.6 Proposed mechanism of FFA uptake of explants

Fatty acid transport across the cell membrane is promoted by CD36 and other membrane proteins. To study the effect of CD36 on fatty acid uptake, HGHI and LGLIS with 2 µM labeled FFA (BODIPY FL C16; green emission) and 2 µM labeled TAMRA-labeled DNA (orange/red emission) was used to stimulate the tissue on this µDAC. In feeding state, the amount of FFA transporter (CD36) are higher than fasting state since gene expression increases the ready to use pool of CD 36 in feeding state where explants exposed with higher glucose and insulin levels (**Figure 2. 23**). On the other hand, gene expression and translation were lower in fasting state because of lower insulin and glucose levels which ultimately results in lower amount storage of fat (**Figure 2. 24**).

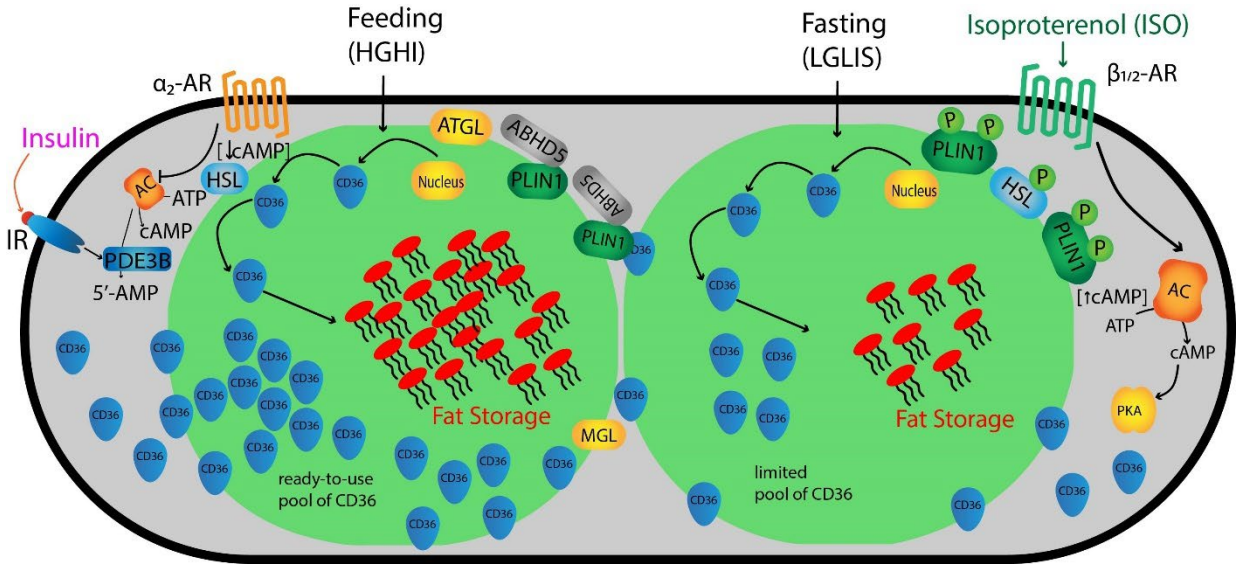

Figure 2. 25 Proposed mechanism for FFA uptake of mice explants. In feeding, the number of ready to use pool of CD 36 (FFA transporter) were high compared to the fasting state, which means in feeding state rate of FFA storage in lipid droplets is much higher than fasting state due to insufficient number of ready to use pool of FFA transporter (CD 36).

2.4 Conclusion

To our knowledge, this μDAC device provides the first tool for stimulating endocrine tissue explants with ~5 s temporal resolution while quantitatively measuring nutrient uptake. Digital nutrient signals (feeding/fasting) were passed over the tissue continuously while monitoring the uptake rates (pmol min^{-1}) downstream in an analog fashion. The slower uptake rate reductions during feeding conditions (compared to fasting conditions) are reasonable, since more fatty acid transporter proteins should be available in the presence of high insulin and glucose. Although further studies are necessary, this work has demonstrated that our μDAC device provides a unique and powerful tool to study the dynamics of function of adipose tissue and perhaps other endocrine tissues.

2.5 References

1. Li, X.; Brooks, J. C.; Hu, J.; Ford, K. I.; Easley, C. J., 3D-templated, fully automated microfluidic input/output multiplexer for endocrine tissue culture and secretion sampling. *Lab on a Chip* **2017,** *17* (2), 341-349.
2. Rosen, E. D.; Spiegelman, B. M., What we talk about when we talk about fat. *Cell* **2014,** *156* (1-2), 20-44.
3. Hull, F. E.; Radloff, J. F.; Sweeley, C., Fatty acid oxidation by ischemic myocardium. *Recent Advances in Studies on Cardiac Structure and Metabolism* **1975,** *8*, 153-165.
4. Drozdowski, L.; Thomson, A. B., Aging and the intestine. *World journal of gastroenterology: WJG* **2006,** *12* (47), 7578.
5. Wu, Q.; Kazantzis, M.; Doege, H.; Ortegon, A. M.; Tsang, B.; Falcon, A.; Stahl, A., Fatty acid transport protein 1 is required for nonshivering thermogenesis in brown adipose tissue. *Diabetes* **2006,** *55* (12), 3229-3237.
6. Boden, G.; Shulman, G., Free fatty acids in obesity and type 2 diabetes: defining their role in the development of insulin resistance and β-cell dysfunction. *European journal of clinical investigation* **2002,** *32*, 14-23.
7. Lee, Y.; Hirose, H.; Ohneda, M.; Johnson, J.; McGarry, J. D.; Unger, R. H., Beta-cell lipotoxicity in the pathogenesis of non-insulin-dependent diabetes mellitus of obese rats: impairment in adipocyte-beta-cell relationships. *Proceedings of the National Academy of Sciences* **1994,** *91* (23), 10878-10882.
8. Trauner, M.; Arrese, M.; Wagner, M., Fatty liver and lipotoxicity. *Biochimica et biophysica Acta (BBA)-Molecular and Cell biology of lipids* **2010,** *1801* (3), 299-310.
9. Fabbrini, E.; Sullivan, S.; Klein, S., Obesity and nonalcoholic fatty liver disease: biochemical, metabolic, and clinical implications. *Hepatology* **2010,** *51* (2), 679-689.
10. Chiu, H.-C.; Kovacs, A.; Blanton, R. M.; Han, X.; Courtois, M.; Weinheimer, C. J.; Yamada, K. A.; Brunet, S.; Xu, H.; Nerbonne, J. M., Transgenic expression of fatty acid transport protein 1 in the heart causes lipotoxic cardiomyopathy. *Circulation research* **2005,** *96* (2), 225-233.
11. Chiu, H.-C.; Kovacs, A.; Ford, D. A.; Hsu, F.-F.; Garcia, R.; Herrero, P.; Saffitz, J. E.; Schaffer, J. E., A novel mouse model of lipotoxic cardiomyopathy. *The Journal of clinical investigation* **2001,** *107* (7), 813-822.
12. Carvalho, R. A.; Sousa, R. P.; Cadete, V. J.; Lopaschuk, G. D.; Palmeira, C. M.; Bjork, J. A.; Wallace, K. B., Metabolic remodeling associated with subchronic doxorubicin cardiomyopathy. *Toxicology* **2010,** *270* (2-3), 92-98.
13. Kahn, S. E.; Hull, R. L.; Utzschneider, K. M., Mechanisms linking obesity to insulin resistance and type 2 diabetes. *Nature* **2006,** *444* (7121), 840-846.
14. A Dar, T.; A Sheikh, I.; A Ganie, S.; Ali, R.; R Singh, L.; Hua Gan, S.; A Kamal, M.; A Zargar, M., Molecular linkages between diabetes and Alzheimer's disease: current scenario and future prospects. *CNS & Neurological Disorders-Drug Targets (Formerly Current Drug Targets-CNS & Neurological Disorders)* **2014,** *13* (2), 290-298.
15. MacLaren, R.; Cui, W.; Cianflone, K., Adipokines and the immune system: an adipocentric view. *Current topics in complement II* **2008**, 1-21.

16. Li, X.; Hu, J.; Easley, C. J., Automated microfluidic droplet sampling with integrated, mix-and-read immunoassays to resolve endocrine tissue secretion dynamics. *Lab on a Chip* **2018,** *18* (19), 2926-2935.
17. Li, X.; Easley, C. J., Microfluidic systems for studying dynamic function of adipocytes and adipose tissue. *Analytical and bioanalytical chemistry* **2018,** *410*, 791-800.
18. Hu, J.; Li, X.; Judd, R. L.; Easley, C. J., Rapid lipolytic oscillations in ex vivo adipose tissue explants revealed through microfluidic droplet sampling at high temporal resolution. *Lab on a Chip* **2020,** *20* (8), 1503-1512.
19. Shackman, J. G.; Dahlgren, G. M.; Peters, J. L.; Kennedy, R. T., Perfusion and chemical monitoring of living cells on a microfluidic chip. *Lab on a Chip* **2005,** *5* (1), 56-63.
20. Dishinger, J. F.; Reid, K. R.; Kennedy, R. T., Quantitative monitoring of insulin secretion from single islets of Langerhans in parallel on a microfluidic chip. *Analytical chemistry* **2009,** *81* (8), 3119-3127.
21. Easley, C. J.; Karlinsey, J. M.; Bienvenue, J. M.; Legendre, L. A.; Roper, M. G.; Feldman, S. H.; Hughes, M. A.; Hewlett, E. L.; Merkel, T. J.; Ferrance, J. P., A fully integrated microfluidic genetic analysis system with sample-in–answer-out capability. *Proceedings of the National Academy of Sciences* **2006,** *103* (51), 19272-19277.
22. Bandak, B.; Yi, L.; Roper, M. G., Microfluidic-enabled quantitative measurements of insulin release dynamics from single islets of Langerhans in response to 5-palmitic acid hydroxy stearic acid. *Lab on a Chip* **2018,** *18* (18), 2873-2882.
23. Godwin, L. A.; Brooks, J. C.; Hoepfner, L. D.; Wanders, D.; Judd, R. L.; Easley, C. J., A microfluidic interface for the culture and sampling of adiponectin from primary adipocytes. *Analyst* **2015,** *140* (4), 1019-1025.
24. Brooks, J. C.; Ford, K. I.; Holder, D. H.; Holtan, M. D.; Easley, C. J., Macro-to-micro interfacing to microfluidic channels using 3D-printed templates: application to time-resolved secretion sampling of endocrine tissue. *Analyst* **2016,** *141* (20), 5714-5721.
25. Bruzewicz, D. A.; McGuigan, A. P.; Whitesides, G. M., Fabrication of a modular tissue construct in a microfluidic chip. *Lab on a Chip* **2008,** *8* (5), 663-671.
26. Sung, J. H.; Esch, M. B.; Prot, J.-M.; Long, C. J.; Smith, A.; Hickman, J. J.; Shuler, M. L., Microfabricated mammalian organ systems and their integration into models of whole animals and humans. *Lab on a Chip* **2013,** *13* (7), 1201-1212.
27. Lomasney, A. R.; Yi, L.; Roper, M. G., Simultaneous monitoring of insulin and islet amyloid polypeptide secretion from islets of Langerhans on a microfluidic device. *Analytical chemistry* **2013,** *85* (16), 7919-7925.
28. Lin, J.; Jordi, C.; Son, M.; Van Phan, H.; Drayman, N.; Abasiyanik, M. F.; Vistain, L.; Tu, H.-L.; Tay, S., Ultra-sensitive digital quantification of proteins and mRNA in single cells. *Nature communications* **2019,** *10* (1), 3544.
29. Zhang, C.; Tu, H.-L.; Jia, G.; Mukhtar, T.; Taylor, V.; Rzhetsky, A.; Tay, S., Ultra-multiplexed analysis of single-cell dynamics reveals logic rules in differentiation. *Science advances* **2019,** *5* (4), eaav7959.
30. Glieberman, A. L.; Pope, B. D.; Zimmerman, J. F.; Liu, Q.; Ferrier, J. P.; Kenty, J. H.; Schrell, A. M.; Mukhitov, N.; Shores, K. L.; Tepole, A. B., Synchronized stimulation and continuous insulin sensing in a microfluidic human Islet on a Chip designed for scalable manufacturing. *Lab on a Chip* **2019,** *19* (18), 2993-3010.

31. Clark, A. M.; Sousa, K. M.; Jennings, C.; MacDougald, O. A.; Kennedy, R. T., Continuous-flow enzyme assay on a microfluidic chip for monitoring glycerol secretion from cultured adipocytes. *Analytical chemistry* **2009,** *81* (6), 2350-2356.
32. Dugan, C. E.; Cawthorn, W. P.; MacDougald, O. A.; Kennedy, R. T., Multiplexed microfluidic enzyme assays for simultaneous detection of lipolysis products from adipocytes. *Analytical and bioanalytical chemistry* **2014,** *406*, 4851-4859.
33. Negou, J. T.; Avila, L. A.; Li, X.; Hagos, T. M.; Easley, C. J., Automated microfluidic droplet-based sample chopper for detection of small fluorescence differences using lock-in analysis. *Analytical chemistry* **2017,** *89* (11), 6153-6159.
34. Shi, N.; Mohibullah, M.; Easley, C. J., Active flow control and dynamic analysis in droplet microfluidics. *Annual Review of Analytical Chemistry* **2021,** *14*, 133-153.
35. Bhatia, S. N.; Ingber, D. E., Microfluidic organs-on-chips. *Nature biotechnology* **2014,** *32* (8), 760-772.
36. Van Der Meer, A. D.; Van Den Berg, A., Organs-on-chips: breaking the in vitro impasse. *Integrative Biology* **2012,** *4* (5), 461-470.
37. Huh, D.; Torisawa, Y.-s.; Hamilton, G. A.; Kim, H. J.; Ingber, D. E., Microengineered physiological biomimicry: organs-on-chips. *Lab on a Chip* **2012,** *12* (12), 2156-2164.

Chapter 3

Automated, high-resolution sampling from *ex vivo* adipose tissue using droplet-based microfluidics with multiplexed sensing of glycerol and fatty acid secretion

This chapter is adopted from the in-preparation publication "Automated, high-resolution sampling from ex vivo adipose tissue using droplet-based microfluidics with multiplexed sensing of glycerol and fatty acid secretion" (Md Moniruzzaman,[a] Andresa B. Bezerra,[a] Robert L. Judd,[b] James G. Granneman,[c] and Christopher J. Easley*)*

In this chapter we will talk about the development of microfluidic analog-to-digital converter for developing multiplexed assays. This device allowed automated and highly precise temporal sampling of tissue explants at high resolution followed by programmable downstream merging with multiple assay reagents, revealing unique biological information. Such device features should be applicable to various other tissue or spheroid types and to other assay formats.

3.1 Introduction

Adipose tissue, also known as body fat, performs a vital function in storing energy and regulating metabolism. It is a multifaceted and diverse tissue composed of various cell types, such as adipocytes, immune cells, and vascular components. Investigating the physiology of adipose tissue and its implications in health and disease necessitates the utilization of accurate and high-resolution techniques for both sampling and analysis.

Abnormalities in fat metabolism have a significant impact on the development of type 2 diabetes associated with obesity[1-4], and increased concentrations of free fatty acids (FFAs) in the bloodstream are linked to insulin resistance in peripheral tissues and the liver[5-7]. Adipose tissue, a dynamic organ, plays a crucial role in maintaining glucose homeostasis, regulating whole-body energy utilization, influencing feeding behaviour, and determining body composition. In a study conducted by Getty et al.[8] using dogs, it was demonstrated that in the fasted state, both FFAs and glycerol exhibited oscillatory patterns in plasma, with an average of nine pulses per hour and an average pulse duration of five minutes. Furthermore, oscillatory lipolysis from the omentum was observed, characterized by an average of 10 pulses per hour and an average pulse length of six minutes[9].

Song and Ismagilov demonstrated the ability to overcome dispersion in flowing channels by utilizing droplet-based microfluidics[10]. Building upon this work, they later introduced the "chemistrode" concept, which offers high temporal, spatial, and chemical resolution[11]. A remarkable application of this concept was recently demonstrated by the Kennedy group, who combined droplet sampling with nano electrospray ionization-mass spectrometry (nESI-MS)[12]. Our group first applied this droplet sampling concept toward high-resolution temporal sampling of endocrine tissue in 2009[13], and we have since refined these techniques and integrated mix-and-read assays to give automated, fluidic μADC devies[14, 15]. Recently, droplet microfluidics has helped to commercialize the digital assay readout and single-cell sequencing, although there are a number of sectors remained to be improved[16].

Corkey and coworkers showed that, isoproterenol caused a significant increase in the amplitude of NFFA and glycerol oscillations since isoproterenol mimics norepinephrine for stimulating the nervous system during the glycerol and fatty acid secretion from perifused isolated rat adipocytes[17]. Bergman et al. showed similar burst like oscillatory effects for glycerol and fatty acid secretion in male mongrel dogs (average weight, 25.0 ± 3.0 kg) in vivo[18].

In recent years, the Kennedy group has shown that isoproterenol has a significant impact on glycerol and NEFA secretion from 3T3-L1 adipocytes[19]. All the studies previously done for multiplexed glycerol and NEFA secretion by separate groups focused on adipocytes either in dog or rat and their microfluidic device temporal resolution was several minutes or more. Oscillatory effects or burst were found in glycerol and NEFA in continuous laminar flow. Our group observed fast responses of glycerol secretion from white adipose tissue by introducing a droplet system in the microfluidic device. Hu et al. observed glycerol release sampled at $\Delta t = 3.5$ seconds from primary murine eWAT explants (12-week-old mice). They showed glycerol release was increased during fasting conditions, and oscillations of period (~30–300 s periods) were observed[14].

Recently, significant advancements have been made in microfluidic technologies, enabling researchers to overcome traditional limitations associated with adipose tissue analysis. One such breakthrough is the development of a droplet-based microfluidic analog-to-digital converter (ADC) with on-chip merging electrodes. This cutting-edge technology allows for high-resolution sampling from adipose tissue and simultaneous quantification of glycerol and fatty acids, major components of adipose tissue metabolism.

The pioneering research conducted by different groups has been instrumental in advancing our understanding of adipose tissue biology and metabolic processes. Dr. Robert Judd's collaboration with our group developed microfluidic devices and applied these devices in biological research which actually laid the foundation for the development of innovative tools for adipose tissue analysis integrating with electrochemical sensing for highly sensitive and multiplexed detection method[14, 20-22]. Dr. Granneman's expertise in adipocyte biology and lipid metabolism has provided valuable insights into the molecular mechanisms underlying adipose tissue function[23-26].

Recent advancements in the field of cellular co-culture, tissue engineering[27] and organs-on-chips have showcased the ability of microfluidic analysis systems to mimic physiological processes at the single-cell, tissue, and even organ level. Notably, our research group has previously developed a fully automated, 16-channel microfluidic input/output multiplexer (μMUX) designed for endocrine tissue culture and secretion sampling[15]. In their review, Shi et al. delved into the development of microfluidic-based analog-to-digital converters (μADCs) and digital-to-analog converters (μDACs), which serve as crucial components for signal processing in microfluidic systems[28]. These devices enable precise and reliable control of fluidic flow rates and volumes, thereby enhancing the capabilities of microfluidic systems for various applications, including chemical and biological analysis, drug discovery, and lab-on-a-chip systems[16].

However, employing microfluidic devices for tissue stimulation poses several challenges. One key challenge involves ensuring the accuracy and consistency of the applied stimulus. The microfluidic system must be meticulously designed to enable precise

control of the stimulus type, whether electrical, mechanical, or chemical, while preventing interference from other stimuli[29]. Additionally, it is essential to establish a physiologically relevant environment for the tissue, maintaining appropriate temperature, humidity, oxygen, and carbon dioxide levels, and facilitating nutrient and waste exchange[30]. Furthermore, considering the compatibility of materials used in the microfluidic device with the stimulated tissue is crucial to prevent any potential toxicity or damage to the tissue[31]. Lastly, the design of the microfluidic device should align with the specific requirements of the tissue under study, including its size, shape, and mechanical properties, in order to ensure accurate and meaningful results. Maintaining high temporal resolution while interfacing the tissue is another challenge addressed in these devices.

In summary, this chapter highlights the significance of the droplet-based microfluidic analog-to-digital converter (ADC) with on-chip merging electrodes as a powerful tool for high-resolution sampling and multiplexed quantification of glycerol and non-esterified fatty acid secreted from adipose tissue. We are presenting an integrated device with six input reservoirs for assay reagents, one oil input reservoir, one tissue reservoir, one merging tool with some zigzag channel for mixing the reactants, and several incubation channels, and one output reservoir. Fifteen pneumatic valves were used for controlling the fluid flow through the flow channel which is able quantify multiplexed glycerol and non-esterified fatty acid (NEFA) secreted from white adipose tissue with high temporal resolution (~20 s for single assay and ~37 s for multiplexed assays).

3.2 Experimental

3.2.1 Reagents and Materials

All buffers used for this study were prepared with deionized, ultrafiltered water collected from BarnsteadTM MicroPureTM Water Purification system (Thermo Fisher Scientific, serial No. 42034239). The following reagents were used without further purification: Polydimethylsiloxane (PDMS) precursors (Sylgard 184, Dow Corning, Midland, MD); SU-8 2015 photoresist (Microchem, Newton, MA); AZ-40-XT photoresist (MicroChem, Westborough, MA); insulin, D-glucose, 4-2-hydroxyethyl-1-piperazineethanesulfonicacid (HEPES), (3-Aminopropyl)trimethoxysilane, trimethylsilyl chloride (Me3SiCl), sodium dodecanoate, fluorescein isothiocyanate (FITC), KH2PO4, NaH2PO4, and NaOH were all obtained from Sigma-Aldrich (St. Louis, Missouri); Bovine serum albumin (BSA), fetal bovine serum (FBS), NaCl, EtOH, MeOH, and DMF were purchased from VWR (West Chester, PA). For glycerol assay, a glycerol assay kit (catalog # MAK117) was purchased from Millipore Sigma. This kit consisted of ATP, enzyme mixture (glycerol kinase, glycerol phosphate oxidase), and dye reagent (Amplex red). For non-esterified fatty acid assay, a free fatty acid quantification kit (catalog # MAK044) was purchased from Millipore Sigma. This kit consisted of ATP, coenzyme A (CoA), enzyme mixture (acyl-CoA synthetase, acyl-CoA oxidase), and dye reagent (Amplex red). Cell culture reagents were received from Life Technologies (Carlsbad, CA). Isoproterenol hydrochloride, sodium dodecyl sulfate (SDS), dimethyl sulfoxide (DMSO), and hexamethyldisilazane (HMDS) were obtained from Sigma-Aldrich (St. Louis, MO).

3.2.2 Microfluidic Master Wafer Fabrication

The study utilized standard multilayer soft lithography methods with 3D-printed templating for tissue culture interfaces to fabricate three-layer microfluidic devices. To create the fluidic channel, merging channel, incubation channel and pneumatic valve control channels, two master wafers were first made using soft lithography. The channel design was created using Adobe Illustrator and printed by Fineline Imaging (Colorado Spring, CO) at 50800 dpi resolution to serve as the photolithographic mask. For the control channel (thin lower layer), a silicon wafer was spin-coated with 30-µm thick negative photoresist (SU-8 2015) and baked at 105 °C for 5 min. UV exposure through the mask was done at ~330 mJ/cm2 on an in-house built UV LED exposure unit, followed by hard baking for 5 min at 105 °C and development in the SU-8 developer solution for 5 min. For the merging and incubation channel (thick layer in flow channel), a silicon wafer was spin-coated with 60-µm thick negative photoresist (SU-8 2050) and baked at 105 °C for 5 min. UV exposure through the mask was done at ~330 mJ/cm2 on an in-house built UV LED exposure unit, followed by hard baking for 5 min at 105 °C and development in the SU-8 developer solution for 5 min. For the fluidic channel layer, a 40-µm thick positive photoresist (AZ 40 XT) was spun onto the same silicon wafer where already merging and incubation channel were patterned beforehand, baked at 105 °C for 5 min, and exposed to UV at ~330 mJ/cm2. After hard baking at 105 °C for 5 min and developing the wafer in AZ developer for about 5 min, the master wafer was annealed at 115 °C for 10 min to round out the cross-section of the fluidic channel template. Prior to use, the silicon wafers were exposed to trimethylsilyl chloride vapor for 30 min to enhance PDMS removal. The

channels were later characterized by imaging the channel cross section after slicing an assembled PDMS device.

3.2.3 3D-printed interface templates for tissue culture regions

3D printed templates were used for culture the tissue in 96 well plate and to hold the tissue in the tissue trap inlet of this μADC. Both 3D-printed templates were designed in SketchUp 3D modeling software and printed on an Any Cubic 3D printer (50 μm layer resolution in the z direction) with pre-made resin in laboratory.

5.1 Microdevice Fabrication

The upper layer of the microfluidic device was fabricated by pouring 36 g of a mixed PDMS precursor mixture (with a 5:1 ratio of monomer to curing agent) onto a flowing channel wafer. Meanwhile, 7.5 g of PDMS precursor (with a 20:1 ratio of monomer to curing agent) were spin-coated onto a separate silicon wafer, which served as the lower pneumatic membrane, at 2100 rpm for 45 s. Both layers were baked in an oven at 60°C for approximately 30 minutes.

Next, the thick fluidic layer was peeled off, cut, punched, and washed before being aligned to the valve channel. The assembled layers were then baked overnight in the oven at 60°C. To irreversibly bind the PDMS to a thin cover glass, plasma oxidization was used after the PDMS was peeled from the wafer, diced, and punched. After plasma oxidation, devices were baked overnight in the oven at 60°C. Finally, the microfluidic device was assembled and ready to use, and it was stored at room temperature.

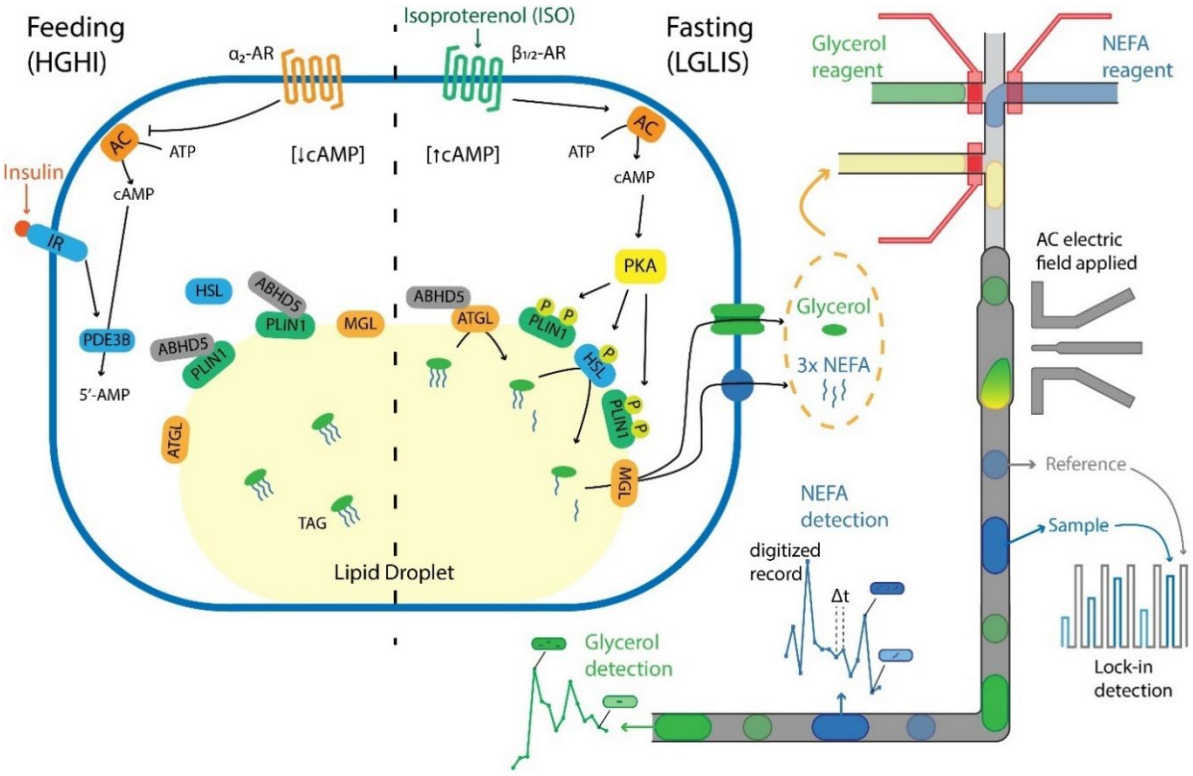

Figure 3. 1 Feeding and fasting state biological reactions. In fasting state Triglyceride converts into glycerol and NEFA which are our interest to quantify secreted from adipose explants.

3.2.5 Extraction of Murine Epidydimal Adipose Tissue (eWAT)

In this study, male C57BL/6J mice were used, and all animal experiments were conducted in accordance with relevant laws and institutional guidelines. The protocols of 2017-3101 were approved by the institutional animal care and use committee (IACUC) of Auburn University. Epididymal white adipose tissue (eWAT) pads were extracted from the mice as previously described in published papers[15, 32]. After extraction, the pads were placed in a 60 mm Petri dish with 10 mL phosphate-HEPES buffer (10 mM HEPES, 135.3 mM NaCl,

2.2 mM CaCl2·2H2O, 1.2 mM MgSO4·7H2O, 0.4 mM KH2PO4, 2.2 mM Na2HPO4, 0.4 mM D-glucose, 2% BSA, pH 7.4), and excess vasculature was removed using Iris micro-dissecting scissors. Next, 2-mm diameter explants were punched from the fat pads with a sterile disposable biopsy punch and placed in a glass tube containing 4 mL phosphate-HEPES buffer. The explants were washed three times with the buffer, and after each centrifugation at 1000 rpm for 3 min, 3 mL of buffer was removed using a syringe and replaced with 3 mL of fresh buffer. The phosphate-HEPES buffer was then replaced with fat serum media (DMEM + low glucose and phenol red with 12% fetal bovine serum, 120 units/mL Nystatin, 120 units/mL Penicillin-Streptomycin and 1.2X MEM NEAA), and the explants were washed twice more in the serum media. Once washed, they were stored in a sterile 96-well plate containing 200 μL fat serum media. Specific 3D-printed anchors were used to prevent the buoyancy of the fat tissue, and each explant was placed in a separate well. The explants were cultured at 37 °C in a 5% CO_2 incubator and could survive for up to 7-10 days with the serum media being refreshed twice daily. Prior to loading the explant on the microchip, it was washed and pretreated with on-demand media without serum for 30 min.

3.2.6 Quantification of Glycerol and Non-esterified Fatty Acid Release by eWAT

Ex vivo adipose tissue explants were extracted from C57BL/6J mice and cultured for up to 5 days until ready for transfer to tissue traps on the microfluidic devices (μADC). Glycerol and non-esterified fatty acid (FFA) secretion on this automated device was quantified using fluorescence imaging (TRITC) of a Amplex red dye and secreted glycerol

and NEFA, at a region-of-interest (ROI) (~middle of 15th incubation channel) far from the tissue reservoir. By using a LabVIEW application to automate valves on the μADC device, we stimulate tissue with high-glucose/high-insulin solution (HGHI) for ~15 minutes and low-glucose/low-insulin with isoproterenol (LGLIS) for ~20 minutes, mimicking feeding and fasting states, respectively. Since the trapped tissue is minimally disturbed during flow, fluorescence emission in droplets at ROI can be calibrated for quantitative glycerol and FFA secretion analysis. As an imaging control, two different droplets were generated which are not merged with droplets generated from tissue inlet. Same experiment was performed with known concentration of glycerol and NEFA for calibrate the system and device.

3.2.7 Droplet formation and control for enzymatic reaction

To generate droplets and flow the droplets as expected for occurring the enzymatic reaction, microfluidic analog-to-digital converter (μADC) utilized 27 pneumatic push-up valves. These valves were under the control of a LabVIEW application developed in-house, which interfaced with a specialized manifold of solenoid switches (LHDA0533115H; the Lee Company, Westbrook, CT, USA) through a multifunction data acquisition system (PCI-6259, National Instruments). The actuation of these solenoid valves was carried out by 5 V signals, enabling the controlled switching of a pressurized nitrogen supply at 25 psi. The redundancy in the operation of pumping valves in the peristaltic pumping meant that only 15 solenoids were necessary although there were 27 valves in operation for droplet generation and flow. And a hand-held 100-mL syringe connected via Tygon tubing (0.02" I.D. X 0.06" O.D.; Cole-Parmer, Vernon Hills, IL, USA) was used to apply a slight vacuum

to the outlet for rinsing the flow channels of this microfluidic analog-to-digital converter (μADC).

As previously mentioned[14, 33], droplets were produced utilizing three-valve peristaltic pumps. Aqueous segments were separated by oil segments at a T-junction channel to create aqueous-in-oil droplets. The precise and automated control of this formation process was achieved using LabVIEW.

3.2.8 Merging of Reference and Reaction Droplets with Salt-Water Electrodes

Reaction droplet formed from tissue inlet and reference droplets formed from either glycerol assay reagents or NEFA assay reagents were merged by applying a 10 kHz alternating current (AC) signal of 500 V to merging channels, specially designed for amplifying voltage filled with 5 M NaCl. To control the high voltage amplifier (Trek, Inc., Lockport, NY, USA; Model 2220), an in-house LabVIEW program was developed. The merging region was intentionally widened compared to incoming and outgoing channels to enable slower migration and improve droplet contact during merging. Detailed information about this methodology can be found in Sciambi and Abate's work[34].

An in-house LabVIEW program was used to preload user-defined time and channel programs for creating six total droplets sequentially. Droplets flow sequentially like droplet from tissue, droplet from glycerol assay reagents, droplet from tissue, droplet from NEFA assay reagents, and then two reference droplets from glycerol and NEFA assay reagents respectively. Subsequently, electro coalescence downstream was utilized to merge these droplet pairs into larger droplets (12 nL each). Two types of oil segments were programmed: very short oil

segments to keep droplets within the tissue droplet and assay reagents droplet close together, and longer oil segments to separate the next pair and two reference droplets.

3.3 Results and discussion

3.3.1 Device Design and Operation

In the device (**Figure 3. 2 A)**, the microfluidic analog-to-digital converter (μADC) has eight different aqueous inlet reservoirs (black colour in **Figure 3. 3 A**) including three glycerol assay reagent reservoirs, three non-esterified fatty acid assay reagent reservoirs, one tissue inlet reservoir and an oil inlet reservoir. There are three T-junction channels for aqueous-in-oil droplet generation. This device has fifteen pneumatic control channels which can control actually twenty-seven valves (red colour in **Figure 3. 4 A**) for automated chip operation with the help of LabVIEW (National Instruments, Austin, TX, USA) and NI-DAQ system, with some large and one extra large valves pumping integrated to improve efficiency and high-volume fluid flow. There is a salt-water electrode channel located near a widened merging region, at the sharpest electric field gradients for droplet merging with a high AC voltage. A zig-zag channel was introduced just after merging region for quickly and completely mixing reagents contained in different droplets. A long incubation channel was added to the design in this μADC for giving enough time to the mixing droplets for happening the enzymatic reactions, storing the mixed droplets, and analysing the target droplets where we choose our region of interest (ROI) to collect the data. There were three different channel depth in this μADC for better performance of the device like droplet generations, merging and controlling valves. Droplet generation channels were 35 μm in depth where are droplet merging and storing channels were 55 μm in depth. The valves

control channels were 20 μm depth. Valve-controlled 35 μm depth droplet generation channels were AZ-defined rounded channels whereas droplet merging, incubation and control channels were SU-8 defined rectangular channels. LabVIEW application was used to precisely control the droplet formation, keeping the expected distance between droplets and droplet flow rates. Six droplets were generated in one cycle by the LabVIEW application, one from glycerol assay reagents, one from tissue secreted in fasting and feeding conditions, one from NEFA assay reagents, again another one from tissue inlets, one from glycerol assay reagents and one from NEFA reagents sequentially. First pair of droplets (glycerol assay reagents droplet and tissue droplet) was merged in merging region and second pair of droplets (NEFA assay reagents droplet and tissue droplet) in a same merging region, other two droplets was used as references for glycerol and NEFA quantification secreted from adipose tissue.

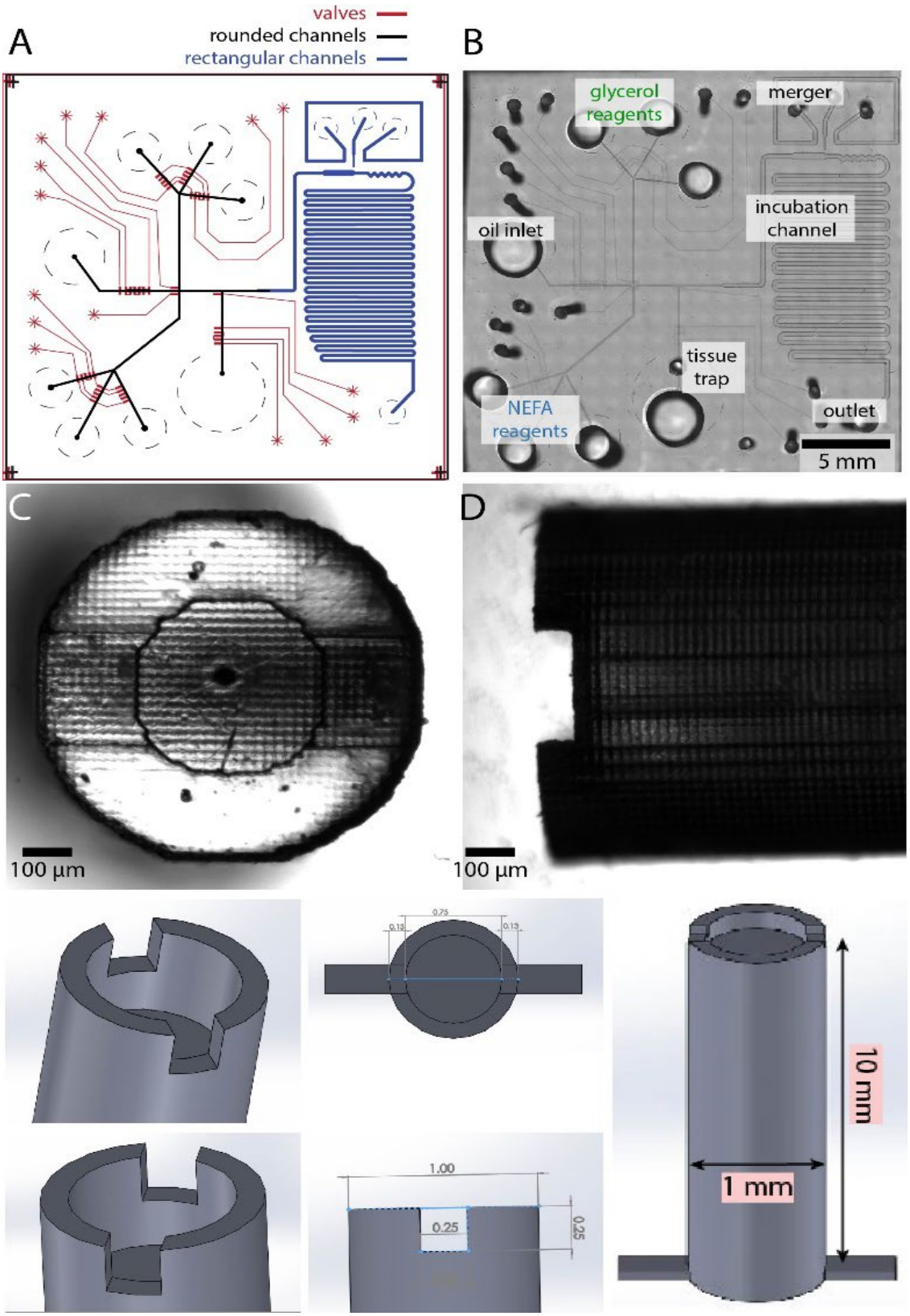
A
valves
rounded channels
rectangular channels
B
glycerol reagents
merger
incubation channel
oil inlet
tissue trap
NEFA reagents
outlet
5 mm
C
100 µm
D
100 µm
0.75
0.13
0.13
1.00
0.25
0.25
10 mm
1 mm

Figure 3. 5 Device design and fabrication with 3D printed tissue holder. **A.** Complete chip design with all components of chip **B.** Fabricated PDMS-based chip contains glycerol and NEFA assay reagents tissue trap inlet, oil inlet, droplet merger system, few incubation channels and outlet. **C.** Top view of 3D printed tissue trapper **D.** Side view of 3D printed tissue trapper E. Schematic designs of tissue trapper from different view with their sizes.

3.3.2 Automated droplet formation

The custom LabVIEW application was designed to produce droplets by alternately pumping aqueous and oil fluids, providing precise control over various droplet parameters. Adjusting the number of cycles for pumping the aqueous phase allowed for variable droplet sizes, while varying the pump cycles of the oil phase regulated the spacing between droplets. Moreover, the pumping codes enabled control over the sample and reference droplet ratio as well as the frequency of droplet generation. These capabilities closely resembled the features reported by Zeng et al., who utilized normally closed valves in PDMS/glass devices[35].

Since the process of droplet formation was under digital control, the droplets were directed sequentially into the merging and storage channels, offering the advantage of individually addressable incubation times for each droplet. Ideally, this ensured that all components inside each droplet had the same reaction time as they passed through the detection region. However, it was observed that the space between droplets decreased as they advanced downstream, especially when dealing with smaller droplets, due to the lower oil fluidic resistance. To mitigate this issue, SU-8 patterned rectangular channels were employed, providing a partial solution.

Lastly, in long-term experiments, it was crucial to regularly empty the outlet reservoir to prevent the accumulation of hydraulic pressure differentials that could affect the device's performance.

The droplet formation mechanism utilized in this study differed from various other reported mechanisms such as T-junction, co-flow, flow-focusing, and step emulsification[26]. In this case, the hydrophobic PDMS surface allowed for the confinement of a small amount of oil between the membranes positioned above the sample and reference gate valves. When the aqueous solution was pumped, the gate valve closed, leading to the formation of a new oil-water interface.

Compared to the passive T-junction droplet formation mechanism, which can experience droplet size variations due to pressure and flow rate differences, the valve segmentation-based method employed in this study, also supported by previous research from our group and others[25, 27, 28], has demonstrated precise and accurate volumetric control of droplets.

3.3.3 Tissue Trap and Device Characterization

One unique aspect of this μADC device is using a 10 mm long 3D printed tissue holder with an outer & inner diameter of 1.0 mm & 0.5 mm respectively, while inner depth of tissue holder was 0.25 mm, connection with the device flow channel was 0.3 mm wide. The tissue piece was placed in this tissue holder and inserted in tissue reservoir by aligning the flow channel of the device and connection of tissue trap. This connection allows fluids to stimulate the tissue and pass the tissue inlet with a negligible dead volume which is very important for measuring the secretion amount from the adipose tissue in picomolar scale.

pH responsive glass beads[14] were placed in tissue inlet reservoir to mimicking the tissue while solution exchange time were measured. With pH responsive glass beads experiments, we found the solution exchange time in tissue inlet was ~ 5 seconds while the resolution of this device was measure ~20 seconds for single assay development and ~37 seconds for multiplexed assay development. Although we have studied single glycerol secretion assay with better resolution in a different device[13], we developed fully automated μADC device concentrating on multiplex assay development which makes this device more complex compared to the device used other single assay development study. Other studies either used a method of pre-mixing the assay reagents with tissue secreted glycerol or NEFA, or mixing the assay reagents with secreted nutrients before droplet formation which makes their device resolution might be few seconds less compared to this μADC. But in this study, we used a method of occurring on-chip real-time reaction between the glycerol or NEFA assay reagents and secreted glycerol or NEFA from adipose tissue, which takes a few seconds more for completing the enzymatic reaction. Thus, this automated device's resolution is few seconds longer compared to previously used device for glycerol study in our laboratory. Although the resolution of this device is few seconds longer compared to our previous device, it exhibited higher resolution compared to the devices used in other group's studies.

3.3.4 Single Assay Calibrations

For single assay calibrations, either glycerol or NEFA, we used respective assay reagents in three different inputs without pre-mixing the reagents. All three inputs dispense same

amount of fluid volume in specific time as those channels were pumped with same number of valves with exactly same amount of external pressure.

For glycerol calibration we used six different concentrated glycerol solution prepared from 100 nM standard and filled tissue inlet reservoir. Glycerol assay reagents like enzyme mixture (glycerol kinase, glycerol phosphate oxidase), dye reagent (Amplex Red) and ATP were prepared as described in the technical bulletin of the MAK117 kit and filled three assay reagents input reservoir of this device. The initial concentration of the glycerol was 0, 37.5, 75, 150, 225, 300 µM but after mixing with assay reagents final concentration was calculated as 0, 12.5, 25, 50, 75, 100 µM, because droplets (generating from assay reagents and glycerol) were mixed with a volume ratio 2:1. The lowest intensity (reaction/reference) ratio was found as 0.37001 for 0 µM final concentration and highest intensity (reaction/reference) ratio was found as 0.73805 for 100 µM final concentration. A calibration curve was determined by nonlinear fitting as enzyme reaction with higher concentrated glycerol or NEFA became saturated. For plotting the calibration curve, we used two-parameter Hill fit equation (**Figure 3. 6**).

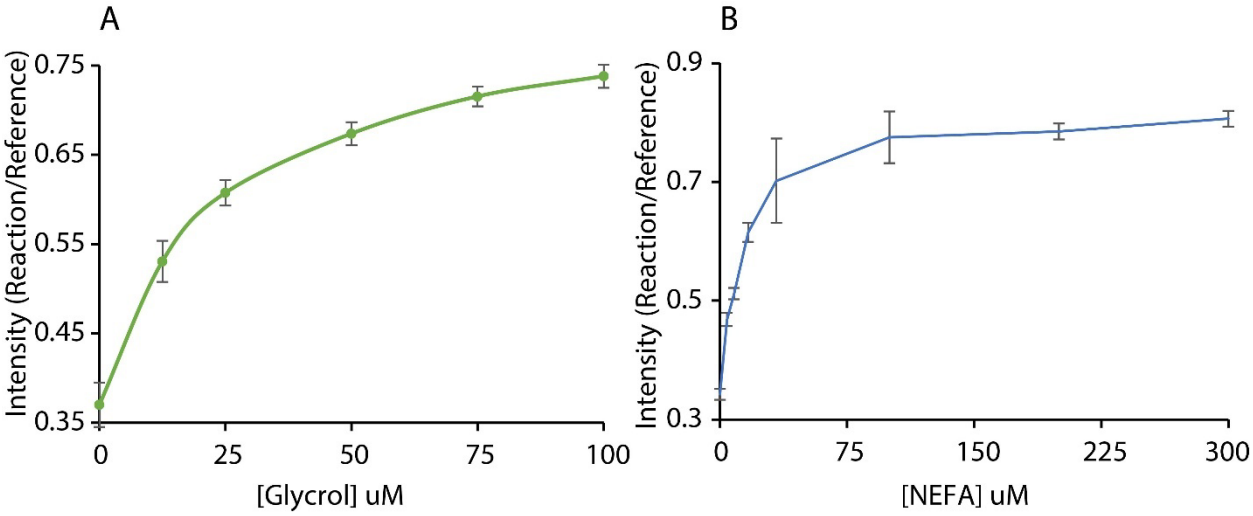

Figure 3. 7 Calibration curve for glycerol and NEFA. **A.** $I_{reaction}/I_{reference}$ droplets within 0 to 100 μM glycerol. **B.** $I_{reaction}/I_{reference}$ droplets within 0 to 300 μM non-esterified fatty acid (NEFA). Two parameter Hill fit equation was used to justify the curve for both calibration curve.

3.3.5 Multiplexed Calibration

For multiplex calibration curves, we actually use same data from single assay calibration. We did the same experiments for NEFA calibrations using 8 different initial concentrations such as 0, 12.5, 25, 50, 100, 300, 600, 900 μM. When we did the single calibrations either glycerol or NEFA, other assay reagents inlet reservoirs (NEFA or glycerol respectively) was filled with buffer but was not pumped as we have a flexibility of closing and opening any pumping operation through automated LabVIEW program. We follow the same method of plotting calibration curve (**Figure 3. 8)** for NEFA as we did for glycerol.

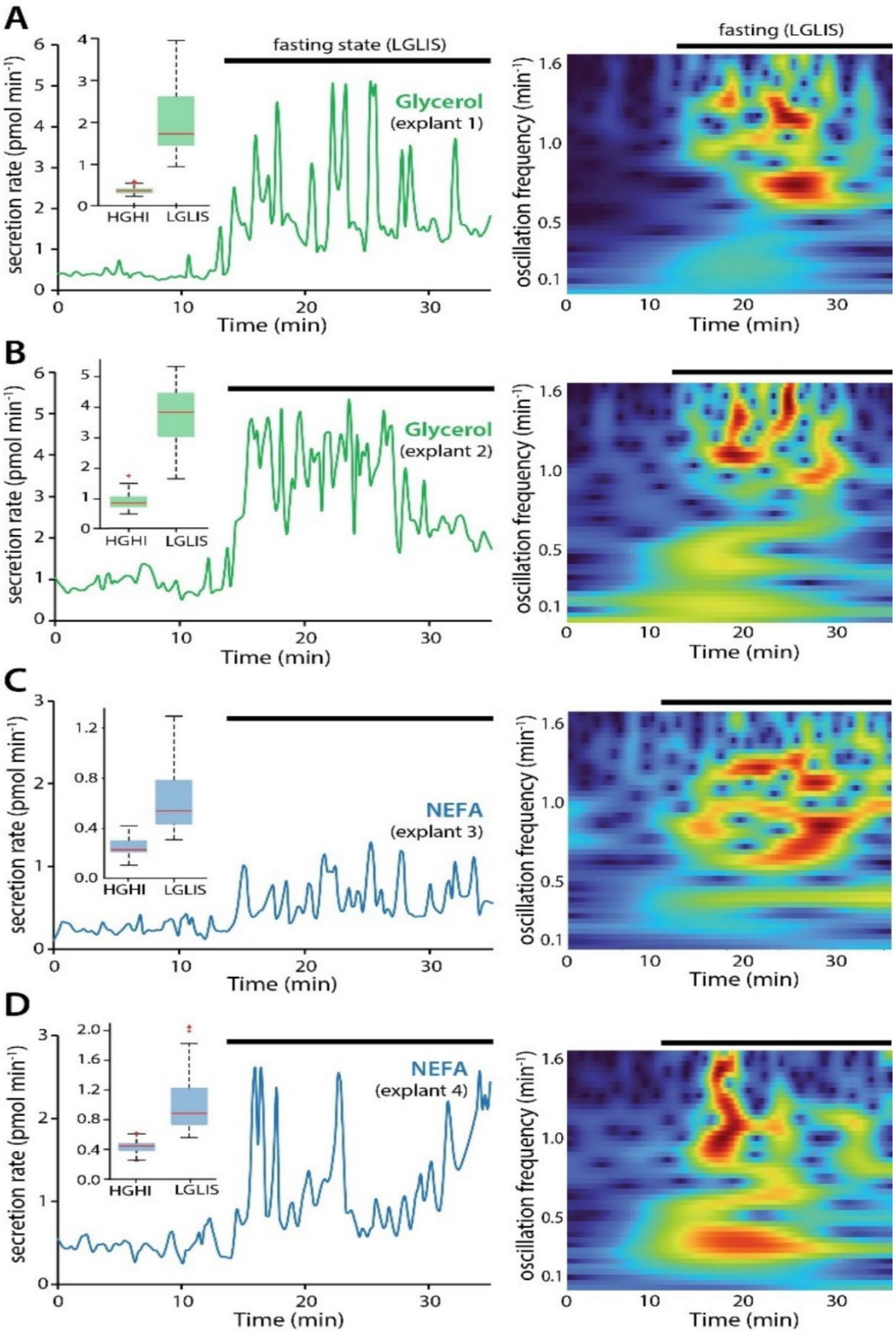
A
fasting state (LGLIS)
Glycerol
(explant 1)
secretion rate (pmol min-1)
HGHI
LGLIS
Time (min)
fasting (LGLIS)
oscillation frequency (min-1)
Time (min)
B
Glycerol
(explant 2)
secretion rate (pmol min-1)
HGHI
LGLIS
Time (min)
oscillation frequency (min-1)
Time (min)
C
NEFA
(explant 3)
secretion rate (pmol min-1)
HGHI
LGLIS
Time (min)
oscillation frequency (min-1)
Time (min)
D
NEFA
(explant 4)
secretion rate (pmol min-1)
HGHI
LGLIS
Time (min)
oscillation frequency (min-1)
Time (min)

Figure 3. 9 Glycerol and NEFA quantification data as single assay development. **A.** Secretion rate for explant 1 shows that in fasting state, release of glycerol is way higher compared to feeding state. To confirm that box plot (inset) and CWT (right) data shows similar patterned in feeding state where fasting state is not that much prominent. **B.** This data shows similar results for glycerol release from another explants (explant 2). Here, we can also watch the similar effect of feeding state **C.** Secretion of NEFA from explants 3, where we can see the isoproterenol effect in fasting state releasing of NEFA. In feeding state, NEFA release is much lower than fasting state due to presence of isoproterenol in fluids **D.** Secretion rate against time, box plot (inset), CWT plot (right) all shows that release of NEFA is much higher in fasting state compared to feeding state for explants 4 due to the presence of isoproterenol which actually mimicking the norepinephrine.

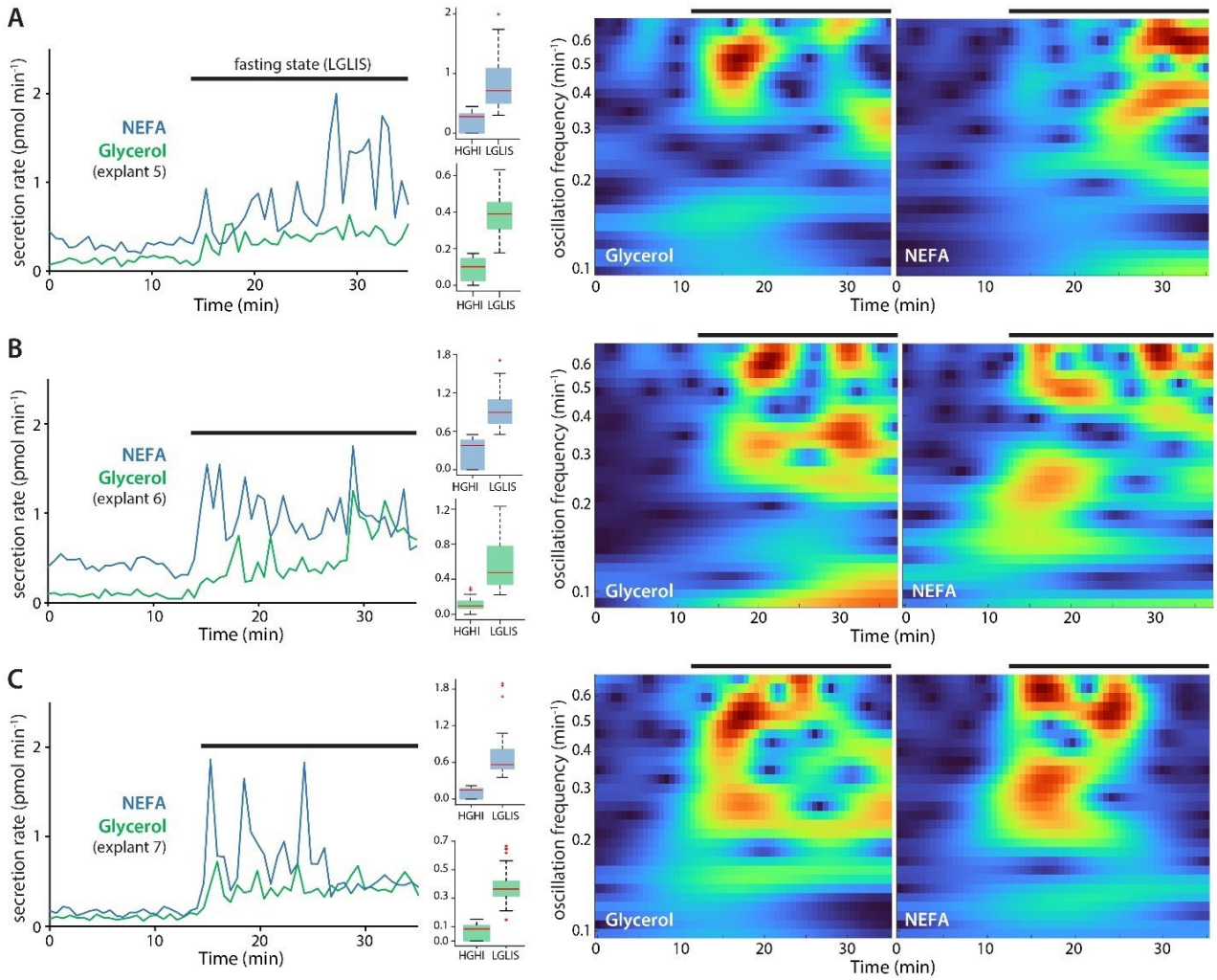

Figure 3. 10 Multiplex assay development on microfluidic devices. **A.** Secretion of glycerol and NEFA from same piece of explant 5, here we found that both glycerol and NEFA release rate is higher in fasting state than feeding state. Box plot for both glycerol and NEFA release shows that in LGLIS release rate is higher. CWT data for both nutrients also proved that in fasting states glycerol and NEFA releasing in higher amount, that's why in these area colors are very intense where in feeding state colors are not intense **B.** Explant 6 is also used for multiplexed assay development. Secretion rate plot against time, box plot and CWT plot agrees with the previous experiment with explant 5 **C.** Here, we can also found that secretion of glycerol and NEFA is higher in fasting state as isoproterenol is present in the LGLIS which actually mimicking the norepinephrine, stimulates the brain system to release glycerol and NEFA.

3.3.6 Explant secretion Sampling and Quantification

Ex vivo adipose tissue explants were extracted from C57BL/6J mice and cultured for up to 5 days until the microfluidic devices are ready for transfer in tissue traps inlet. Glycerol and non-esterified fatty acid (NEFA) secretion on this automated device was quantified using fluorescence imaging as the reaction of assay reagents and respective nutrients produces resorufin like product, which is fluorescence sensitive, at a region-of-interest (ROI) downstream of the tissue. By using manual pipetting, on the μADC device, we alternatively pulsed either high-glucose/high-insulin solution (HGHI) or low-glucose/low-insulin with isoproterenol (LGLIS), mimicking feeding and fasting states, respectively. Since the tissue is minimally disturbed during pipetting and flow and generating droplet in suitable distance before merging with assay reagents droplet, fluorescence emission at the downstream ROI can be calibrated for quantitative glycerol and NEFA secretion analysis. As an imaging control, we used only assay reagents droplets which were not merged with any nutrients secreted from explants. Reference droplets and merged droplets showed

significant differences in fluorescence intensity which helps us to quantify the secreted amount of glycerol or NEFA from tissue. The μADC converter was used to measure tissue secreted nutrients dynamics by monitoring glycerol and fatty acid release in fasting and feeding conditions. In fasting condition (LGLIS), the β-adrenergic activator isoproterenol is known to stimulate lipolysis and the release of glycerol and NEFAs by activating protein kinase A[36]. Multiple explants showed dynamic function during lipolytic conditions (low glucose and insulin, with isoproterenol) with glycerol released at 0.5 – 6 pmol min^{-1} and NEFA at 0.5 – 3.0 pmol min^{-1} for single assays while release of glycerol and NEFA was 0.3 – 1.0 pmol min^{-1} and 0.5 – 2.0 pmol min^{-1} respectively for multiplexed. Levels at high glucose and insulin remained steady around 1.0 and 0.2 pmol min^{-1}, respectively. While other groups[37] have previously developed microfluidics for monitoring these analytes from adipocytes, our work is the first to monitor glycerol and NEFA dynamics from ex vivo adipose tissue (~0.75 mm explants) and at sub-minute temporal resolution.

3.3.7 Continuous Wavelet Transform (CWT) Analysis

The Continuous Wavelet Transform (CWT) employs time-frequency analysis to offer an assessment of the timescale/time-frequency characteristics present within signals and images. This technique is particularly suitable for scrutinizing nonstationary signals, where the representation of their frequency-domain undergoes changes over time. In our present investigation, we have gathered a sequence of droplet data across time, yielding intensity data correlated with temporal instances.

To determine instances of frequency alterations in various reaction and reference droplets, the short-time Fourier transform (STFT) methodology segments the signal into distinct portions and conducts Fourier transforms on each segment. This is necessary since the Fourier transform lacks temporal data. Nevertheless, the selection of the window (segment) size is a critical consideration.

In the context of time-frequency analysis via the short-time Fourier transform, selecting for a smaller window size accelerates improved temporal resolution but at the cost of frequency resolution. Conversely, choosing a larger window size yields improved frequency resolution while sacrificing temporal resolution. It is essential to bear in mind that once a window size is chosen, it remains constant throughout the analysis. If there is an ability to predict the anticipated frequency components within the signal, this information can guide the selection of an appropriate window size for the analysis. In figure 3 and 4 shows CWT analysis of glycerol and NEFA secretion for single and multiplex assays. CWT analysis in both types of nutrients secretion shows unique pattern where in fasting state shows prominent burst compared to feeding state and this changes in color started just after change in fluids for different conditions.

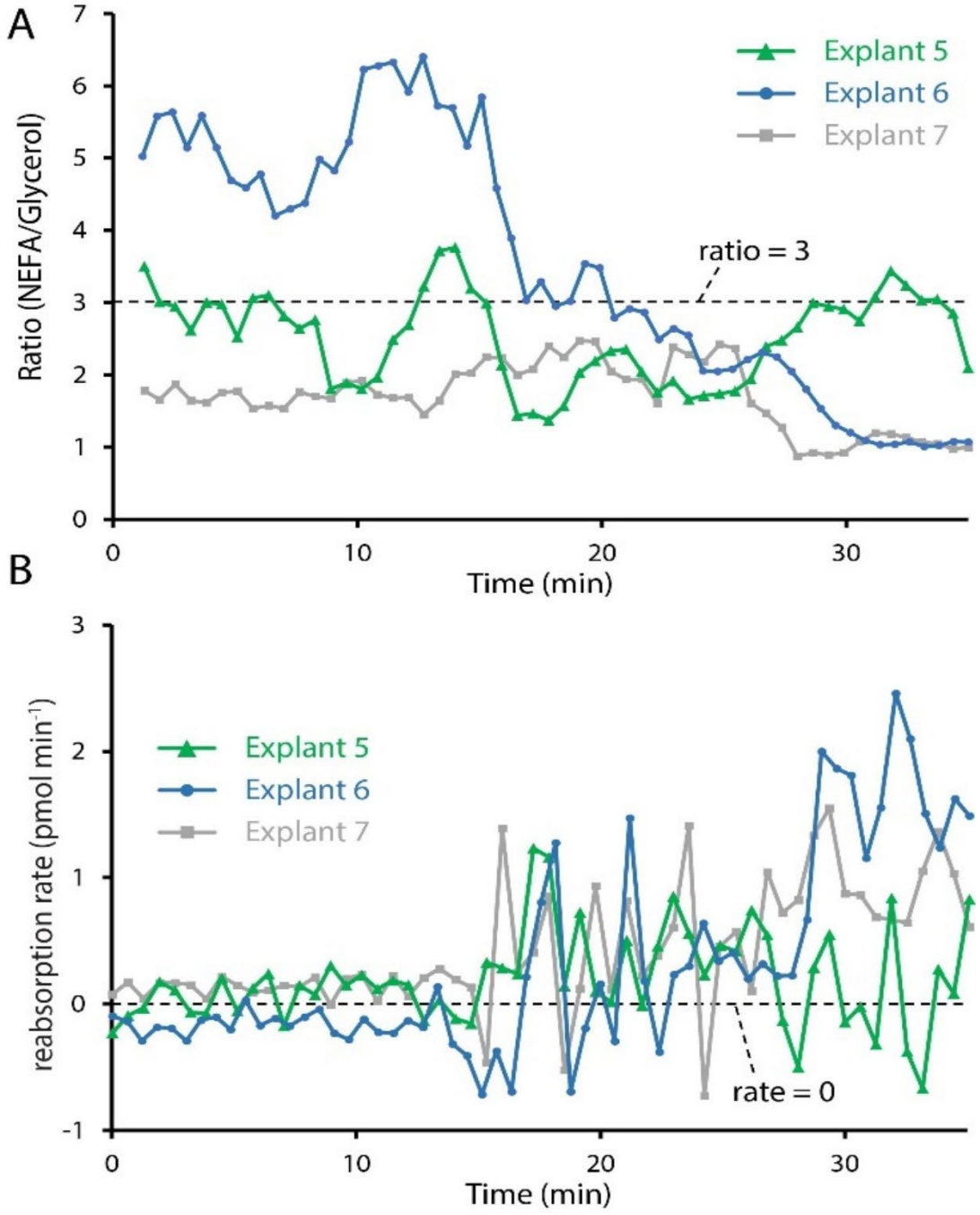

Figure 3. 11 Ratio and reabsorption rate of NEFA and glycerol release. **A.** In feeding state ration of NEFA and glycerol release are random although in fasting state the release ratio of NEFA and glycerol is under three which actually gives us the idea of NEFA reabsorption **B.** Reabsorption

rate of NEFA is higher in fasting state than feeding state as the release of NEFA is also higher in fasting state. And we are also quantifying all forms of NEFA which makes a sense of higher reabsorption rate.

3.3.8 Burst Analysis

Burst like lipolysis first observed in dog by Dr. Bergman group[18]. But they did not use any microfluidic platform and quantify glycerol and plasma FFA in vivo. To test the system for monitoring dynamic changes in glycerol release from adipocytes, we monitored glycerol and NEFA secretion during treatment of explants with feeding (HGHI) and fasting state (LGLIS) for 15 and 20 minutes respectively. In fasting state, we added the adrenergic agonist isoproterenol for mimicking norepinephrine, known to elevate cellular cAMP by activating protein kinase A to stimulate lipolysis reaction in the system[36]. We collected the data in total of 35 minutes by loading the explants in the tissue reservoir and generating droplets as described before for merging corresponding droplets for fast enzymatic reaction with secreted glycerol and NEFA while comparing the merged, reacted droplets with reference, unmerged droplets generated from tissue inlets. The tissue was minimally disturbed during fluid change from HGHI to LGLIS. Without isoproterenol explants were stimulated for 15 minutes and with isoproterenol explants were stimulated for 20 minutes. In feeding state, glycerol and NEFA multiplex secretion three different explants were average of 0.115 pmol min^{-1} and 0.308 pmol min^{-1} respectively, whereas in fasting state secretion amount were 0.466 pmol min^{-1} and 0.868 pmol min^{-1} respectively. After switching feeding to fasting state, a transient burst of glycerol and NEFA secretion was observed, and burst was approximately 4-fold for glycerol and 3-fold for NEFA. This

number actually proved that secretion of glycerol and NEFA for multiplex assay was found 75% and 64% respectively, higher in fasting state compared to feeding state, which indicates significant effect of isoproterenol in lipolysis. The bursts in glycerol and NEFA secretion were found more prominent in fasting state compared to feeding state. As soon as isoproterenol stimulated the explants, burst frequency and height was more prominent in the collected data for both nutrients. The average burst area considering all explants in feeding state and fasting state for glycerol was found to be 0.178 pmol and 0.969 pmol, stating ~5 times higher in fasting state. For NEFA, the burst area considering all explants in feeding and fasting state was 0.777 pmol and 2.255 pmol, represents ~3 times higher in fasting state. For single assay, both glycerol and NEFA shows burst in secretion with almost similar patterns as with multiplex assays.

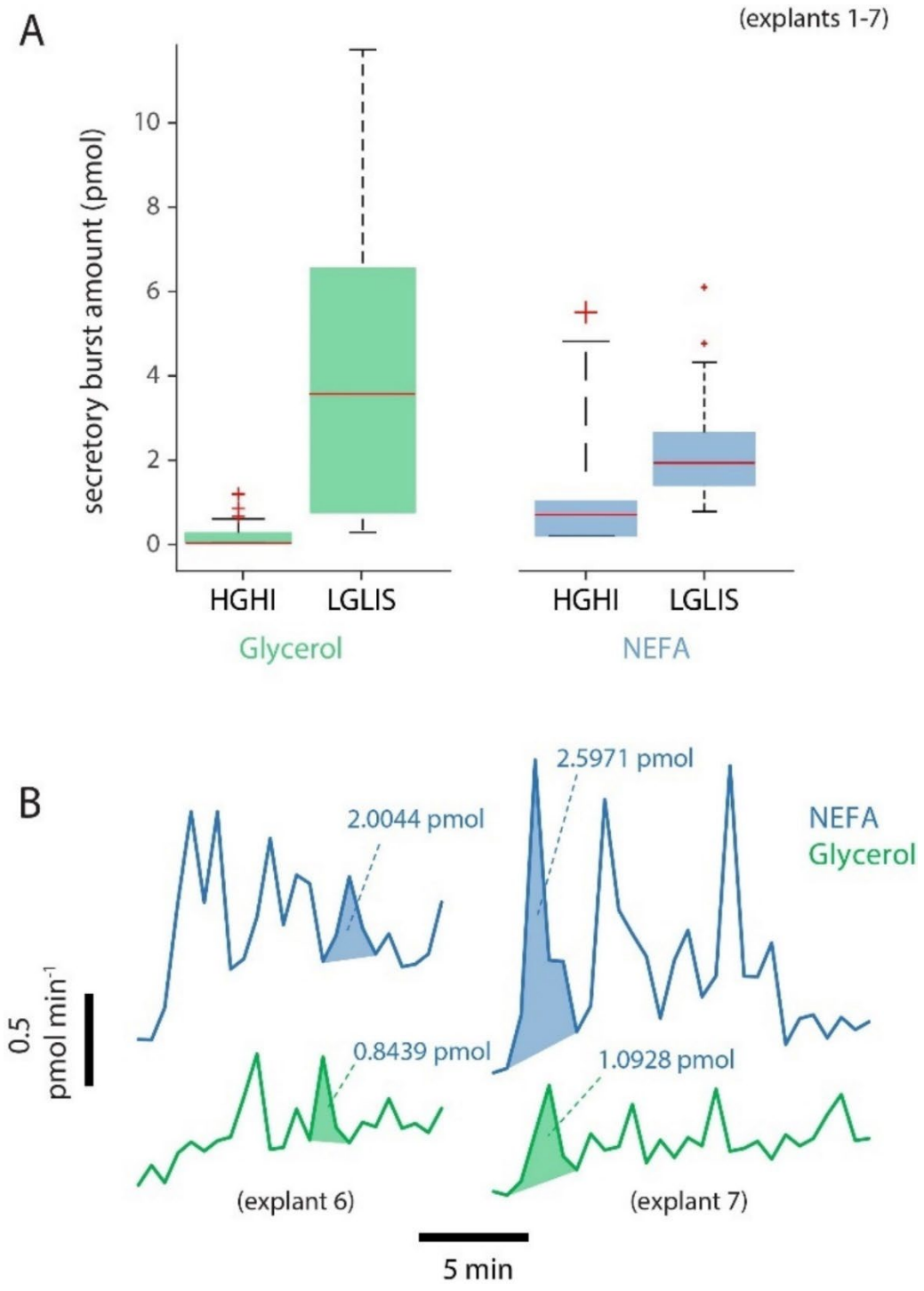

Figure 3. 12 Secretory burst amount and specific burst area for both glycerol and NEFA release. **A.** Box plot of glycerol and NEFA burst amount shows higher in LGLIS B. Two multiplex tissue

data for quantifying glycerol and NEFA release show similar patterns although we need more explants data to come a conclusion for this pattern of both nutrients release.

3.3.9 NEFA Reabsorption

The ratio of NEFA/glycerol should be 3:1 as glycerol has three -OH groups[38] to facilitate NEFA attachment. The NEFA can be reabsorbed by the tissue after secretion, so the ratio of NEFA/glycerol was not found to be consistently 3:1 by our experiments for any explants. For three multiplex assays, the average ratios of NEFA/glycerol were calculated as 2.58, 3.56 and 1.71. In feeding state, reabsorption was not profound compared to fasting state. All explants show almost similar trend in NEFA reabsorption, meaning that in fasting state reabsorption rate is much higher compared to feeding state reabsorption while we were expecting more reabsorption in fasting state. In **Figure 3. 13 B**, all three explants show similar patterns for rate NEFA reabsorption and ratio of NEFA to glycerol over time. Although some ratios show represents more than the theoretical value in feeding state where actually the rate of both nutrients secretion is very low. As the NEFA reabsorption occurring abruptly in feeding state while secretion amount is pretty low, additional experiments with more explants need to perform to identify the secretion ratios under varying treatments.

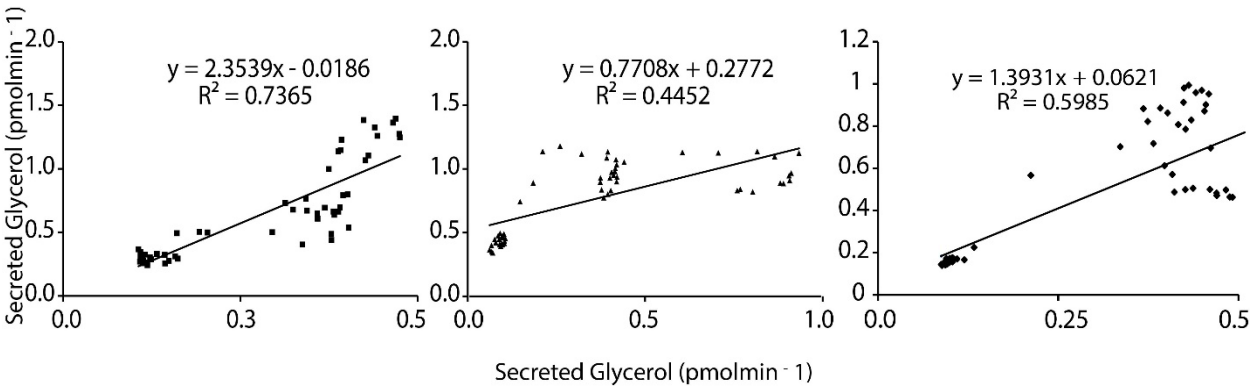

Figure 3. 14 Correlation plot for glycerol and NEFA release for three different explants. All correlation between glycerol and NEFA plot for three different explants follow similar patterns bur R^2 value varies from 0.44 to 0.74

3.4 Conclusions

A multilayer microfluidic analog-to-digital device was developed to study the lipolytic products from ex-vivo adipose tissue. Multiplexed enzyme assay for glycerol and NEFA from same adipose tissue and singled assay for both glycerol and NEFA from different piece of adipose tissue was developed with this μADC. While other groups have previously developed microfluidics for monitoring these analytes from adipocytes, our work is the first to monitor glycerol and NEFA dynamics from *ex vivo* adipose tissue (~0.75 mm explants) and at much higher temporal resolution.

The μADC has thus enabled the collection of unique biological information. While it appears that NEFA reabsorption is occurring thus far, additional studies should be done to identify the secretion ratios with more explants under varying pharmacological treatments.

3.5 References

1. Milburn, J. L.; Hirose, H.; Lee, Y. H.; Nagasawa, Y.; Ogawa, A.; Ohneda, M.; BeltrandelRio, H.; Newgard, C. B.; Johnson, J. H.; Unger, R. H., Pancreatic β-Cells in Obesity: EVIDENCE FOR INDUCTION OF FUNCTIONAL, MORPHOLOGIC, AND METABOLIC ABNORMALITIES BY INCREASED LONG CHAIN FATTY ACIDS (∗). *Journal of Biological Chemistry* **1995,** *270* (3), 1295-1299.
2. McGarry, J.; Dobbins, R., Fatty acids, lipotoxicity and insulin secretion. *Diabetologia* **1999,** *42* (2), 128-138.
3. McGarry, J. D., Banting lecture 2001: dysregulation of fatty acid metabolism in the etiology of type 2 diabetes. *Diabetes* **2002,** *51* (1), 7-18.
4. Prentki, M.; Corkey, B. E., Are the β-cell signaling molecules malonyl-CoA and cystolic long-chain acyl-CoA implicated in multiple tissue defects of obesity and NIDDM? *Diabetes* **1996,** *45* (3), 273-283.
5. Boden, G.; Chen, X., Effects of fat on glucose uptake and utilization in patients with non-insulin-dependent diabetes. *The Journal of clinical investigation* **1995,** *96* (3), 1261-1268.
6. Kim, J. K.; Wi, J. K.; Youn, J. H., Plasma free fatty acids decrease insulin-stimulated skeletal muscle glucose uptake by suppressing glycolysis in conscious rats. *Diabetes* **1996,** *45* (4), 446-453.
7. Boden, G., Role of fatty acids in the pathogenesis of insulin resistance and NIDDM. *Diabetes* **1997,** *46* (1), 3-10.
8. Getty, L.; Panteleon, A. E.; Mittelman, S. D.; Dea, M. K.; Bergman, R. N., Rapid oscillations in omental lipolysis are independent of changing insulin levels in vivo. *The Journal of Clinical Investigation* **2000,** *106* (3), 421-430.
9. Getty, L. E., *The characterization of rapid oscillations in plasma free fatty acids and omental lipolysis: the role of insulin and the central nervous system*. University of Southern California: 1999.
10. Song, H.; Ismagilov, R. F., Millisecond kinetics on a microfluidic chip using nanoliters of reagents. *Journal of the American Chemical Society* **2003,** *125* (47), 14613-14619.
11. Chen, D.; Du, W.; Liu, Y.; Liu, W.; Kuznetsov, A.; Mendez, F. E.; Philipson, L. H.; Ismagilov, R. F., The chemistrode: a droplet-based microfluidic device for stimulation and recording with high temporal, spatial, and chemical resolution. *Proceedings of the National Academy of Sciences* **2008,** *105* (44), 16843-16848.
12. Steyer, D. J.; Kennedy, R. T., High-throughput nanoelectrospray ionization-mass spectrometry analysis of microfluidic droplet samples. *Analytical chemistry* **2019,** *91* (10), 6645-6651.
13. Easley, C. J.; Rocheleau, J. V.; Head, W. S.; Piston, D. W., Quantitative measurement of zinc secretion from pancreatic islets with high temporal resolution using droplet-based microfluidics. *Analytical chemistry* **2009,** *81* (21), 9086-9095.
14. Hu, J.; Li, X.; Judd, R. L.; Easley, C. J., Rapid lipolytic oscillations in ex vivo adipose tissue explants revealed through microfluidic droplet sampling at high temporal resolution. *Lab on a Chip* **2020,** *20* (8), 1503-1512.

15. Li, X.; Brooks, J. C.; Hu, J.; Ford, K. I.; Easley, C. J., 3D-templated, fully automated microfluidic input/output multiplexer for endocrine tissue culture and secretion sampling. *Lab on a Chip* **2017,** *17* (2), 341-349.
16. Shi, N.; Mohibullah, M.; Easley, C. J., Active flow control and dynamic analysis in droplet microfluidics. *Annual Review of Analytical Chemistry* **2021,** *14*, 133-153.
17. Getty-Kaushik, L.; Richard, A.-M. T.; Corkey, B. E., Free fatty acid regulation of glucose-dependent intrinsic oscillatory lipolysis in perifused isolated rat adipocytes. *Diabetes* **2005,** *54* (3), 629-637.
18. Hücking, K.; Hamilton-Wessler, M.; Ellmerer, M.; Bergman, R. N., Burst-like control of lipolysis by the sympathetic nervous system in vivo. *The Journal of clinical investigation* **2003,** *111* (2), 257-264.
19. Clark, A. M.; Sousa, K. M.; Jennings, C.; MacDougald, O. A.; Kennedy, R. T., Continuous-flow enzyme assay on a microfluidic chip for monitoring glycerol secretion from cultured adipocytes. *Analytical chemistry* **2009,** *81* (6), 2350-2356.
20. Godwin, L. A.; Pilkerton, M. E.; Deal, K. S.; Wanders, D.; Judd, R. L.; Easley, C. J., Passively operated microfluidic device for stimulation and secretion sampling of single pancreatic islets. *Analytical chemistry* **2011,** *83* (18), 7166-7172.
21. Godwin, L. A.; Brooks, J. C.; Hoepfner, L. D.; Wanders, D.; Judd, R. L.; Easley, C. J., A microfluidic interface for the culture and sampling of adiponectin from primary adipocytes. *Analyst* **2015,** *140* (4), 1019-1025.
22. Brooks, J. C.; Judd, R. L.; Easley, C. J., Culture and sampling of primary adipose tissue in practical microfluidic systems. *Thermogenic Fat: Methods and Protocols* **2017**, 185-201.
23. Lee, Y.-H.; Petkova, A. P.; Konkar, A. A.; Granneman, J. G., Cellular origins of cold-induced brown adipocytes in adult mice. *The FASEB Journal* **2015,** *29* (1), 286.
24. Burl, R. B.; Ramseyer, V. D.; Rondini, E. A.; Pique-Regi, R.; Lee, Y.-H.; Granneman, J. G., Deconstructing adipogenesis induced by β3-adrenergic receptor activation with single-cell expression profiling. *Cell metabolism* **2018,** *28* (2), 300-309. e4.
25. Varghese, M.; Kimler, V. A.; Ghazi, F. R.; Rathore, G. K.; Perkins, G. A.; Ellisman, M. H.; Granneman, J. G., Adipocyte lipolysis affects Perilipin 5 and cristae organization at the cardiac lipid droplet-mitochondrial interface. *Scientific reports* **2019,** *9* (1), 4734.
26. Rondini, E. A.; Granneman, J. G., Single cell approaches to address adipose tissue stromal cell heterogeneity. *Biochemical Journal* **2020,** *477* (3), 583-600.
27. Shi, N.; Moniruzzaman, M.; Easley, C. J., Tissue engineering and analysis in droplet microfluidics. In *Droplet Microfluidics*, R. Soc. Chem. Cambridge, UK: 2020; pp 223-260.
28. Shi, N.; Mohibullah, M.; Easley, C. J., Active Flow Control and Dynamic Analysis in Droplet Microfluidics. *Annual Review of Analytical Chemistry* **2021,** *14* (1), 133-153.
29. Bhatia, S. N.; Ingber, D. E., Microfluidic organs-on-chips. *Nature biotechnology* **2014,** *32* (8), 760-772.
30. Van Der Meer, A. D.; Van Den Berg, A., Organs-on-chips: breaking the in vitro impasse. *Integrative Biology* **2012,** *4* (5), 461-470.
31. Huh, D.; Torisawa, Y.-s.; Hamilton, G. A.; Kim, H. J.; Ingber, D. E., Microengineered physiological biomimicry: organs-on-chips. *Lab on a Chip* **2012,** *12* (12), 2156-2164.

32. Brooks, J. C.; Ford, K. I.; Holder, D. H.; Holtan, M. D.; Easley, C. J., Macro-to-micro interfacing to microfluidic channels using 3D-printed templates: application to time-resolved secretion sampling of endocrine tissue. *Analyst* **2016,** *141* (20), 5714-5721.
33. Li, X.; Hu, J.; Easley, C. J., Automated microfluidic droplet sampling with integrated, mix-and-read immunoassays to resolve endocrine tissue secretion dynamics. *Lab on a Chip* **2018,** *18* (19), 2926-2935.
34. Sciambi, A.; Abate, A. R., Accurate microfluidic sorting of droplets at 30 kHz. *Lab on a Chip* **2015,** *15* (1), 47-51.
35. Pourmand, A.; Shaegh, S. A. M.; Ghavifekr, H. B.; Aghdam, E. N.; Dokmeci, M. R.; Khademhosseini, A.; Zhang, Y. S., Fabrication of whole-thermoplastic normally closed microvalve, micro check valve, and micropump. *Sensors and Actuators B: Chemical* **2018,** *262*, 625-636.
36. Arner, P., Human fat cell lipolysis: biochemistry, regulation and clinical role. *Best practice & research Clinical endocrinology & metabolism* **2005,** *19* (4), 471-482.
37. Dugan, C. E.; Cawthorn, W. P.; MacDougald, O. A.; Kennedy, R. T., Multiplexed microfluidic enzyme assays for simultaneous detection of lipolysis products from adipocytes. *Analytical and bioanalytical chemistry* **2014,** *406*, 4851-4859.
38. Coppack, S. W.; Persson, M.; Judd, R. L.; Miles, J. M., Glycerol and nonesterified fatty acid metabolism in human muscle and adipose tissue in vivo. *American Journal of Physiology-Endocrinology and Metabolism* **1999,** *276* (2), E233-E240.

Chapter 4

Automated Microfluidic Device For Electrode Preparation and Nucleic Acid Detection

This chapter was re-written from the dissertation "Development of Nucleic Acid Driven Peptide and Protein Sensors and Their Integration with Automated Microfluidics" (Niamat E Khuda, Adapted from dissertation with permission from Niamat E Khuda, Copyright 2020 by Niamat E Khuda) as this was an collaborative project with her where we tried to combine the microfluidics with electrochemistry.

4.1 Introduction

The interaction between microfluidic and electrochemical technologies creates a mutually beneficial relationship, enhancing their individual strengths and opening up new possibilities for advancing point-of-care (POC) analysis[1]. Microfluidics offers advantages such as device miniaturization, the integration of multiple components into one unit, precise manipulation of small sample volumes, simultaneous detection of multiple samples, portability, and cost-effectiveness[2, 3]. However, when applied to POC scenarios, downsizing the detection system is essential for seamless integration into microfluidic platforms. Electrochemical detection methods align well with POC setups and can be easily combined with microfluidics due to their compatibility with microfabrication techniques[4, 5]. This seamless integration improves fluid control through electrodes, reducing sample and reagent usage. The smaller microchannel size accelerates reactions by shortening diffusion times, and automated operations minimize local variations, enhancing sensor reproducibility.

In recent times, integrated microfluidic devices with electrochemical detection methods have been employed to monitor blood metabolites, quantify disease biomarkers, and study cell cultures[6-12]. This integration has also shown promise in other research areas, particularly in pharmaceuticals, environmental analysis, and food testing[13-18]. Microfluidics enables high-throughput analysis by directing samples to various electrochemical cells, allowing multiplexing and simultaneous detection of multiple target molecules within a single device[19, 20].

An illustrative example of this fusion is the work of Lee and colleagues, who combined an electrochemical detection system with a digital microfluidic platform to concurrently detect multiple biomarkers associated with pulmonary hypertension[21]. Their device featured five fluidic chambers controlled by pneumatic microvalves, linked to an electrochemical sensor capable of detecting four biomarkers. Similarly, Panini et al. demonstrated a sensitive technique for quantifying prostate-specific antigen (PSA) in human serum samples using continuous flow microfluidics[22]. They utilized carbon nanotubes/horseradish peroxidase/anti-tPSA immobilized glassy carbon electrodes in a microfluidic Plexiglas biochip, achieving an electrochemical readout with a superior detection limit compared to conventional ELISA methods.

In a similar vein, Uliana and team contributed to this field by developing a cost-effective, fully disposable microfluidic electrochemical array device (μFED) for detecting the estrogen receptor alpha biomarker[23]. The device featured estrogen response element-modified carbon-based working electrodes, capturing nanoparticles loaded with estrogen receptor alpha and horseradish peroxidase. Introduction of H_2O_2 and hydroquinone into the microfluidic device prompted an electrochemical readout.

These examples only scratch the surface of the diverse range of studies showcasing the immense potential of combining microfluidic platforms with electrochemical detection for biomolecule analysis. In this context, we present our own contribution: the integration of an electrochemical sensor into an automated microfluidic device (Figure 4.3). This microdevice incorporates a gold working electrode combined with microfluidics, featuring three input channels regulated by active microvalves to achieve versatile dynamic control over fluids. Our study underscores the utility of automated, valve-controlled microfluidics for electrode preparation and analyte detection using a DNA-based surface assay platform employing square wave voltammetry (SWV). Our future objective is to employ this automated microfluidic biosensor for real-time detection of secretions from cells and tissues.

4.2 Reagents and Materials

All solutions were prepared using deionized water that had been filtered through a Barnstead MicroPure Water Purification system (Thermo Fisher Scientific, Waltham, MA, USA). This water had a resistance value of 18.2 MΩ·cm at 23.5 °C and contained particles smaller than 0.2 μm.

The following reagents were used as received: 4-(2-hydroxyethyl)-1-piperazineethanesulfonic acid (HEPES) and sodium chloride from BDH, Tris-(2-carboxyethyl) phosphine hydrochloride (TCEP), mercaptohexanol (MCH), gold etchant, and chromium etchant from Sigma-Aldrich, Gold-sputtered on glass (GoG) (Au 100 nm with Cr adhesion layer 5 nm) was obtained from Deposition Research Lab, Inc (St. Charles, MO) with dimensions of 1” x 3” x 1.1 mm, Silicon wafers were sourced from the Polishing Corporation of America (Santa Clara, CA, USA), Negative photoresists (SU-8 2015) and SU-8 developer were obtained from MicroChem

(Westborough, MA, USA), AZ 40XT (positive thick photoresist) and AZ 300 MIF developer from AZ Electronic Materials USA (Somerville, NJ, USA), Polydimethylsiloxane (PDMS) precursors, SYLGARD 184 silicone elastomer base, and curing agent were acquired from Dow Corning Corp. (Midland, MI, USA), Dimethyl sulfoxide (DMSO) was obtained from Anachemia, Bovine serum albumin (BSA) was sourced from VWR (West Chester, PA), Fluorescein was purchased from Alfa Aesar (Ward Hill, MA, USA). Fluorescence excitation and emission measurements were performed using a Nikon Ti-E inverted fluorescence microscope (40X objective, 0.75 NA; Nikon Instruments Inc., Melville, NY, USA) connected to a CCD camera (CoolSnap HQ2; Photometrics Scientific, Tucson, AZ, USA). Fluorescence images were captured by focusing on a designated region of interest (Figure 4.5) and collected through the green fluorescence filter cube ($\lambda ex = 470 \pm 20$ nm, $\lambda em = 525 \pm 25$ nm).

Methylene blue-conjugated DNA was acquired from Biosearch Technologies (Novato, CA) and underwent purification by RP-HPLC. Thiolated DNA was obtained from Integrated DNA Technologies (IDT; Coralville, Iowa) and confirmed for purity through mass spectroscopy. Details of the DNA samples used are listed inTable: 4.1.

Table 4. 1: Single-Stranded DNA Sequences Used in Oligonucleotide Quantification

Sequence Name	Abbreviation	DNA sequence, listed 5′ to 3′
Thiolated DNA	thio-DNA	/**5ThioMC6-D**/AAA AGC ATG GTG ACG TGT GAG AGA TAG GAA AAG GAC AAT AAC AA
Methylene Blue DNA	MB-DNA	TTG UTA TTG UCC TTU TCC UAT CTC TCA CAC GUC ACC AUG C/**MB-C7**/

Abbreviations: /5ThioMC6-D/ = disulfide bond flanked by two six-carbon spacers (IDT), /MB-C7/ = methylene blue modification (Biosearch).

4.3 Experimental Methods

4.3.1 Preparation of Gold Electrodes

The electrode design photomask for our experiment was created using Adobe Illustrator. The design files were then sent to Fineline Imaging in Colorado Springs, Colorado, where a positive photomask was generated based on our design. You can see the mask design in **Figure 4.1A**. In total, we were able to produce eighteen autonomous gold working electrodes, each with a diameter of 2 mm, on a single microscope slide using this photomask. The production process followed the standard photolithographic procedure. We applied AZ 40XT photoresist to create the desired pattern on the gold-on-glass slide (GoG). Afterward, the GoG underwent treatment with gold etchant for 30 seconds, followed by chromium etchant for 15 seconds. This treatment selectively removed the non-protected gold and chromium, shaping the gold electrodes according to the design on the photomask. To remove the positive photoresist layer from the gold, the electrode patterned GoG was heated in DMSO at 110°C for 30 minutes. The GoG electrodes then underwent a series of rinsing steps, which included deionized water and ethanol, followed by drying with nitrogen.

4.3.2 3D-printed Template For The Fabrication of Electrochemical Cell

A 3D computer-aided design (CAD) file was designed in Sketchup© (Trimble Navigation Limited) and printed the 3D mold by Makerbot Replicator 2 (200 μm layer resolution in the z-

direction) with Hatchbox's polylactic acid filament (PLA, 1.75 mm diameter). The 3D CAD depiction and an example of a printed template is shown **in Figure 4.1B & 4.1C**.

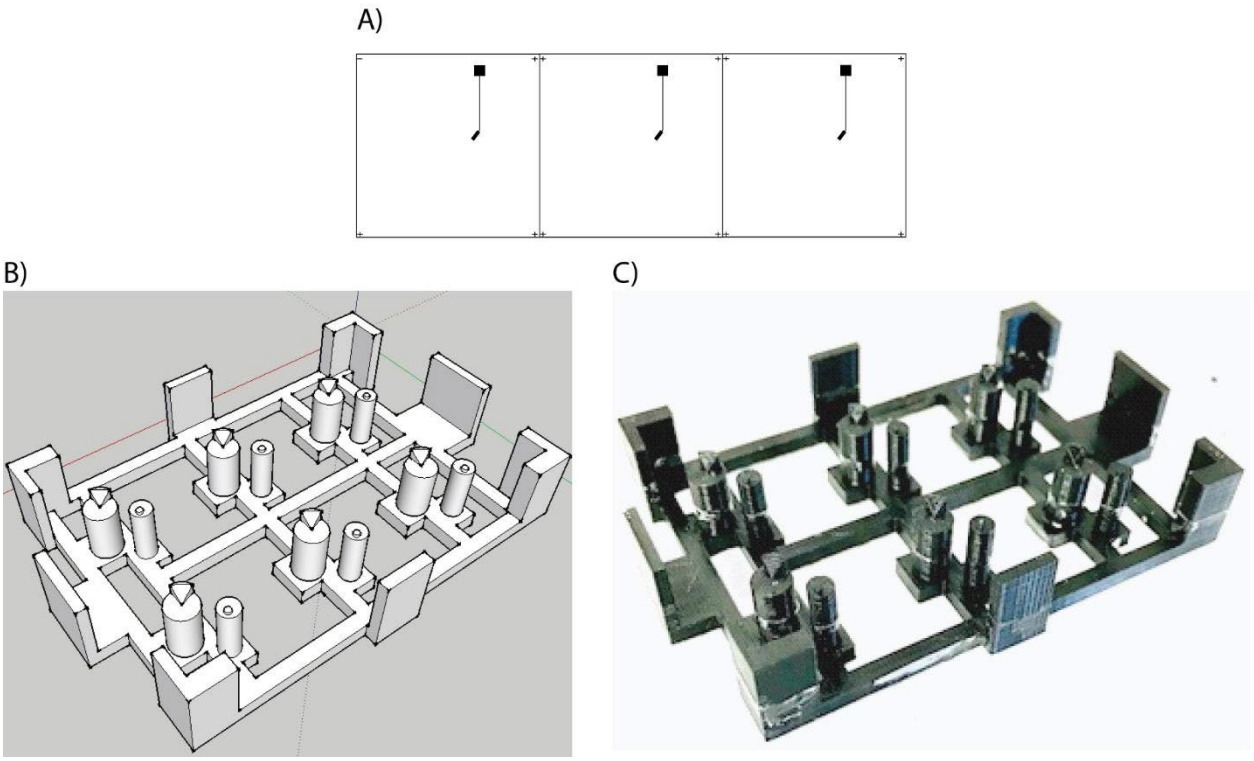

Figure 4. 1 A) Photomask design used for gold-on-glass (GoG) preparation. **B)** 3D CAD of the master to prepare electrochemical cell. **C)** 3D printed PLA used for molding PDMS electrochemical cells.

4.3.3 Master Wafer Fabrication

To create templates for the liquid channels and pneumatic control channels, we employed traditional photolithography techniques to produce two master wafers. The configurations for these

channels were designed using Adobe Illustrator software, and high-resolution plastic film photomasks were produced by Fineline Imaging in Colorado Springs, CO, USA, at a resolution of 50,800 dpi. To prepare the silicon wafers for use, they underwent a series of steps. First, they were agitated in a 1.0 M H2SO4 solution at a speed of 300 rpm for 30 minutes. This was followed by a thorough wash and agitation in deionized water for 30 minutes, concluding with air drying.

For the pneumatic control channel layer, we applied a layer of SU-8 2015 photoresist, approximately 30 μm in thickness, onto the silicon wafer using spin-coating at 2000 rpm for 45 seconds. The wafer was then subjected to a soft bake at 95°C for 5 minutes, followed by a gradual cooling to room temperature. Next, the photomask was precisely positioned on the photoresist-coated wafer, and UV exposure was carried out for 2 minutes using our in-house UV lithography light exposure unit. Following UV exposure, the wafer underwent a 5-minute development process in a SU-8 developer solution, followed by a 5-minute hard bake at 95°C on a hot plate.

For the fluidic layer wafer, we used a positive photoresist called AZ40 XT. We allowed the AZ40 XT photoresist to reach room temperature before use. Subsequently, a layer of AZ 40 XT photoresist, approximately 40 μm in thickness, was spin-coated onto the silicon wafer at 2000 rpm for 45 seconds. The wafer then underwent a sequence of soft-bake steps: first at 65°C for 5 minutes, then at 95°C for 5 minutes, and finally at 115°C for 5 minutes, with gradual cooling to room temperature. The photomask was carefully aligned on the AZ photoresist-coated wafer and exposed to UV for 120 seconds. Afterward, a hard bake was performed at 65°C for 1.5 minutes, followed by 95°C for 1.5 minutes, and finally 105°C for 1.5 minutes. Cooling was allowed to occur naturally, bringing the wafer back to room temperature. The AZ portion of the wafer underwent

annealing, which facilitated the templating of rounded channel cross-sections, achieved by baking at 120°C for 10 minutes.

4.3.4 Microchip Fabrication

The process began with the careful alignment of the 3D template onto the flow channel wafer. After a degassing procedure conducted under vacuum conditions, we poured a total of 45 grams of a well-mixed PDMS precursor mixture (with a 5:1 ratio of monomer to curing agent) onto the silicon wafer that had been patterned with flow channels. This wafer was placed within an aluminum foil container. The fluid layer was then baked in an oven at 65°C for a period of 1 hour. During the halfway point of the fluid layer's baking, we prepared another mixture of PDMS precursor (10.5 grams) with a different ratio, specifically a 20:1 ratio of monomer to curing agent. This mixture underwent a degassing process and was spin-coated onto the control layer at a rotation speed of 2100 rpm for 45 seconds, resulting in a layer approximately 30 μm thick. The control layer was then baked at 60°C for 30 minutes.

After removing the bulk PDMS material from both the 3D template and the wafer, we created the reservoir for the electrochemical cell. Subsequently, the flow channel layer was shaped by cutting, inlets were generated using Miltex disposable biopsy punches, and alignment with the valve channel layer was achieved under 3X microscopy. These two interconnected layers were placed in an oven at 65°C overnight to achieve permanent bonding.

Further steps included peeling the PDMS from the wafer, segmenting it into individual devices, punching the inlet for control valves, establishing connections for fluidic channels and via

channels using a punch with a 0.35-mm inner diameter, and cleaning the surfaces with methanol, followed by drying using N2 gas.

Before the PDMS device underwent plasma oxidation, the electrodes were cleaned with a piranha solution. This solution, freshly prepared, consisted of H2SO4 and H2O2 in a 3:1 ratio. It was applied to the electrode surface for one minute and then rinsed with deionized water. Each device was subsequently permanently bonded to Gold-sputtered on glass (GoG) using plasma oxidation carried out with the Harrick Plasma system (Ithaca, NY, USA), making the devices ready for use.

4.3.5 Automated Flow Control System of Microchip

The microfluidic chip was equipped with seven pneumatic push-up control valves, and their operation was controlled by an in-house-developed LabVIEW application. This application was connected to a customized manifold of solenoid switches (LHDA0533115H; the Lee Company, Westbrook, CT, USA) through a multifunction data acquisition system (PCI-6259, National Instruments).

To activate these pneumatic solenoid valves, a nitrogen gas source was employed, generating a pressure of 20 psi, which was regulated by a pressure regulator. The microchip's control valves were attached to the corresponding solenoid valves using 22-gauge blunt 304 stainless steel needles (Jensen Global JG22-0.5HPX-90, Santa Barbara, CA) at a 90-degree angle. They were connected through Tygon microbore tubing (0.02” I.D. X 0.06” O.D., Cole-Parmer, Vernon Hills, IL). The inlet points for the valves interfacing with the control system were created using a 0.75-mm inner diameter punch (69039-07, Electron Microscopy Sciences, Hatfield, PA).

In this configuration, an in-house-coded LabVIEW application managed the control of valve opening and closure. When a valve needed to be closed, the corresponding solenoid switch released nitrogen gas into the dead-end channel of the control layer, which had been filled with deionized water to prevent air from entering the channels. This action caused the PDMS membrane to deflect upwards, effectively sealing the flow channel in the upper layer, a mechanism known as the push-up valve.

4.3.6 Mixer Performance Evaluation

The microfluidic chip was placed onto the stage of a fluorescence microscope, which was equipped with a Tokai Hit microscope stage top incubator. To prepare the microchip for experimentation, the valve inlets were filled with deionized (D.I.) water. A 20 μL solution containing 100 nM fluorescein was introduced into the probe inlet, while 20 μL of D.I. water was added to the sample and reference inlets. Following this, the device was configured for fully automated operation, utilizing either 6 or 5-step peristaltic pumping with a pumping time of 600 ms and a total of 50 pump cycles.

Fluorescence imaging was performed at consistent intervals of 150 ms within the region of interest (as shown in Figure 4.5A). This imaging process used a FITC filter cube ($\lambda ex = 470 \pm 20$ nm, $\lambda em = 525 \pm 25$ nm) in combination with a CCD camera (CoolSnap HQ2; Photometrics Scientific), integrated with a Nikon inverted Ti-E fluorescence microscope (40X objective, 0.75 NA). The obtained fluorescence intensity data from these images underwent analysis using ImageJ software, and subsequent data processing was conducted within Excel.

4.3.7 Custom Reference Electrode

In our experiments, we used a custom-made L-shaped reference electrode, which is illustrated in Figure 4.2A. This electrode was crafted using a 2 mm outer diameter (OD) glass tubing and included a CoralPor glass frit (BASi, West Lafayette, IN), as well as a 0.5 mm silver wire (Alfa Aesar). The silver wire was filled with a solution of 3 M KCl. We obtained a 60-mm section of silver wire from our available stock and created a rubber plug with a 2 mm diameter from a rubber stopper using a 2-mm biopsy punch. This plug was attached to the silver wire, positioned approximately 30 mm from the wire's end. To chlorinate the lower 15 mm of the wire, we immersed it in a 3 M KCl solution while applying 9 V (direct current) for about 10 seconds, with the wire serving as the positive terminal with respect to ground and a platinum electrode functioning as the return electrode. This process resulted in the formation of a gray/white AgCl coating on the wire's surface.

The chlorinated silver wire was then inserted into the L-shaped glass structure, with the rubber plug positioned 5 mm below the end of the glass tube. We applied epoxy (Loctite, Düsseldorf, Germany) to the end and allowed it to cure. After the curing process, we introduced 3 M KCl into the glass tubing and securely placed the frit at the end of the glass tubing. It was held in place by transparent heat shrink tubing. This reference electrode underwent a 24-hour equilibration period before it was used.

Additionally, we designed and produced another 3D CAD template to assist in positioning the counter electrode on the electrochemical cell, as shown in **Figures 4.2B and 4.2C**.

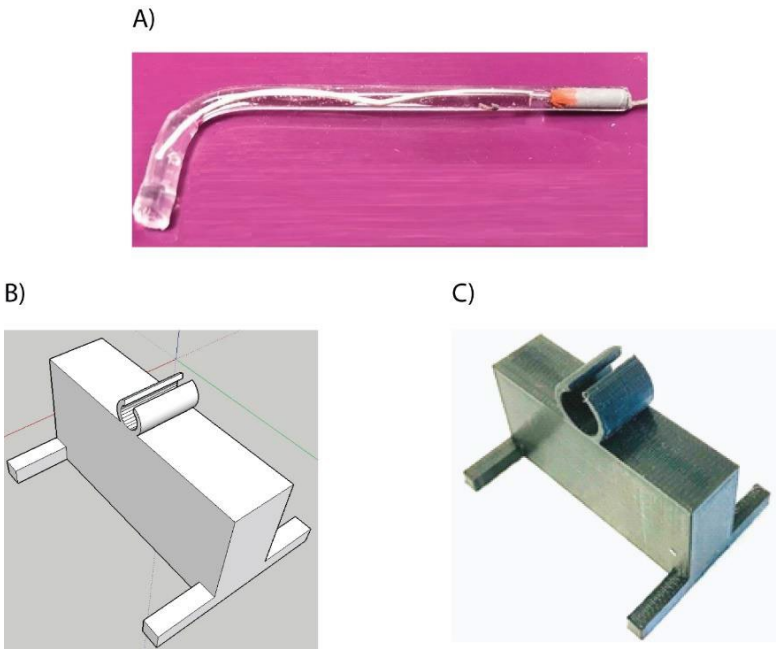

Figure 4. 2 A) Assembled Ag/AgCl L-shaped reference electrode, filled with 3M KCl and closed by porous frits. **B)** 3D CAD of the reference electrode holder. **C)** 3D printed PLA used as a reference electrode holder.

4.3.8 Electrochemical Measurements

Electrochemical measurements were conducted using a custom-built potentiostat. We introduced a customized silver/silver chloride reference electrode (3 M KCl) and a platinum counter electrode (CH Instruments) into the electrochemical cell, which had previously been filled with a 0.1 M potassium chloride buffer solution. In the sample inlet, we added 20 µL of a mixture containing equimolar concentrations of potassium ferricyanide and potassium ferrocyanide, while 20 µL of a 0.1 M potassium chloride buffer was placed in both the probe and reference inlets.

For complete automation, the device was configured to operate using peristaltic pumping, with a pumping time of 600 ms, and was run for either 50 or 400 pump cycles, corresponding to each

sample concentration. The resulting current, generated by varying concentrations (0, 1, 5, 10 nM) of the ferri/ferrocyanide redox couple in a 0.1 M potassium chloride buffer, was then monitored every minute using square-wave voltammetry (SWV). This SWV procedure covered a potential range from -0.2 to +0.6 V (versus the reference electrode). It utilized a step size of 1 mV, a pulse height of 25 mV, and an SWV frequency of 100 Hz.

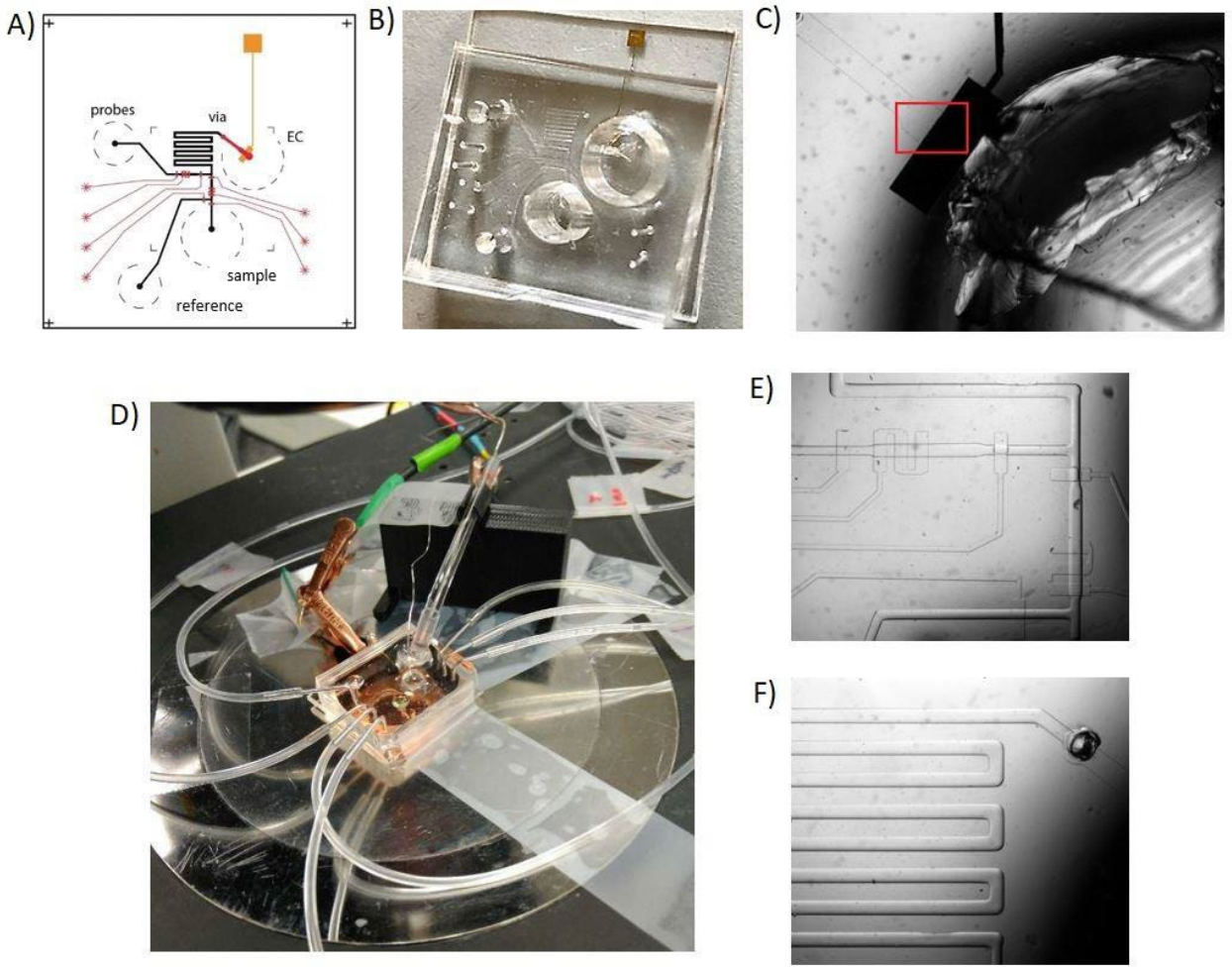

Figure 4. 3 A) Schematic of the channel layouts, with fluidic channels shown in black and pneumatic control channels and detection channel in red. **B)** Photo of assembled device. **C)** Gold electrode placed inside the detection channel. **D)** Photo of working device in the microscope stage.

Tubing was connected to control channels. Reference and counter electrodes were positioned on top of the 3D-templated reservoir to serve as the full sensor. **E)** Microvalves controlling the fluid flow. **F)** Serpentine-shaped incubation channel for homogenization of fluids.

4.3.9 Electrode Preparation and Detection of Nucleic Acid

Following the preparation of the device, we loaded all three inlets with 20 µL of a 10 mM HEPES buffer containing 0.5 M NaCl at pH 7. We then guided this solution through the channel using valve-based peristaltic pumps. Next, we prepared the electrochemical cell by introducing a custom silver/silver chloride reference electrode (3 M KCl) and a platinum counter electrode (CH Instruments). The electrochemical cell was pre-filled with the same HEPES buffer solution. An initial square-wave voltammetry (SWV) measurement was conducted in the potential range of -0.45 to 0 V (versus the reference electrode). This measurement used a step size of 1 mV, a pulse height of 25 mV, and an SWV frequency of 100 Hz.

To reduce the thio-DNA, we employed the reducing agent TCEP. To achieve this, we combined 1 µL of a 200 µM thio-DNA solution with 3 µL of a 10 mM TCEP solution. The mixture was then incubated in darkness at room temperature for 1 hour. The resulting solution was diluted to achieve a final thio-DNA concentration of 1.25 µM in a HEPES buffer containing 10 mM HEPES and 0.5 M NaCl at pH 7. We emptied the electrochemical cell and introduced 50 µL of the thio-DNA solution into the cell. This mixture was incubated at room temperature for an additional hour. Afterward, the thio-DNA solution was replaced with buffer, and another measurement was taken. In the subsequent step, we loaded the inlets with 20 µL of a 3 mM mercaptohexanol (MCH) solution in a HEPES buffer containing 10 mM HEPES and 0.5 M NaCl at pH 7. This solution

flowed through the channel for 1 hour, during which SWV measurements were conducted at 10-minute intervals. Following the MCH passivation step, we loaded the inlets with 20 μL of a 1% BSA solution in a HEPES buffer. This solution flowed through the channel for 30 minutes, and SWV measurements were performed at 10-minute intervals.

For electrochemical detection of MB-labeled complementary DNA, we loaded the sample inlet with 20 μL of a 100 nM sample solution. This solution was introduced into the microfluidic biosensor at a flow rate of 4.35 nL/min and then subjected to SWV measurement. In the kinetics experiment, a 20 μL sample of 50 nM concentration was utilized.

4.3.10 Data Analyses

4.3.10.1 Peak Height

The raw data from SWV, which included both Vstep and Idiff values, was imported into Microsoft Excel. To create a smoother representation of the data, a 9-point moving average was applied. To eliminate the influence of capacitance current, a third-order polynomial baseline was established using Excel's "Linest" function. Specifically, data points falling within the ranges of -0.421 to -0.358 V and -0.140 to -0.005 V were used for this baseline calculation. The calculated baseline was then subtracted from the original raw data. You can observe an example of this process in **Figure 3.2**. The peak height measurement was determined by extracting the highest current value from the resulting difference graph (not shown).

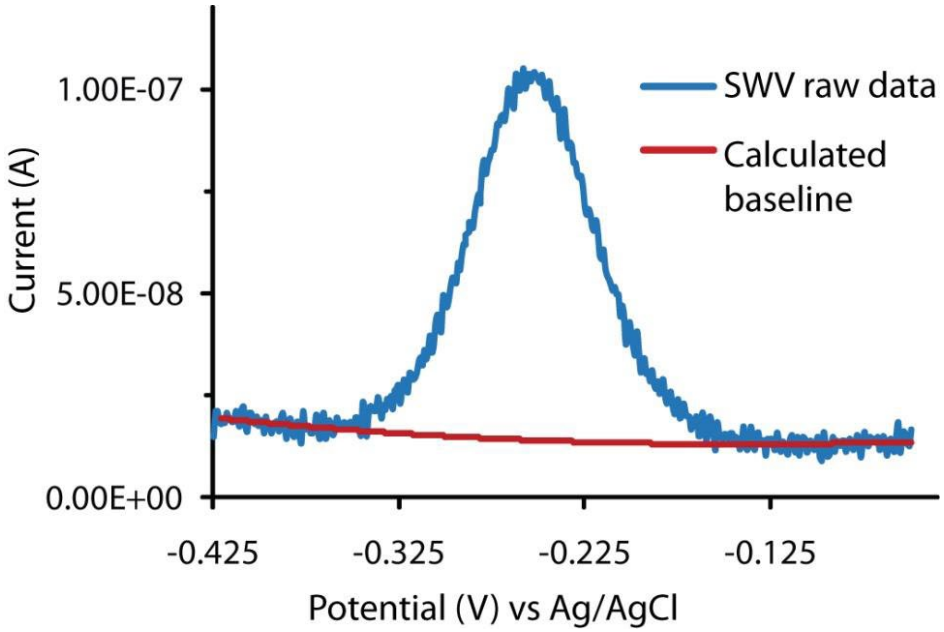

Figure 4. 4 Example MB-DNA redox current sampled during SWV (raw data) along with the calculated baseline curve used for Faradaic current extraction. The maximum current from the difference curve (not shown here) was used as the peak height of each individual measurement.

4.3.10.2 Average Distance Between Nanostructures

The number of moles of nanostructure, N_{tot}, was determined using a previously established relationship[24, 25] using the following relationship,

$$i_p = 2nfFN_{tot} \times \frac{sinh\left(\frac{nFE}{RT}\right)}{cosh\left(\frac{nFE}{RT}\right) + 1}$$

where *ip* is the peak height of the current measurement, *n* is the number of electrons transferred per redox event (with MB label, n = 2), *F* is the Faraday constant, *R* is the universal gas constant, *T* is the temperature, *E* is the applied voltage amplitude, and *f* is the SWV frequency.

We assumed that electron transfer occurs exclusively between MB and the electrode surface once the nanostructure is formed. This assumption was based on previous findings that indicated MB is washed away in the absence of proper formation[26]. To determine the nanostructure surface density in units of mol cm^{-2}, we divided the number of nanostructure moles by the electrode surface area. By taking the reciprocal of this density value (strands cm^{-2}), we estimated a circular area around each DNA-nanostructure, and from the diameter of this circle, we calculated the distance between nanostructures.

4.3.10.3 Signal Suppression

The following equation was used to calculate signal suppression, where i_p *(initial)* is the peak height of the initial current measurement (before target incubation) and i_p *(final)* is the peak height of the final current measurement (after target incubation).

$$\textbf{\textit{Signal Suppression}}\ (\%) = -100 \times \frac{\boldsymbol{i_p\ (final) - i_p\ (initial)}}{\boldsymbol{i_p\ (initial)}}$$

4.4 Results and Discussion

4.4.1 Microchip Design and Operation

The microchip design consists of two PDMS layers, as illustrated in **Figure 4.4** the lower layer, known as the control layer and highlighted in red, contains 7 pneumatic channels to enable fully automated chip operations, along with a dedicated detection channel. The upper layer is designed for the fluidic channel, shown in black, which includes a T-junction channel to facilitate the mixing of reagents and samples. This layer also features a serpentine-shaped incubation channel, essential

for thorough homogenization of the two components. A connection point (via) exists between these two layers to ensure seamless integration.

In the operational process, the sample follows the serpentine-shaped channel until it reaches the detection channel. Within this region, the downstream profile of the sample solution allows for direct contact with the electrode. This design minimizes sample diffusion within the bulk solution. At the end of the detection channel, you'll find the electrode, accompanied by a 3D-templated reservoir positioned above it. This reservoir serves as a container for the supporting electrolyte, reference electrode, and counter electrode, which are all crucial components for facilitating electrochemical measurements.

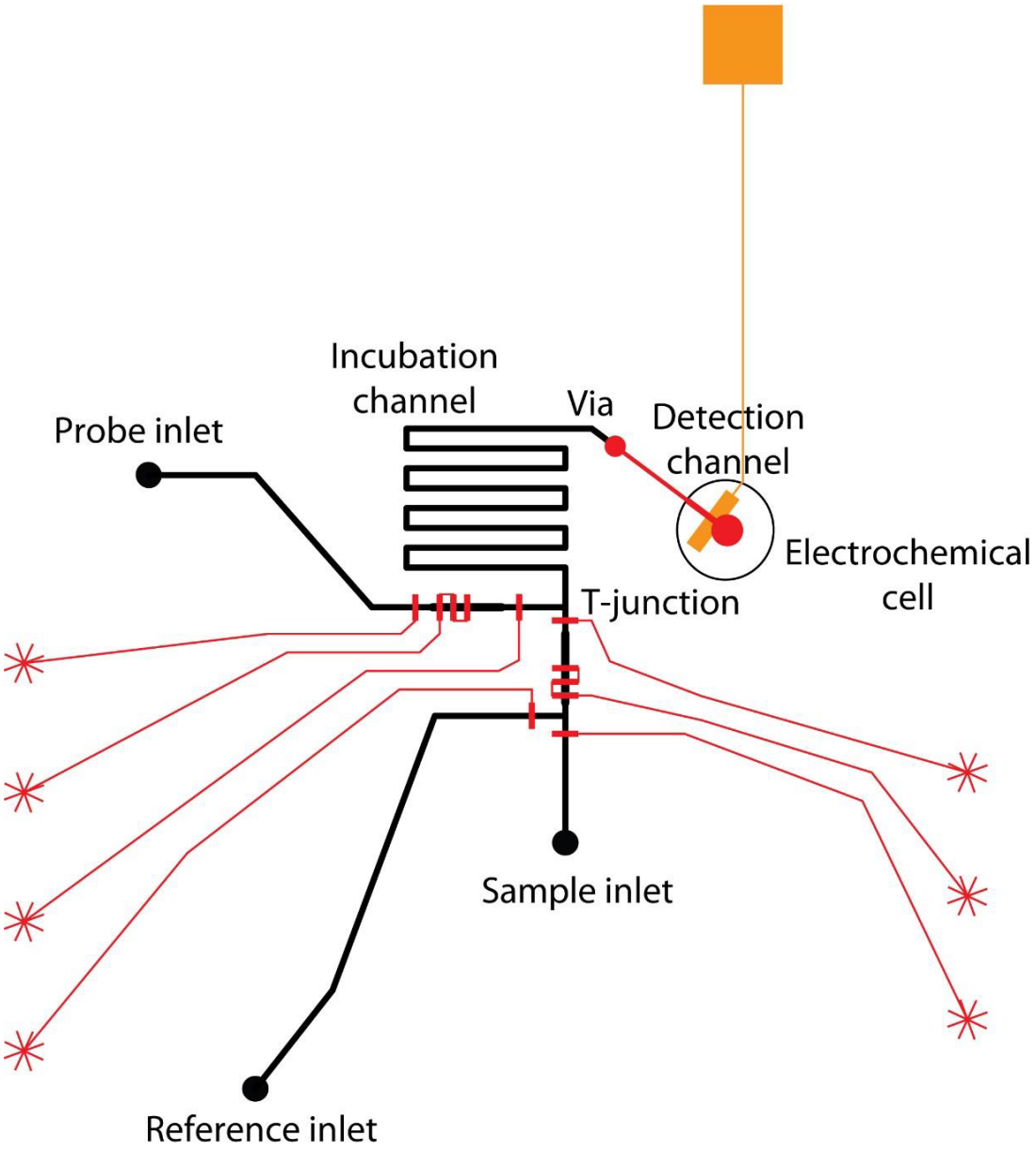

Figure 4. 5 Schematic of the channel design at higher resolution. Two-layer microfluidic chip design: the short red lines, representing the microvalves, is the bottom layer for controlling. Via is the connection point between the two layers, which connects the fluidic channel and detection channel. The inlets and incubation channel are in the top layer for fluid flow.

In this system, fluid movement along the channels is achieved using valve-based peristaltic pumps. One significant feature of this device is the deliberate alignment of fluids from the probe inlet and the sample or reference inlet, ensuring their orthogonal convergence at the T junction. This alignment is facilitated by coordinating the activation of valves within their respective channels, programmed to pump simultaneously. Each channel is equipped with three valves arranged within a single channel configuration.

Peristaltic pumping occurs when these valves are actuated following either a 6-step pattern (101, 100, 110, 010, 011, 001) or a 5-step pattern (100, 110, 011, 001, 101), where the binary representation of 0 and 1 corresponds to open and closed valves, respectively. In each pumping cycle, the volume dispensed downstream precisely matches the volume occupied by the central valve membrane when it closes. This mechanism allows for precise control over the sample volume by adjusting the number of cycles pumped.

Compared to more passive microfluidic setups relying on methods like syringe pumps, pressure, or vacuum, this peristaltic pumping system offers significantly enhanced precision in volume metering. Additionally, passive systems often rely on laminar flow to control the mixing ratio of components and are susceptible to fluctuations over extended operation periods.

4.4.2 Evaluation of Mixer Performance

The microchip incorporates a lengthy incubation channel with a distinct serpentine shape. This channel plays a crucial role in ensuring thorough and complete mixing of the two assay solutions while maintaining a predefined flow rate. In this context, a solution containing 100 nM fluorescein

was introduced through the probe inlet, while water was simultaneously pumped in through the sample/reference inlet. The flow rate for this process was precisely set at 4.35 nL/min.

During this operational phase, the sample solution loaded with fluorescein travels through the extensive serpentine channel, undergoing a deliberate mixing process with the introduced water. The resulting fluorescence intensity measurements were taken from various regions of interest (ROIs). As shown in **Figure 4.5**, a combination of the sample and water becomes evident after traversing 8 turns of the serpentine channel. This blending ultimately yields a consistent fluorescence signal, particularly at ROI#11, which corresponds to the detection channel.

An interesting phenomenon occurs as these two fluids move along the serpentine channel. The center of each fluid stream advances at a faster rate than the edges, causing the interface between the fluids to stretch. This stretching effect significantly enhances the rate of diffusion across this interface, facilitating rapid and efficient mixing and equilibration of the solution.

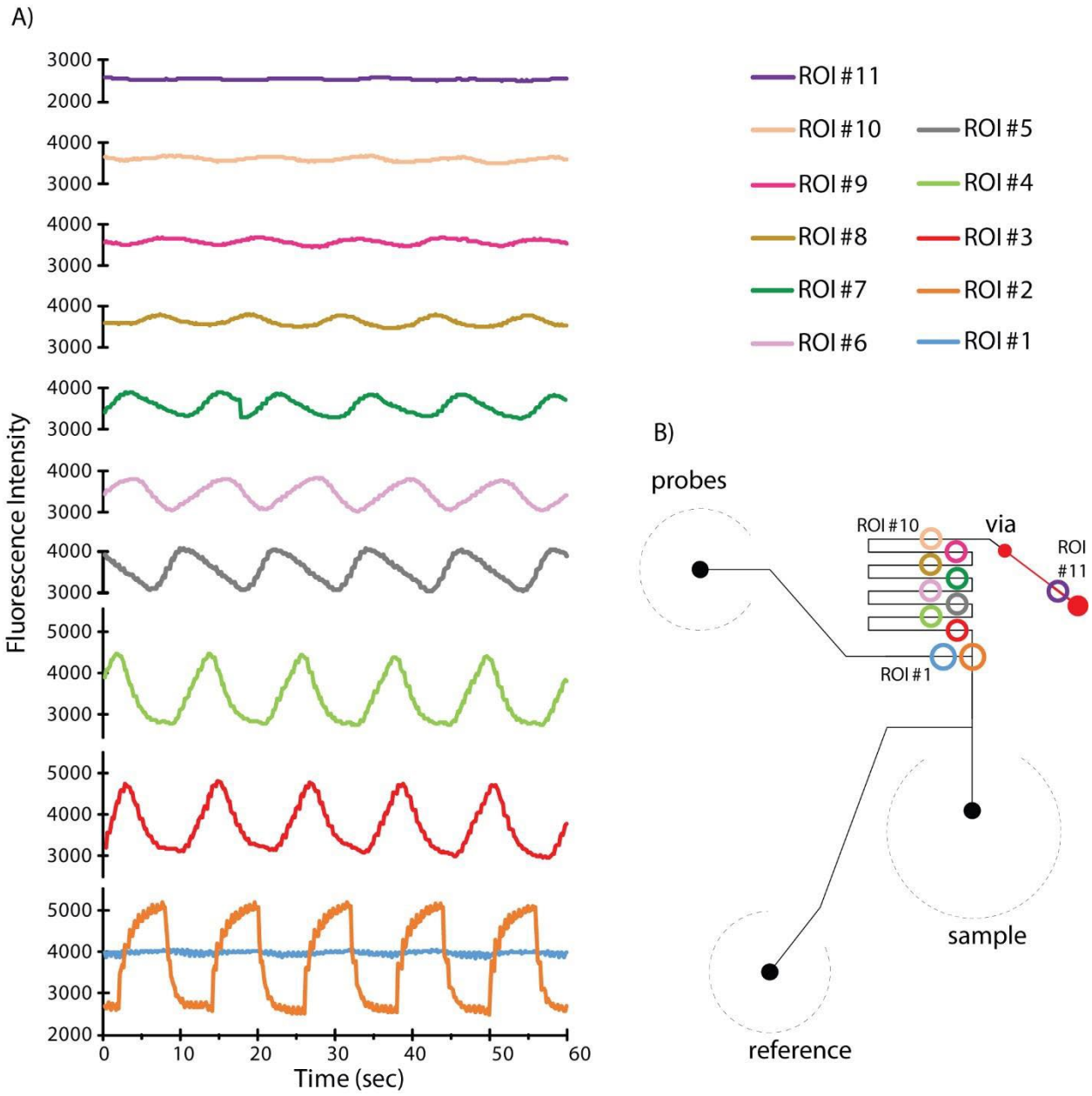

Figure 4. 6 A) Fluorescence intensity measured at different region of interest (ROI) to evaluate the extent of mixing. Steady fluorescence signal at ROI#11 indicates homogenization of two fluids. **B)** Channel layout with color coded circles to represent ROI.

4.4.3 Dynamic Electrochemical Measurement

To validate the simultaneous operation of both fluidic and electrical components within the device, an experiment was conducted involving the concurrent flow of a sample and electrochemical detection. The microfluidic system functioned as a flow injection apparatus, where a sample containing potassium ferri/ferrocyanide was injected into a continuous buffer stream. Inside the microchannel, a steady flow of 0.1 M potassium chloride solution, serving as the supporting electrolyte, was maintained through the probe inlet. Simultaneously, a sample solution with varying concentrations of potassium ferri/ferrocyanide was introduced through the sample inlet. This solution traveled through the incubation channel, mixed with the buffer, and then progressed through the detection channel after dilution.

A gold electrode located at the end of the microfluidic detection channel played a crucial role in confirming the system's electrochemical response. As expected, a distinct and well-defined SWV peak corresponding to the $[Fe(CN)6]^{-3/-4}$ redox couple was obtained. An illustrative example of this phenomenon for the 10 nM concentration is presented in Figure **4.6A**. Interestingly, the system effectively differentiated between four distinct sample concentrations. Notably, a decrease in signal intensity was observed as the sample concentration decreased, as shown in Figure **4.6B**. However, it's important to note that the signal was detected approximately 3 minutes after the sample injection. This delay may be attributed to the positioning of the electrode outside the detection channel.

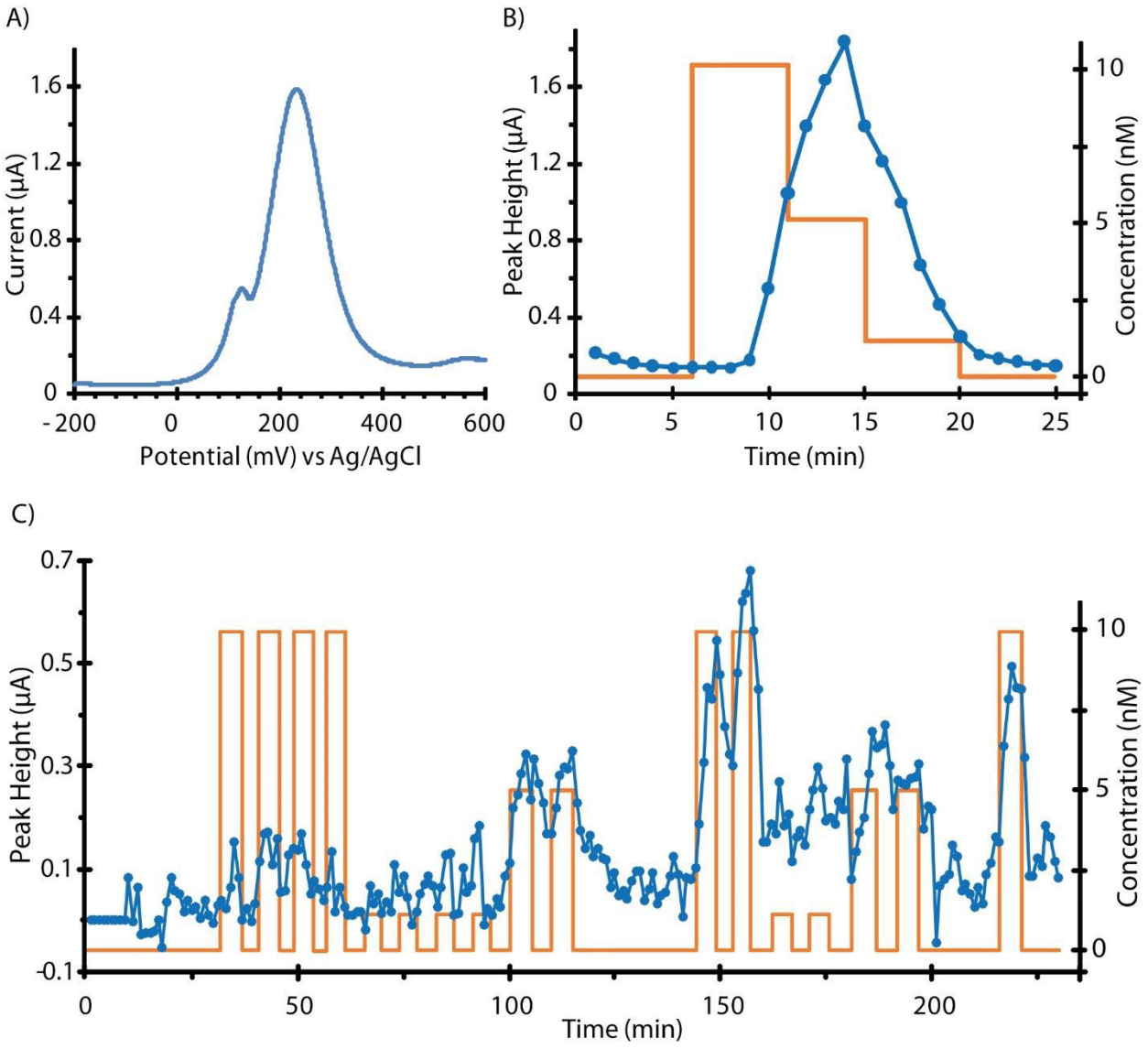

Figure 4. 7 A) SWV peak of [Fe(CN)6]-3/-4 redox couple obtained by simultaneous sample flow and electrochemical measurement. **B)** Profile of the sensor current signal in response to three concentrations of [Fe(CN)6]-3/-4 injected into a stream of buffer flowing through the electrode. **C)** Profile of the sensor current signal in response to programmed square wave of buffer and sample at different concentrations.

We conducted an additional experiment involving the placement of the electrode within the detection channel. The device was systematically operated using a square wave approach, with

the automated introduction of buffer and sample solutions at various concentrations. This setup aimed to demonstrate the functionality of the temporal sampling mode. In this specific scenario, the reference inlet was used to inject the buffer solution into the channel.

As depicted in Figure **4.7C**, the microfluidic flow-injection mechanism resulted in a noticeable increase in peak current when the sample was introduced into the channel. Subsequently, a decrease in peak current was observed as the buffer solution was injected. These electrochemical measurements performed within the integrated microfluidic system not only validated the operational performance of both the electrochemical system and the fluidic mixer but also highlighted the device's capability to operate in temporal sampling mode. It is worth noting, however, that the device remained unresponsive for the initial 100 minutes of operation. This delay could potentially be attributed to channel clogging or valves adhering to the flow channel, causing slow or restricted fluid movement.

4.4.4 Automated Microfluidic Electrode Preparation

Upon the initial confirmation of device functionality, we proceeded to adapt our automated, valve-controlled microfluidics for the purpose of electrode preparation. The entire process of gold electrode preparation, which included the following steps, was carried out on-chip:

1. Deposition of bare gold.
2. Formation of a DNA monolayer.
3. Passivation using mercaptohexanol (MCH).
4. Passivation with bovine serum albumin (BSA) in a buffer solution.

As shown in **Figure 4.7**, the introduction of a DNA monolayer resulted in an increased capacitive current (1.6 μA). This increase can be attributed to the negatively charged phosphate backbone of the nucleic acid. Subsequently, upon the injection of MCH through the channel, the capacitive current gradually decreased. This decline indicates the surface-blocking effect of MCH and the removal of weakly and nonspecifically adsorbed nucleic acids, leading to the formation of a dense MCH sublayer. Finally, the introduction of BSA further reduced the capacitive current to 74 nA. These results convincingly demonstrate that electrodes can be effectively prepared using minimal reagent volumes (Dead volume: 20 μL) through the application of automated microfluidic techniques.

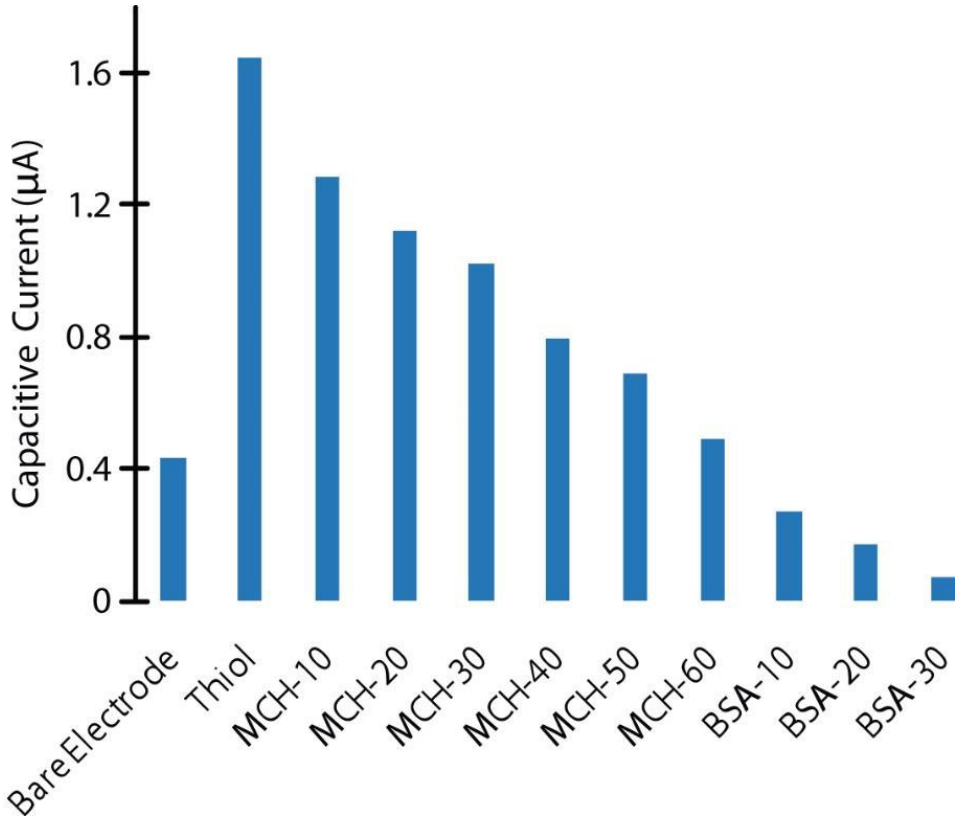

Figure 4. 8 Multiple, automated electrode preparation steps conducted on-chip. DNA monolayer formation resulted in high capacitive current, which was gradually decreased by MCH and BSA passivation.

4.4.5 Detection of Nucleic Acid

To detect complementary DNA, we introduced a sample solution labeled with a redox tag into a continuous buffer stream through the sample inlet. This allowed the sample solution to interact with the thiolated-DNA immobilized on the electrode surface, resulting in the generation of an electrochemical signal. As depicted in Figure 4.8A, the MB-labeled DNA was rapidly detected in real-time within just one minute after its introduction into the channel (indicated by the red arrow). This detection was achieved through the use of on-chip valve-based peristaltic pumps. The signal reached a stable state after approximately 20 minutes.

Subsequently, the device underwent a square wave of buffer and sample introduction, with buffer solution being introduced through the reference inlet. Figure 4.8B illustrates the sequence of events, where a signal emerged upon the injection of the sample into the well. A consistent signal was maintained in the buffer stream, followed by an increase in signal magnitude during the second cycle of sample injection. These results once again confirmed the device's suitability for temporal sampling mode.

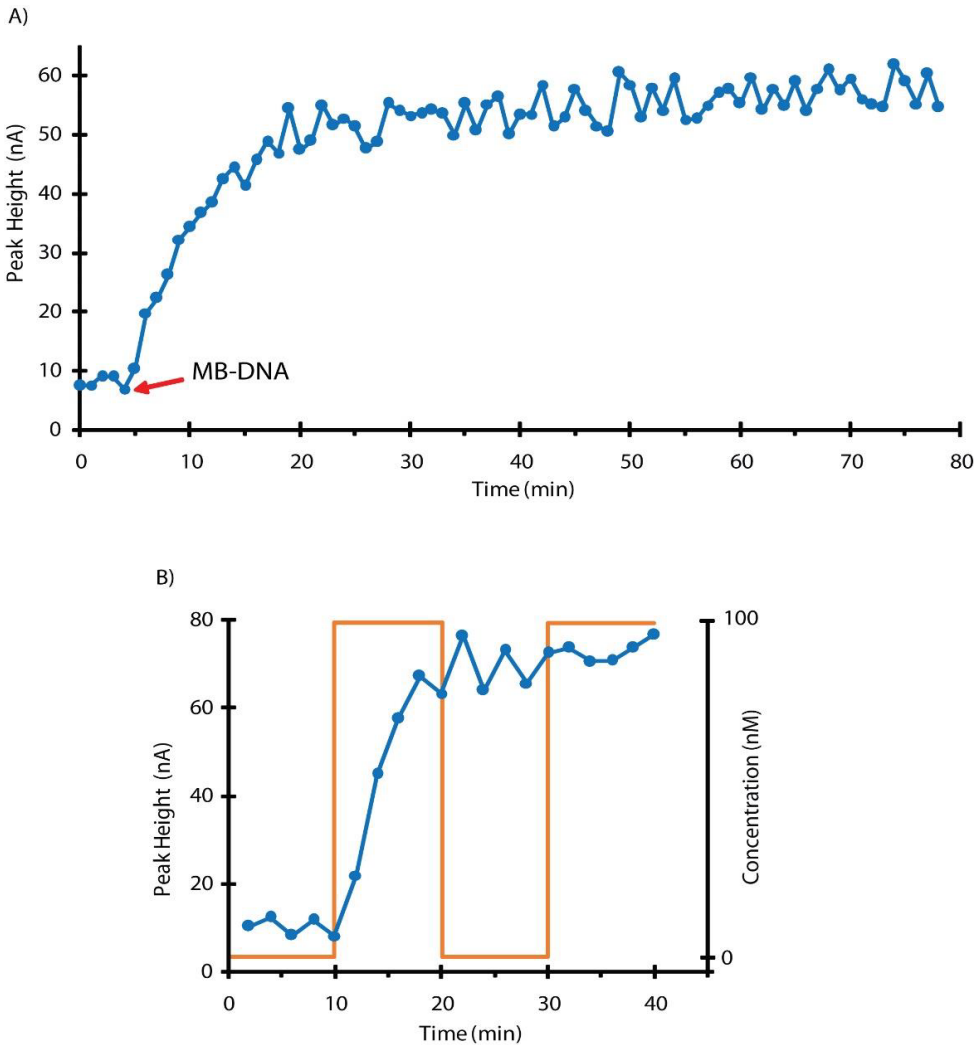

Figure 4. 9 A) Real-time detection of 50 nM MB-DNA strand. **B)** Sensor response to programmed square wave of buffer and 100 nM MB-DNA strand.

4.5 Conclusions

We have successfully demonstrated the integration of an electrochemical detection system with automated microfluidics for electrode preparation and nucleic acid detection. Through the use of valve-controlled automated microfluidics, we achieved a reduction in reagent consumption during the multi-step electrode fabrication process. Furthermore, the real-time detection of target DNA

was achieved within just one minute of injection into the microchannel. The microchannel system demonstrated efficient fluid mixing, suggesting its potential for conducting biochemical assays that require sample-reagent premixing directly on the chip. While further advancements are required, this automated microfluidics-linked electrochemical detection system establishes a foundation for studying real-time cell secretion scenarios

One practical application of this device involves the utilization of the electrochemical proximity assay (ECPA)[27, 28] to monitor insulin secretion from live murine pancreatic islets over time, triggered by stimuli such as glucose. By simultaneously injecting secreted insulin and antibody-oligo probes into the microchannel, their combination becomes feasible. Subsequently, the complex can be captured on the thiolated-DNA modified electrode surface, resulting in an electrochemical signal. As a result, this integrated device provides a promising avenue for gaining enhanced insights into the dynamic functionality of endocrine tissues.

4.6 References

1. Rackus, D. G.; Shamsi, M. H.; Wheeler, A. R., Electrochemistry, biosensors and microfluidics: a convergence of fields. *Chemical Society Reviews* **2015,** *44* (15), 5320-5340.
2. Chiu, D. T.; Demello, A. J.; Di Carlo, D.; Doyle, P. S.; Hansen, C.; Maceiczyk, R. M.; Wootton, R. C., Small but perfectly formed? Successes, challenges, and opportunities for microfluidics in the chemical and biological sciences. *Chem* **2017,** *2* (2), 201-223.
3. Nikoleli, G.-P.; Siontorou, C. G.; Nikolelis, D. P.; Bratakou, S.; Karapetis, S.; Tzamtzis, N., Biosensors based on microfluidic devices lab-on-a-chip and microfluidic technology. *Nanotechnology and biosensors* **2018**, 375-394.
4. Abdulbari, H. A.; Basheer, E. A., Electrochemical biosensors: electrode development, materials, design, and fabrication. *ChemBioEng Reviews* **2017,** *4* (2), 92-105.
5. da Everson, T.; Souto, D. E.; Barragan, J. T.; Giarola, J. d. F.; de Moraes, A. C.; Kubota, L. T., Electrochemical biosensors in point-of-care devices: recent advances and future trends. *Chemelectrochem: fundamentals and applications* **2017**.
6. Evans, D.; Papadimitriou, K. I.; Vasilakis, N.; Pantelidis, P.; Kelleher, P.; Morgan, H.; Prodromakis, T., A novel microfluidic point-of-care biosensor system on printed circuit board for cytokine detection. *Sensors* **2018,** *18* (11), 4011.
7. Kaur, G.; Tomar, M.; Gupta, V., Development of a microfluidic electrochemical biosensor: Prospect for point-of-care cholesterol monitoring. *Sensors and Actuators B: Chemical* **2018,** *261*, 460-466.
8. Shin, S. R.; Kilic, T.; Zhang, Y. S.; Avci, H.; Hu, N.; Kim, D.; Branco, C.; Aleman, J.; Massa, S.; Silvestri, A.; Kang, J.; Desalvo, A.; Hussaini, M. A.; Chae, S.-K.; Polini, A.; Bhise, N.; Hussain, M. A.; Lee, H.; Dokmeci, M. R.; Khademhosseini, A., Label-Free and Regenerative Electrochemical Microfluidic Biosensors for Continual Monitoring of Cell Secretomes. *Advanced Science* **2017,** *4* (5), 1600522.
9. Wang, R.; Xu, Y.; Sors, T.; Irudayaraj, J.; Ren, W.; Wang, R., Impedimetric detection of bacteria by using a microfluidic chip and silver nanoparticle based signal enhancement. *Microchimica Acta* **2018,** *185*, 1-8.
10. Li, Y.; Sella, C.; Lemaître, F. d. r.; Guille-Collignon, M.; Amatore, C.; Thouin, L., Downstream simultaneous electrochemical detection of primary reactive oxygen and nitrogen species released by cell populations in an integrated microfluidic device. *Analytical chemistry* **2018,** *90* (15), 9386-9394.
11. Liu, Z. J., M.; Cao, J.; Niu, R.; Li, P.; Zhou, G.; Yu, Y.; van den Berg, A.; Shui, L.,, Electrochemical sensor integrated microfluidic device for sensitive and simultaneous quantification of dopamine and 5-hydroxytryptamine. *Sensors and Actuators B: Chemical* **2018,** *273*, 873-883.
12. Lakey, A.; Ali, Z.; Scott, S. M.; Chebil, S.; Korri-Youssoufi, H.; Hunor, S.; Ohlander, A.; Kuphal, M.; Marti, J. S., Impedimetric array in polymer microfluidic cartridge for low cost point-of-care diagnostics. *Biosensors and Bioelectronics* **2019,** *129*, 147-154.
13. Li, S.; Zhang, C.; Wang, S.; Liu, Q.; Feng, H.; Ma, X.; Guo, J., Electrochemical microfluidics techniques for heavy metal ion detection. *Analyst* **2018,** *143* (18), 4230-4246.

14. Kudr, J.; Zitka, O.; Klimanek, M.; Vrba, R.; Adam, V., Microfluidic electrochemical devices for pollution analysis–A review. *Sensors and Actuators B: Chemical* **2017,** *246*, 578-590.
15. Holmes, J.; Pathirathna, P.; Hashemi, P., Novel frontiers in voltammetric trace metal analysis: Towards real time, on-site, in situ measurements. *TrAC Trends in Analytical Chemistry* **2019,** *111*, 206-219.
16. Gallardo-Gonzalez, J.; Baraket, A.; Boudjaoui, S.; Metzner, T.; Hauser, F.; Rößler, T.; Krause, S.; Zine, N.; Streklas, A.; Alcácer, A., A fully integrated passive microfluidic Lab-on-a-Chip for real-time electrochemical detection of ammonium: Sewage applications. *Science of the total environment* **2019,** *653*, 1223-1230.
17. Lu, L.; Gunasekaran, S., Dual-channel ITO-microfluidic electrochemical immunosensor for simultaneous detection of two mycotoxins. *Talanta* **2019,** *194*, 709-716.
18. Pol, R.; Céspedes, F.; Gabriel, D.; Baeza, M., Microfluidic lab-on-a-chip platforms for environmental monitoring. *TrAC Trends in Analytical Chemistry* **2017,** *95*, 62-68.
19. Liao, Z.; Wang, J.; Zhang, P.; Zhang, Y.; Miao, Y.; Gao, S.; Deng, Y.; Geng, L., Recent advances in microfluidic chip integrated electronic biosensors for multiplexed detection. *Biosensors and Bioelectronics* **2018,** *121*, 272-280.
20. Cincotto, F. H.; Fava, E. L.; Moraes, F. C.; Fatibello-Filho, O.; Faria, R. C., A new disposable microfluidic electrochemical paper-based device for the simultaneous determination of clinical biomarkers. *Talanta* **2019,** *195*, 62-68.
21. Lee, G.; Lee, J.; Kim, J.; Choi, H. S.; Kim, J.; Lee, S.; Lee, H., Single microfluidic electrochemical sensor system for simultaneous multi-pulmonary hypertension biomarker analyses. *Scientific reports* **2017,** *7* (1), 7545.
22. Panini, N. V.; Messina, G. A.; Salinas, E.; Fernández, H.; Raba, J., Integrated microfluidic systems with an immunosensor modified with carbon nanotubes for detection of prostate specific antigen (PSA) in human serum samples. *Biosensors and Bioelectronics* **2008,** *23* (7), 1145-1151.
23. Uliana, C. V.; Peverari, C. R.; Afonso, A. S.; Cominetti, M. R.; Faria, R. C., Fully disposable microfluidic electrochemical device for detection of estrogen receptor alpha breast cancer biomarker. *Biosensors and Bioelectronics* **2018,** *99*, 156-162.
24. Somasundaram, S.; Easley, C. J., A nucleic acid nanostructure built through on-electrode ligation for electrochemical detection of a broad range of analytes. *Journal of the American Chemical Society* **2019,** *141* (29), 11721-11726.
25. D O'Connor, S.; Olsen, G. T.; Creager, S. E., A Nernstian electron source model for the ac voltammetric response of a reversible surface redox reaction using large-amplitude ac voltages. *Journal of Electroanalytical Chemistry* **1999,** *466* (2), 197-202.
26. Mahshid, S. S.; Camiré, S. b.; Ricci, F.; Vallée-Bélisle, A., A highly selective electrochemical DNA-based sensor that employs steric hindrance effects to detect proteins directly in whole blood. *Journal of the American Chemical Society* **2015,** *137* (50), 15596-15599.
27. Hu, J.; Wang, T.; Kim, J.; Shannon, C.; Easley, C. J., Quantitation of femtomolar protein levels via direct readout with the electrochemical proximity assay. *Journal of the American Chemical Society* **2012,** *134* (16), 7066-7072.

28. Jiaming, H.; Yajiao, Y.; Subramaniam, S.; Ferdous, T.; Joonyul, K.; Curtis, S., A Reusable Electrochemical Proximity Assay for Highly Selective, Real-Time Protein Quantitation in Biological Matrices. *Journal of the American Chemical Society* **2014,** *136* (23), 8467-8474

5.4

Conclusions and Future Directions: Development of of FFA uptake and secretion quantification assay from same explant on microfluidic platform

5.1 Final words for dissertation

In this dissertation, we developed a few microfluidic devices for free fatty acid (FFA) uptake assay, glycerol, and non-esterified fatty acid (NEFA) multiplex secretion assay and also for preparing DNA nanostructure on gold electrodes. We also have a future plan to expand the research on quantifying free fatty acid uptake and secretion from same piece of tissue at the same time by combining μDAC (**Figure 2. 26**) to μADC (**Figure 3. 15 A**).

As this research was advanced, the plan was to enhance the system's efficiency and accuracy by concurrently detecting two eWAT explants in future projects. This modification would broaden the scope of investigations and improve data acquisition. In summary, the research background underscores the significance of microfluidic devices for studying endocrine tissue dynamics, particularly in the context of adipose tissue metabolism and fatty acid and glycerol uptake or secretion. The development and integration of the μDAC and μADC designs into the microfluidic platform represents significant advancements in the field, with the potential to improve our understanding of endocrine tissue functions in health and disease.

Based on the outcomes of this research, my career aspirations revolve around advancing microfluidic technology to study endocrine tissue functions, particularly in the context of adipose tissue dynamics and metabolic processes, bridging the fields of engineering and biology. In the

future, I aim to apply these findings to clinical and translational research while collaborating with experts in biology, medicine, and other engineering disciplines.

5.2 Future directions : Development of µDAC to µADC converter for FFA uptake and secretion quantification assay from same explant simultaneously

Microfluidic devices have gained recognition as valuable tools for simulating in vivo conditions and interfacing with cultured or primary cells to explore the dynamics of endocrine tissue functions[1]. These devices enable the creation of microenvironments that replicate conditions within endocrine tissues, offering a valuable platform for studying their roles in normal and diseased states[2].

In the context of my research, I aimed to leverage microfluidics to emulate endocrine tissue microenvironments and gain novel insights into their functions. I designed, fabricated, and characterized several microfluidic devices to stimulate tissues with higher resolution during different physiological states, such as feeding and fasting. These devices provided the capability to investigate time-dependent responses of endocrine tissues to various stimuli, including nutrient uptake or secretion.

To examine the timing of stimulation in microfluidic devices, I developed an innovative method involving fluorescein-labeled glass beads as tissue mimics. These beads were used to modulate fluorescence emissions by exposing them to solutions with varying pH levels, enabling precise control over the stimulation conditions[3]. This approach allowed for a temporal resolution (Δt) of approximately 5 seconds for the microfluidic digital-to-analog converter (µDAC), showcasing its ability to capture rapid tissue response dynamics.

Building upon the capabilities of the μDAC, I integrated it into a microfluidic device featuring a 3D-printed adipose tissue trap. This automated laminar flow-based setup enabled real-time monitoring of free fatty acid uptake dynamics in adipose tissue. By subjecting the tissue to sequences of "fasting" and "feeding" treatments, I observed rapid, insulin-dependent dynamics of fatty acid uptake in ex vivo adipose tissue explants from mice.

I emphasize that this microfluidic device allowed for the first-time quantitative analysis of dynamics in epididymal white adipose tissue (eWAT) free fatty acid uptake rates and amounts at high temporal resolution (sub-minute), offering new possibilities for exploring adipose tissue function and metabolism with unprecedented precision.

The prevalence of diabetes and prediabetes in the United States and worldwide underscores the urgent need for improved tools to monitor and understand adipose tissue dynamics, which play a pivotal role in whole-body lipid buffering and various physiological processes. Microfluidic technology offers a promising avenue to investigate these dynamic processes and acquire novel biological insights.

My research further involved the development of a pneumatic valve-controlled, customized microfluidic analog-to-digital converter (μADC) capable of sampling adipose tissue secretions into droplets at high temporal resolution. This device facilitated multiplexed analysis of glycerol and non-esterified fatty acids (NEFA) by merging sampled droplets with coupled enzyme assay reagents using on-chip merging electrodes. Calibration and optimization of the assays for glycerol and NEFA characterized the device's capabilities, enabling the monitoring of their dynamics from ex vivo adipose tissue explants at high temporal resolution.

These results provided valuable insights into adipose tissue function during lipolytic conditions and varying glucose and insulin levels. Notably, the study suggested the occurrence of NEFA reabsorption, warranting further investigations with more explants and varying pharmacological treatments to accurately determine secretion ratios. The μADC demonstrated its potential to gather unique biological information, positioning it as a valuable tool for future research in endocrine tissue dynamics.

From our analysis of **chapter 2** and **chapter 3,** it has become evident that adipose tissue cells secrete significant molecules such as glycerol and non-esterified fatty acids in a dynamic and phased manner. To delve deeper into the dynamics of this secretion process, advanced tools like our μADC devices are imperative. Glycerol is a product by complete lipolysis as illustrated in **Figure 3. 16** and it is released through a protein channel known as AQP7. The synchrony of NEFA release with glycerol remains unknown, but it is well-established that NEFA follows a distinctly different metabolic pathway compared to glycerol. Hence, it is crucial to measure glycerol and NEFA concurrently and with high precision within a short timeframe, for which our novel device proves to be exceptionally valuable. Our microfluidic digital-to-analog circuit (μDAC), depicted in **Figure 2. 27** is seamlessly integrated with μADC (**Figure 3. 17 A**) sampling for quantifying protein efflux in white adipocytes. To optimize valve timings for rapid stimulation to the tissue reservoir, we employ pH-responsive beads as surrogates, mimicking tissue properties. These beads serve as on-site solution sensors of equivalent size to tissue explants, a critical factor for achieving high-resolution results. While interfacing with tissue in a μDAC/μADC device poses a challenge, Easley and Judd possess extensive expertise in adipose-focused interfacing techniques, including the use of 3D-printed reservoir templates (**Figure 5. 1**)[2, 4-9]. We have previously demonstrated that

the extended incubation channel on the μADC (**Figure 3. 18 A**) allows for continuous tissue imaging followed by subsequent assay readout in droplets[7, 8]. The release of metabolites in a cyclic or pulsatile manner is observed in circulation and likely plays a role in coordinating systemic/hepatic metabolism with the repackaging of NEFA into lipoproteins and glycerol into glucose. While these mechanisms in adipose tissue remain unknown, they likely involve feedback loops associated with cAMP, NEFA, acyl-CoA (lipase inhibition), or protein-regulated NEFA efflux. Our approach will involve systematic testing of mechanistic controls or protein-regulated NEFA efflux by combining simultaneous efflux assays (NEFA, glycerol, and possibly lactate) with optical FRET-based imaging of intracellular reporters developed by Granneman (cAMP, NEFA, acyl-CoA). Ligands ISO and SR-3420 will be utilized, and quantitative burst analyses (**Figure 3. 19**) and CWT spectrograms will be applied to study glycerol and NEFA release while correlating with real-time imaging. The underlying premise is that vital signaling molecules for systemic insulin sensitivity, including FABP4, are released via lipolysis-dependent non-conventional protein secretion. These molecules are believed to originate either in soluble form[10, 11], from secretory lysosomes[10, 12], or through an endosome/exosome pathway. Prior investigations have primarily focused on static conditions, neglecting the study of mechanisms and dynamics. Given that adipose-secreted FABP4 is elevated in metabolic disease[13], it is imperative that we uncover these mechanisms. Our approach will begin with the development of new mix-and-read proximity immunoassays for both CD63 (an exosome marker) and soluble FABP4. Subsequently, we will stimulate lipolysis in the tissue through PKA-dependent and -independent routes using various treatments (ISO, SR-3420, Aci, Ins). Following this, we will employ μADC droplet devices to

quantify CD63 and FABP4 at high resolution (< 5 s) using the µDAC system (**Figure 2. 28**) for the first time.

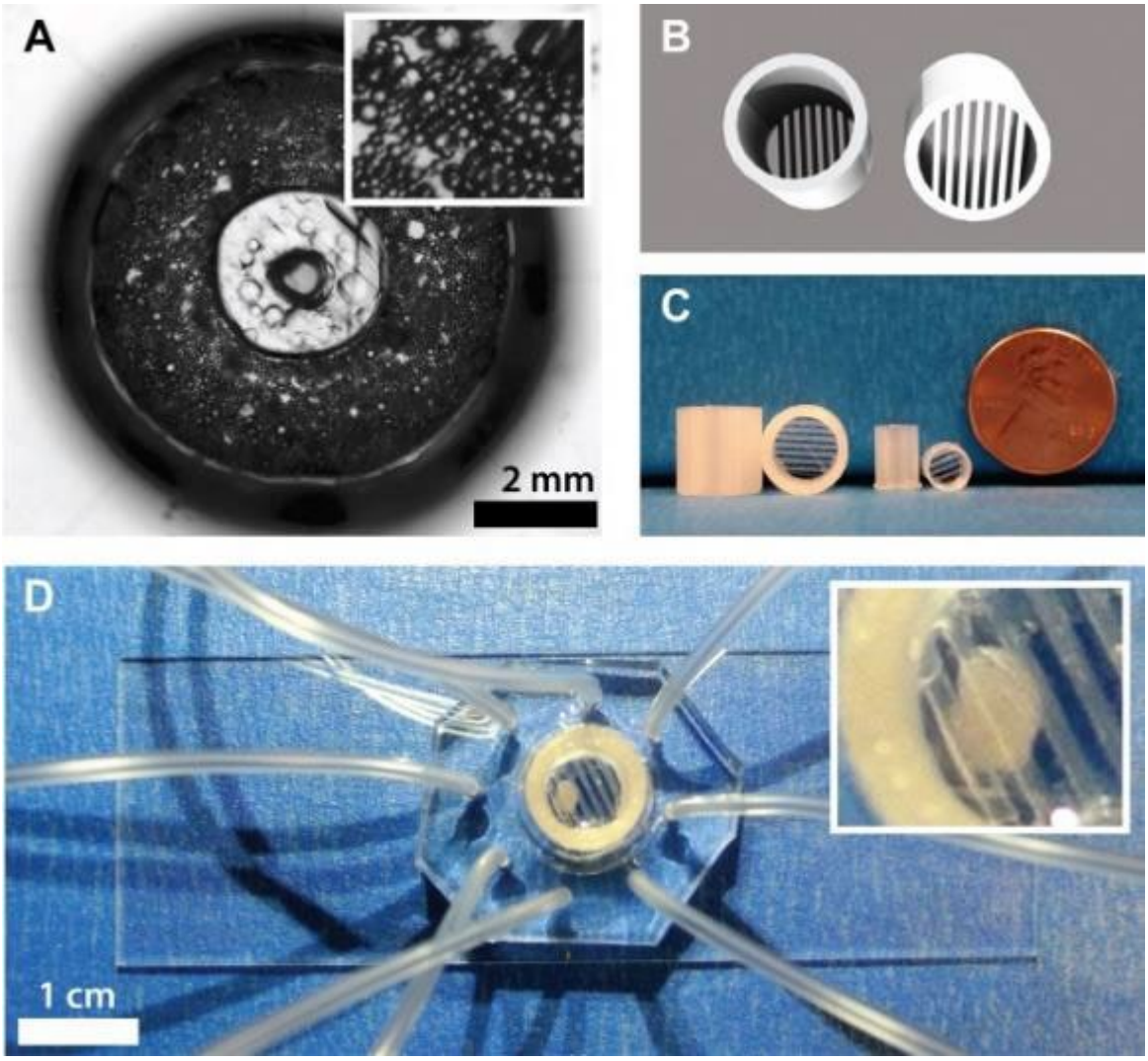

Figure 5. 2 Methods for interfacing dispersed adipocytes and adipose tissue explants to microfluidic devices have been developed by the Easley and Judd laboratories

5.3 New device: µDAC to µADC converter

The upper layer of the microfluidic device was created by pouring a mixture of PDMS precursor, consisting of 36 g with a 5:1 ratio of monomer to curing agent, onto a wafer containing

the flowing channel. Simultaneously, another 7.5 g of PDMS precursor with a 20:1 ratio of monomer to curing agent was spin-coated onto a separate silicon wafer, which acted as the lower pneumatic membrane, at 2100 rpm for 45 seconds. Both layers were then baked in an oven at 60℃ for approximately 30 minutes.

Subsequently, the thick fluidic layer was carefully removed, cut, punched, and cleaned before being precisely aligned with the valve channel. The assembled layers were left to bake overnight in the oven at 60℃. To permanently bond the PDMS to a thin cover glass, plasma oxidation was employed after peeling, cutting, and punching the PDMS. Following plasma oxidation, the devices were once again baked overnight in the oven at 60℃. Finally, the microfluidic device was fully assembled, prepared for use, and stored at room temperature.

5.4 Device

The whole PDMS device (**Figure 5. 3**) is ready to use for its application. This µDAC to µADC converter consists of two fluidic inputs (black in **Figure 5. 4 A** at bottom) for uptake assay, three fluidic inputs (black in **Figure 5. 5 A** at top) for secretion assay, one oil input (black in **Figure 5. 6 A** at middle left) for generating droplets after uptake assay, one tissue trap region, two waste reservoir, a whole system (white in **Figure 5. 7 A** at top right) for applying high voltage to merge the droplets, few incubation channels (white in **Figure 5. 8 A** at right), two region of interest and sixteen rectangular shape valves (red in **Figure 5. 9**) to control and flow the fluid through the microfluidic channels.

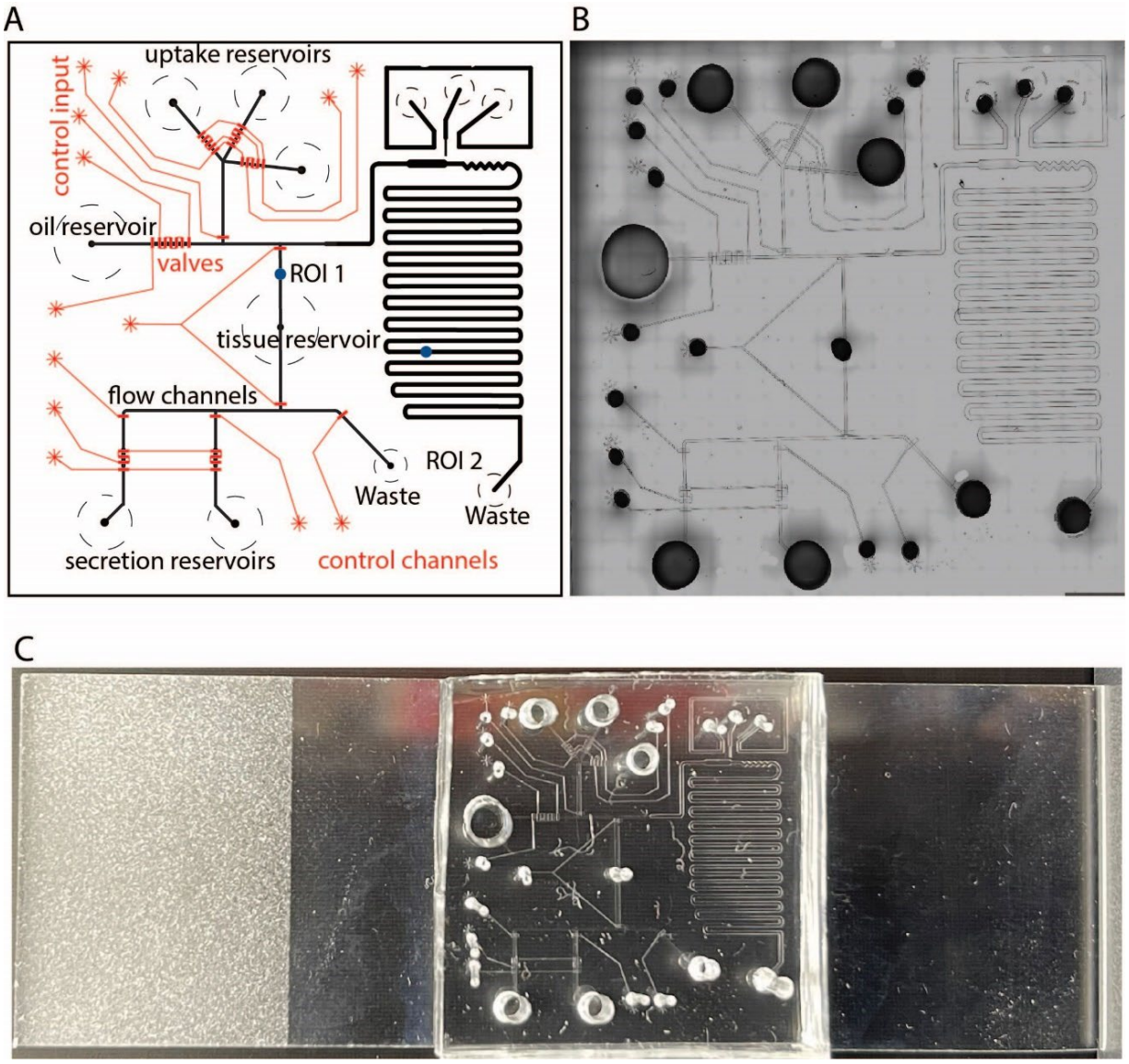

Figure 5. 10 Future device for nutrients uptake and secretion assay from explants simultaneously. **A**. Adobe Illustrator design of µDAC to µADC converter. **B**. Largescale image of the device after fabrication with PDMS. **C**. Whole chip-ready to use

5.5 Limitations of microfluidic devices

Microfluidic devices used in this research are complicated in terms of use as they consist of large number of valves for controlling the fluid flow inside the microfluidic channels. We are

planning to work with a smaller number of valves so that our devices can operate easily, and the efficiency of the devices can increase. Again, these devices need a huge laboratory set up support to make them automated and easy to use. This is another drawback of these devices that we cannot run them in another laboratory without proper set up. Interfacing the tissue on μDAC tissue trap region is complicated without the tissue holder, that's why we used 3D printed tissue holder in our research for holding the tissue inside the tissue reservoir. For μADC, we sacrificed our device temporal resolution due to on chip reactions for multiplexed quantification.

5.6 Conclusion

The research discussed here collectively emphasizes the significance of microfluidic technology in advancing our understanding of adipose tissue dynamics and its role in the broader context of endocrine tissue function. Each project contributes to a comprehensive exploration of these dynamics and provides innovative solutions for monitoring and analyzing key aspects of adipose tissue metabolism.

A microfluidic digital-to-analog converter (μDAC) was developed to study the uptake rates of fatty acids in ex vivo adipose tissue by rapidly stimulating the tissue. By precisely controlling the stimulation timing using innovative fluorescein-labeled glass beads as tissue mimics, we have achieved an input temporal resolution of approximately 5 seconds. The device was further integrated into a microfluidic setup for real-time monitoring of free fatty acid uptake dynamics, offering a novel tool for quantitative analysis of epididymal white adipose tissue (eWAT) uptake rates and amounts. This development is a significant advancement in understanding adipose tissue function and metabolic processes, particularly in the context of obesity and diabetes.

Later we worked on the role of microfluidic devices in emulating endocrine tissue microenvironments and gaining insights into their functions. We designed and fabricated microfluidic devices that enabled the study of time-dependent responses of endocrine tissues to various stimuli. By using pH-responsive beads as surrogates to mimic tissue properties, we achieved high-resolution results. These efforts provided a valuable platform for exploring adipose tissue function and metabolism with unprecedented precision. The importance of understanding adipose tissue dynamics in the context of diabetes and obesity is underscored, emphasizing the potential of microfluidic technology in this research.

In future work, we address the pressing issue of diabetes and prediabetes and the need for improved tools to monitor and understand the dynamics of adipose tissue. The development of a microfluidic analog-to-digital converter (μADC) for high-resolution sampling from adipose tissue is discussed. This device enables the quantification of glycerol and non-esterified fatty acids (NEFA) in a dynamic and phased manner. It is an important step in understanding the dynamics of NEFA reabsorption, a critical aspect of adipose tissue function. The project also emphasizes the potential for microfluidic methods to provide new biological insights and highlights the importance of monitoring these analytes at higher temporal resolution from ex vivo adipose tissue.

In summary, this dissertation collectively demonstrates the power of microfluidic technology in advancing our understanding of endocrine tissue dynamics, with a particular focus on adipose tissue. Microfluidic technology offers innovative solutions, tools, and methodologies for studying the dynamic functions of this vital organ, which plays a central role in whole-body lipid metabolism and is closely associated with conditions such as diabetes and obesity. These

developments have the potential to open new avenues for research and contribute to our knowledge of endocrine tissue function in both health and disease.

5.7 References

1. Bhatia, S. N.; Ingber, D. E., Microfluidic organs-on-chips. *Nature biotechnology* **2014,** *32* (8), 760-772.
2. Li, X.; Easley, C. J., Microfluidic systems for studying dynamic function of adipocytes and adipose tissue. *Analytical and bioanalytical chemistry* **2018,** *410*, 791-800.
3. Li, X.; Brooks, J. C.; Hu, J.; Ford, K. I.; Easley, C. J., 3D-templated, fully automated microfluidic input/output multiplexer for endocrine tissue culture and secretion sampling. *Lab on a Chip* **2017,** *17* (2), 341-349.
4. Godwin, L. A.; Brooks, J. C.; Hoepfner, L. D.; Wanders, D.; Judd, R. L.; Easley, C. J., A microfluidic interface for the culture and sampling of adiponectin from primary adipocytes. *Analyst* **2015,** *140* (4), 1019-1025.
5. Brooks, J. C.; Ford, K. I.; Holder, D. H.; Holtan, M. D.; Easley, C. J., Macro-to-micro interfacing to microfluidic channels using 3D-printed templates: application to time-resolved secretion sampling of endocrine tissue. *Analyst* **2016,** *141* (20), 5714-5721.
6. Brooks, J. C.; Judd, R. L.; Easley, C. J., Culture and sampling of primary adipose tissue in practical microfluidic systems. *Thermogenic Fat: Methods and Protocols* **2017**, 185-201.
7. Li, X.; Hu, J.; Easley, C. J., Automated microfluidic droplet sampling with integrated, mix-and-read immunoassays to resolve endocrine tissue secretion dynamics. *Lab on a Chip* **2018,** *18* (19), 2926-2935.
8. Hu, J.; Li, X.; Judd, R. L.; Easley, C. J., Rapid lipolytic oscillations in ex vivo adipose tissue explants revealed through microfluidic droplet sampling at high temporal resolution. *Lab on a Chip* **2020,** *20* (8), 1503-1512.
9. Shi, N.; Moniruzzaman, M.; Easley, C. J., Tissue engineering and analysis in droplet microfluidics. In *Droplet Microfluidics*, R. Soc. Chem. Cambridge, UK: 2020; pp 223-260.
10. Ertunc, M. E.; Sikkeland, J.; Fenaroli, F.; Griffiths, G.; Daniels, M. P.; Cao, H.; Saatcioglu, F.; Hotamisligil, G. S., Secretion of fatty acid binding protein aP2 from adipocytes through a nonclassical pathway in response to adipocyte lipase activity. *Journal of lipid research* **2015,** *56* (2), 423-434.
11. Mita, T.; Furuhashi, M.; Hiramitsu, S.; Ishii, J.; Hoshina, K.; Ishimura, S.; Fuseya, T.; Watanabe, Y.; Tanaka, M.; Ohno, K., FABP4 is secreted from adipocytes by adenyl cyclase-PKA-and guanylyl cyclase-PKG-dependent lipolytic mechanisms. *Obesity* **2015,** *23* (2), 359-367.
12. Villeneuve, J.; Bassaganyas, L.; Lepreux, S.; Chiritoiu, M.; Costet, P.; Ripoche, J.; Malhotra, V.; Schekman, R., Unconventional secretion of FABP4 by endosomes and secretory lysosomes. *Journal of Cell Biology* **2018,** *217* (2), 649-665.

13. Kralisch, S.; Klöting, N.; Ebert, T.; Kern, M.; Hoffmann, A.; Krause, K.; Jessnitzer, B.; Lossner, U.; Sommerer, I.; Stumvoll, M., Circulating adipocyte fatty acid-binding protein induces insulin resistance in mice in vivo. *Obesity* **2015,** *23* (5), 1007-1013.